NOTICE

The quality of this microform is heavily dependent upon the quality of the original thesis submitted for microfilming. Every effort has been made to ensure the highest quality of reproduction possible.

If pages are missing, contact the university which granted the degree.

Some pages may have indistinct print especially if the original pages were typed with a poor typewriter ribbon or if the university sent us an inferior photocopy.

Reproduction in full or in part of this microform is governed by the Canadian Copyright Act, R.S.C. 1970, c. C-30, and subsequent amendments.

AVIS

La qualité de cette microforme dépend grandement de la qualité de la thèse soumise au microfilmage. Nous avons tout fait pour assurer une qualité supérieure de reproduction.

S'il manque des pages, veuillez communiquer avec l'université qui a conféré le grade.

La qualité d'impression de certaines pages peut laisser à désirer, surtout si les pages originales ont été dactylographiées à l'aide d'un ruban usé ou si l'université nous a fait parvenir une photocopie de qualité inférieure.

La reproduction, même partielle, de cette microforme est soumise à la Loi canadienne sur le droit d'auteur, SRC 1970, c. C-30, et ses amendements subséquents.

COMPUTER-AIDED VEHICLE DESIGN SYNTHESIS

FOR

HANDLING AND STABILITY

ROLAND JONASCH

A Thesis

in

The Department

of

Mechanical Engineering

Presented in Partial Fulfilment of the Requirements
for the Degree of Master of Engineering at
Concordia University
Montreal, Quebec, Canada

December 1991

ISBN 0-315-73697-6

ABSTRACT

COMPUTER-AIDED VEHICLE DESIGN SYNTHESIS FOR HANDLING AND STABILITY

Roland Jonasch

The vehicle design engineer's task is to design or select vehicle components to meet handling and stability criteria. The thesis presents a computer-aided vehicle design synthesis as a tool for the vehicle design engineer.

A mathematical model of the vehicle in lateral, yaw and roll degrees of freedom is developed. A sinusoidal tire model characterizing the lateral force and self-aligning torque as a function of normal load, slip angle and camber angle is used. A planar pullrod A-arm suspension linkage is mathematically modelled and analyzed by the method of velocity coefficients. This provides instantaneous roll center heights and roll stiffnesses. Tire and suspension characteristics are incorporated in the 3DOF vehicle model in a modular computer software for evaluating vehicle handling and stability characteristics. The software selects chassis spring rates, synthesizes the chassis configuration based on selected performance indices, and computes the transient dynamic handling response.

Case studies are presented to demonstrate the vehicle design synthesis procedure. A parametric study showed the influence on vehicle response behaviour as a result of variations in suspension and chassis design.

The main advantage of the vehicle design synthesis used in this thesis is its modularity. The suspension linkage analysis is performed once, at the start of the design synthesis procedure. The results of the suspension analysis are then included in the vehicle handling and stability evaluation in black box form. Thus the problem is solved in small, manageable parts.

ACKNOWLEDGEMENTS

The author wishes to express his gratitude to his thesis supervisors, Dr. S. Sankar and Dr. M. Richard for the encouragement and support extended during the preparation of this thesis.

He would also like to thank all CONCAVE research personnel and other graduate students for their technical support and encouragement. In addition, the author thanks Mr. Valerio Valentini for his help in the preparation of this thesis.

The financial support from CONCAVE Research Center is also gratefully acknowledged.

Thanks are due to the author's family for their encouragement and support, temporal and otherwise. In particular, Dr. Momcilo Gavrilovic contributed many hours of assistance and encouragement.

Finally, many thanks to my wife, Ivana, for her love, encouragement, patience and support.

TABLE OF CONTENTS

LIST OF FIGURES

LIST OF TABLES

NOMENCLATURE

Symbol		Description
a	:	distance from front axle to projection of center of gravity on $\bar{X}$-$\bar{Y}$ plane
a_s	:	distance from sprung mass center of gravity to vehicle center of gravity, in $\bar{X}$-$\bar{Y}$ plane
$\mathbf{A}$	:	a Jacobian matrix in equation (3.12)
A_f, A_r	:	front and rear lateral accelerations
A_y	:	lateral acceleration of whole vehicle
A_0, A_1, A_2	:	constant coefficients in equation (1.2) representing tire side-force properties
b	:	distance from rear axle to projection of center of gravity on $\bar{X}$-$\bar{Y}$ plane
$\mathbf{B}$	:	matrix of partial derivatives of the loop closure equations $\mathbf{f}$ with respect to independent variables $\mathbf{q}$
c_i	:	ith constant that defines the linkage geometry
C_x, C_y	:	longitudinal and lateral tire stiffnesses, respectively, N/radian
DI	:	inertial coupling dynamic index
DOF	:	degrees of freedom
f_i	:	ith function in loop-closure equation (3.11)

ftol	:	tolerance for Newton-Raphson iterative technique
F	:	matrix of forces due to kinematic linkage force generators
F_o	:	outward inertial force during cornering
F_x, F_y, F_z	:	longitudinal, lateral, and vertical tire forces
F_{yfo}	:	lateral force on front outer wheel
F_{yfi}	:	lateral force on front inner wheel
F_{yro}	:	lateral force on rear outer wheel
F_{yri}	:	lateral force on rear inner wheel
g	:	gravitational acceleration
h	:	vertical distance from road to center of gravity
h_f, h_r	:	front and rear roll center heights
h_{rs}	:	perpendicular distance from roll axis to center of gravity of sprung mass
h_{uf}, h_{ur}	:	front and rear unsprung mass center of gravity heights
i	:	sprung mass radius of gyration
I_x	:	sprung mass roll moment of inertia
I_z	:	vehicle yaw moment of inertia
k_f, k_r, k_{tot}	:	front, rear and total roll stiffness
k_i	:	designated stiffness i
K	:	velocity coefficients matrix
K_r	:	roll stiffness of a planar suspension

L	:	wheelbase
L_p	:	total roll damping
m	:	total vehicle mass
m_i	:	designated lumped mass i
m_s	:	sprung mass
m_{uf}, m_{ur}	:	front and rear unsprung masses
M_r	:	total roll moment
M_{zfo}	:	front outer self aligning torque
M_{zfi}	:	front inner self aligning torque
M_{zro}	:	rear outer self aligning torque
M_{zri}	:	rear inner self aligning torque
N_u	:	understeer number
P_{xz}, P_{yz}, P_{xy}	:	product of inertia
p	:	sprung mass roll angular velocity
pg	:	proportion of weight on rear axle
q	:	independent linkage variables (generalized coordinates)
Q	:	matrix of generalized forces
R	:	corner radius
r	:	yaw angular velocity
s	:	wheel slip
t_f, t_r	:	front and rear track width
U	:	vehicle velocity in $\bar{X}$-direction
V	:	vehicle velocity in $\bar{Y}$-direction
W	:	work done

W_{brf}, W_{brr}	:	front and rear lateral weight transfer due to body roll
W_{rcf}, W_{rcr}	:	front and rear lateral weight transfer due to sprung mass inertia forces
W_{tf}, W_{tr}	:	front and rear total lateral weight transfer
W_{uf}, W_{ur}	:	front and rear lateral weight transfer due to unsprung mass inertia forces
X_{cg}	:	X-coordinate of center of gravity in inertial reference frame
X_{RC}	:	X-coordinate of roll center in inertial reference frame
y	:	y position
Y_{cg}	:	Y-coordinate of center of gravity in inertial reference frame
Y_{RC}	:	Y-coordinate of roll center in inertial reference frame
α	:	slip angle
α_f, α_r	:	front and rear slip angles
α_{RC}	:	horizontal coordinate of roll center in inertial reference frame
β_{RC}	:	vertical coordinate of roll center in inertial reference frame
γ	:	camber angle
Δ	:	determinant
δ	:	steer angle

ϵ	:	a road-tire interface-dependent parameter in Dugoff's tire friction model
η_s	:	coordinate in the sprung mass-fixed reference frame
θ	:	sprung mass roll angle
$\mathbf{K}$	:	generalized stiffness matrix
λ	:	a non-dimensional parameter in Dugoff's tire friction model
μ	:	actual friction force coefficient of the road-tire interface
μ_o	:	nominal friction force coefficient of the road-tire interface
ξ_s	:	coordinate in the sprung mass-fixed reference frame
ϕ	:	dependent linkage variables
Ψ	:	vehicle yaw angle
Ω	:	Lagrangian coordinates
$\cdot$	:	differentiation with respect to time

CHAPTER 1

Introduction and Literature Review

1.1 General

The vehicle design engineer's task is to combine a selection of physical components and chassis with the intention of meeting certain control, handling and stability criteria. For the purposes of this work, the vehicle's control, handling and stability criteria will be referred to as the performance requirement. The engineer may have to design a suspension system using a specified combination of components so that the design is simple and is low cost, or he/she may be required to determine what quality of components are required for a specific design in order to meet the performance criteria (i.e. design of sports or racing cars whose handling abilities must be superior to those of the competing models or designs). In either case, it is important to quantitatively evaluate the performance potential of a combination of suspension components and chassis. This will reduce the number of design-build-test cycles necessary to obtain an acceptable product.

An accurate chassis performance estimate requires sufficient detail in both tire models and vehicle models. The automobile industry has the requisite analysis tools and computing power to carry out a thorough vehicle analysis. Unfortunately, these resources are not available to industry

outsiders. There is, however, a great deal of public domain knowledge which can make a valid vehicle design procedure possible. A detailed review of the literature on this subject is outlined below.

1.2 Review of Previous Investigations

1.2.1 Tire Models

A concise review of the theory of theoretical and experimental tire shear force generation at the tire-road interface is now presented.

Bernard, Segel and Wild provided a concise review of tire interfacial force and moment knowledge [1]*. They reported on pioneering efforts by Becker, Fromm, Maruhn and others; the majority of these reported works were based on measurements made on laboratory dynamometers. Knowledge of the limit-state tire-pavement shear forces was of a qualitative nature.

According to Bernard, Segel and Wild, the accepted tire shear force relation during the fifties was

$$\sqrt{F_y^2 + F_x^2} \leq \mu F_z \qquad (1.1)$$

*Numbers in parentheses designate references at end of thesis.

Around 1960, researchers such as Pacejka [2], Radt and Milliken [3], Ellis [4], and Deininger [5] questioned whether the interaction between F_x and F_y was independent of tread and carcass compliance.

In 1967, Krempl published findings to refute the concept of constant tire friction coefficient [6]. Krempl's work provided evidence that tire friction forces were dependent on normal load. He also discovered that the forward velocity had a greater influence on the longitudinal force than on the lateral force.

Further work by the Road Research Laboratory [7] and the University of Michigan's Highway Safety Research Institute [8] confirmed that the tire friction mechanism is more complex than implied by equation (1.1).

Okada et al. (1973) used an empirical tire model in a computer evaluation of vehicle handling and stability [9]. Cornering force and self aligning torque were modelled.

Bernard, Segel and Wild continued by modelling the tire-road interfacial shear forces [1]. Their semi-empirical tire model, published in 1977, was applicable to combined steering and braking maneuvers. The model was a trapezoidal idealized pressure distribution for the contact patch. By determining the position of the sliding boundary point, the resultant longitudinal and lateral forces were obtained by integrating the shear stresses over the contact patch. Closed form solutions were then derived for the sliding boundary point.

A mathematical match to measured tire data was achieved by using friction, contact patch shape, longitudinal stiffness, and cornering stiffness parameters. Adjustment parameters were used to accommodate non-linearities in the test data. Predictions of lateral force versus slip angle were claimed to match measured data within 5 percent.

A report on the dynamics of single vehicle accidents, published in 1968 by the Cornell Aeronautical Laboratory, contained a semi-empirical tire model [10]. Accuracy of predicting lateral, braking and traction forces within the normal ranges of operating conditions for passenger cars was the primary objective.

Radial loading of each tire was calculated in 2 modes, depending on the nature of the tire-terrain contact patch. A point contact model was used for flat terrain, while a radial spring model was used for non-planar contact such as curbs. When calculating the effects of loading on side forces, variations in small-angle cornering stiffnesses and camber stiffnesses due to changes in tire normal load were approximated by parabolic curves fitted to experimental data. The lateral tire force near the limit-state was approximated as independent of tire loading, since artificial reversal of slip angle forces could result for the following cornering stiffness parabola:

$$C_y = A_0 + A_1 F_z - \left(\frac{A_1}{A_2}\right) F_z^2 \qquad (1.2)$$

The actual properties of tires in the region of extreme overload (limit-state) were not known. The side force calculations were based on non-dimensional slip angle variables and the friction circle concept, with modifications for large slip and camber angles.

Dugoff's semi-empirical tire model (1969) calculated longitudinal and lateral tire forces as follows [11]:

$$F_x = -\frac{C_x s}{(1-s)} f(\lambda) \tag{1.3}$$

$$F_y = -\frac{C_y \tan\alpha}{(1-s)} f(\lambda) \tag{1.4}$$

$$\text{where } \lambda = \frac{\mu F_z (1-s)}{2\sqrt{(C_x s)^2 + (C_y \tan\alpha)^2}} \tag{1.5}$$

$$f(\lambda) = (2-\lambda)\lambda \quad \text{if} \quad \lambda < 1 \tag{1.6}$$

$$= 1 \quad \text{if} \quad \lambda \geq 1 \tag{1.7}$$

$$\mu = \mu_0 (1-\varepsilon U s) \tag{1.8}$$

Brewer and Rice [12] examined the influences of vehicle design and tire characteristics on the level of stability and control at the upper limits of vehicle performance. They defined a limit maneuver as any maneuver which causes a motor vehicle's tires to operate at their peak shear force level. If the level of severity of the maneuver is increased, the vehicle responds in a discontinuous manner.

The goals of Brewer and Rice were to determine how changes in vehicle design and tire characteristics could influence the level of stability and control, emphasizing the upper limits of vehicle performance. Their analysis scheme used the method of moments, which is based on solving the generalized steady-state equations of motion to obtain values for the resultant yaw moment and lateral acceleration. Brewer and Rice concluded that a comprehensive knowledge of force coefficients was essential in order to make analytical predictions about a vehicle's near-limit stability and controllability.

Bakker, Nyborg and Pacejka [13] published a steady-state tire model using a formula with coefficients that applied tire data from pure steady-state cornering and pure braking. Steady-state side and braking forces as well as self-aligning torques were measured on a full scale test trailer on a dry road.

The experimental measurements were reduced to three equations with thirty-one coefficients. The influences of normal load and camber change were taken into account in the equations, which calculated side forces, self-aligning torque and brake forces for pure cornering and pure braking. Due to the use of the arctan function and the various correction factors in the equations, very good agreement with the experimental data was achieved, notably in the peak regions.

In a 1989 review, Maalej, Guenther and Ellis [14]

evaluated several tire force and moment models that have been developed for use in the mathematical analysis of vehicle handling. Using empirical data for one particular tire, the sinusoidal tire model by Bakker, Nyborg and Pacejka [13] and a cubic fit polynomial tire model [14] as well as the semi-empirical model developed by Segel [14] were compared to Dugoff's semi-empirical model [11]. Table 1.1 classifies the tire models according to accuracy, solvability and evaluation time.

TABLE 1.1 - Comparison of Tire Friction Models [14]

Model	Accuracy	Parameter Determination	CPU computation time
Sinusoidal	1*	4	3
Polynomial	2	3	2
Segel	4	2	1
Dugoff	3	1	3

*1 denotes best performance on the considered criterion

Maalej, Guenther and Ellis concluded that the sinusoidal model gave the best fit for lateral force, especially at higher normal loads. The third order polynomial tire model did not reach the peak empirical value of the tire lateral force. However, all four tire models provided a reasonable

fit for small slip angles. The model constants for the polynomial model are easily obtained from the experimental data using methods such as the least square method, while the sinusoidal model constants require non-linear regression analysis. In fact, the CPU time required to calculate constants in the sine model exceeded that of the polynomial model by a factor of six. In addition, the CPU time required to compute the side force as a function of normal load and wheel orientation using the sine model was ten percent greater when compared to the polynomial model.

Nalecz' non-linear tire model [15] used the friction ellipse concept to determine the limits of adhesion of all four tires under different loading conditions due to weight transfer, acceleration and braking. The proportions of the friction ellipse are a function of the tire normal load and the frictional properties of the road-tire interface. Peak lateral and braking coefficients as well as cornering stiffnesses were calculated using CALSPAN tire data [16]. This model is of the polynomial type, which underestimates the peak lateral force values of the tires.

1.2.2 Vehicle Models

In 1957, Leonard Segel published a paper which served as a foundation for modern automobile control and stability theory [17]. He stated that published engineering discussions of automotive handling were non-existent before 1925. In

1925, Broulhiet [18] presented the basic concept of wheel side-slip. By 1935, papers were appearing which described the lateral mechanical properties of automotive tires. In 1950, the concept of static margin was presented as representative of steady-state stability [19]. Segel continued by stating that aircraft dynamic stability and control theory was best suited for analyzing automobile behaviour, and that previously-developed vehicle equations of motion were not as comprehensively effective.

Segel defined handling as the vehicle's yawing, rolling and side-slipping motions resulting from road irregularities, aerodynamics, or driver-applied steering inputs. The subjective aspect of handling deals with the driver's evaluation of the ease and precision with which a vehicle can be steered into and maintained on a desired path.

Vehicle control was interpreted in two ways. The first interpretation was as a means of applying forces and moments to a vehicle, resulting in linear and angular accelerations, velocities, or displacements. Additionally, control implies a transient and steady-state vehicle response to control force and moment inputs.

Stability was defined as the ability to maintain a given state of equilibrium. A stable vehicle returns to its initial state after a momentary disturbance is removed, or achieves a new equilibrium state for a constant disturbing force.

Segel's vehicle model was a three degree-of-freedom

linear dynamic system which represents the fixed control automobile with tire dynamics neglected. A vehicle-fixed coordinate system was used. The linearity condition was used up to a lateral acceleration of approximately 0.3g. It was required to model or measure mass and inertia properties, and the suspension and tire characteristics to predict a vehicle's response to steering inputs.

Results from the analytical solution were verified by comparing with instrumented road test results. For the particular test configuration, excellent agreement was found between theory and experiment. Segel concluded that the derived equations of motion adequately defined the lateral dynamic behaviour of the car.

A description was made of the forces and moments acting on a car during a steady turn, due to front wheel steer angle, angular yaw velocity, and lateral velocity. Segel stated that the moment due to side-slip approaches zero, and the yaw damping moment (due to the tires opposing the yawing velocity) is primarily balanced by the steering moment. The total directional stability was described by Segel in terms of the static margin, which was more precisely defined by Scibor-Rylski [20] as the distance between the vehicle's center of gravity and the line of action of the resultant of the tire forces, expressed as a fraction of the wheelbase. In summary, the two most important properties governing the control sensitivity and transient response of an automobile are the

static margin and the yaw damping, according to Segel.

Okada et al. (1973) analysed the vehicle response during skidpad and slalom maneuvers, as well as during straight-running motion with wind and steering inputs [9]. Using a polynomial-type empirical tire model, a 7DOF vehicle model with 63 design parameters was solved. The agreement of analytical results with the response of the car on the test track was generally good. The authors reported that the results for the skidpad test above 0.6 g were limited by innaccuracies in the tire model and the representation of roll characteristics. A distinction was made between the mechanical handling limits of the vehicle and the limits of the driver's ability to steer the vehicle.

Dominy and Dominy (1984) modelled the performance of the Formula 1 racing car [21]. A major goal of this work was to investigate the influence of downforce, drag and center of pressure on lap times. At the time of publication, Formula 1 racing cars featured underbody venturis which developed downforces in the order of three times the vehicle weight. Changes in dynamic ride height were minimized, as it was necessary to strictly control the undertray-to-road dimension. As a result of this, a very simple suspensionless four wheel chassis model was used, which used the overturning moment to calculate load transfer at the front and rear axles. The car was assumed to be under maximum acceleration, maximum braking, or maximum steady-state cornering. A traction circle tire

PAGINATION ERROR.

TEXT COMPLETE.

ERREUR DE PAGINATION.

LE TEXTE EST COMPLET.

roll center loci were calculated. The authors concluded that the suspension damper characteristics did not affect the dynamics of the car due to the strong aerodynamic downforce and very limited suspension travel.

Nalecz (1987) modelled the effects of suspension design on the stability of light vehicles [15]. A three dimensional model was used. The three degrees of freedom are: lateral displacement, yawing and rolling. Non-linear tire and roll center effects are included. Limit-states for various cornering and braking combinations were calculated.

In 1990, Dixon published the equations of lateral motion for a two degree-of-freedom model of the four-wheeled road vehicle [23]. An analogy was made with the single degree-of-freedom linear mass-spring-damper system. Terms expressing the stability, undamped natural frequency, damping ratio, and damped natural frequency were derived. It was suggested that the effects of pneumatic trail, load transfer, compliance steer, roll steer, and roll camber be incorporated by introducing the static margin term from a more extensive steady-state analysis.

1.2.3 Existing Software for Vehicle Design Analysis

Software packages for multibody dynamics analysis and general mechanisms analysis and synthesis are relatively common. They will not be reviewed here, rather, an overview of commercially available vehicle analysis programs is given.

The Racing by the Numbers software (1987) is intended for

the auto racing market [24]. Among seven available program modules are programs for suspension analysis and vehicle dynamics.

The suspension geometry program performs spatial kinematic analysis of double A-arm, MacPherson strut and selected live rear axle systems. Asymmetrical linkages can be analyzed, and steering system kinematics are included. Eighteen kinematic suspension parameters are calculated. The wheelrate calculation neglects the non-linear effects of the rate of change of the motion ratio. A rigid-body force analysis of the suspension components is also carried out.

The Racing by the Numbers software uses a simple tire model which is based on normal load and camber. No further information on this tire model is available.

The TLS100 suspension design software is restricted to the kinematic analysis of double A-arm suspension systems [25]. Spatial kinematics including geometry are included. No vehicle dynamics calculations are performed, thus no tire model is present.

Programme TOUR 3.6 is a simulation program used in race car tuning and performance prediction as well as design analysis [26].

TOUR uses "correction coefficients" to compensate for modelling inaccuracies. The correction coefficients are determined by baseline vehicle tests. A constant forward speed is used in cornering segments, and no road camber,

banking, or elevation changes are considered. The tire model is based on the traction ellipse, with modifications for road-tire friction coefficient adjustment. Tread-width compensation is included as well.

The TOUR simulation procedure is based on straight line acceleration with maximum available or useable engine torque, followed by maximum straight line braking and limit-state cornering. The limit cornering speed is calculated subject to the limit of adhesion of one axle, and the unloading of both inner wheels. The variable EQUIL is used to describe the normalized level of lateral acceleration that each axle can sustain, where EQUIL < 1 = understeer and EQUIL > 1 = oversteer. The difference between 1 and EQUIL is the traction margin of the less-used axle. One lap consists of calculating the maximum speed for each curve, then connecting each adjoining straight with intersecting stretches of maximum acceleration and braking.

1.3 Scope of the Thesis

The objective of this thesis is to create a computer-aided design synthesis procedure for handling and stability. The vehicle should be modelled mathematically with sufficient detail so that changes in handling and stability can be detected. A mathematical tire model is required that accurately describes the tire lateral force and self aligning moment as a function of normal load, slip angle and camber angle. Tire response in the peak lateral force region must be accurately represented. The front and rear suspension linkages must be modelled and analysed so that the characteristics of significant non-linearities such as instantaneous roll center location, roll stiffness and camber change can be extracted.

The tire and suspension characteristics should be incorporated in the vehicle model in a modular way. The programming tools should allow the vehicle design synthesis software to be developed easily and quickly, and should help in rapid program modification and debugging.

The vehicle design should be synthesized according to clear, logical performance objectives. Various studies should be completed during software development to gain confidence in the design synthesis procedure for handling and stability in order to gain confidence in the results and to demonstrate the potential of the software.

CHAPTER 2

Vehicle System Components for Handling and Stability

2.1 General

This chapter will discuss the suspension system components, emphasizing their influence on vehicle handling and stability. The inertial properties of the vehicle (mass, C.G. position, moments and products of inertia) combined with the physical components (tires, linkages, springs and dampers) determine the vehicle handling characteristics.

2.2 A-Arm Suspension Linkage

Real-world road conditions with surface irregularities of diverse amplitudes and wavelengths require a suspension system to minimize dynamic force variations at the tire contact patches for good handling and stability. In addition, a desired level of ride comfort must be provided for the vehicle occupants. The passive suspension system consists of linkages connecting the wheels to the chassis, allowing relative movement between the two.

The state of the art in passive automobile suspension linkages is the independent suspension system, which ideally reacts to a single-wheel disturbance only at that corner of the vehicle, leaving the other three wheels unperturbed. There are many physical configurations providing independency; the example treated in this thesis is the A-arm linkage with

pullrod spring/damper actuation (Fig. 2.1).

As seen in Fig. 2.1, the pullrod suspension has upper and lower frames, commonly called A-arms, wishbones, or tables. Each frame has two revolute joints at the chassis and one spherical joint at the hub. This suspension is a 4-bar linkage where the chassis is the ground link, the A-arms are side links, and the hub/wheel assembly is the coupler link. The 4-bar linkage governs the tire contact patch kinematics, and is found in up-market motorcars (luxury and high-performance) as well as in purpose-built race cars. The advantages of the 4-bar linkage as a wheel locator when compared to the McPherson strut or the non-independent suspension system are light weight, rigidity and accurate wheel control; disadvantages are cost, complexity and space inefficiency.

To the 4-bar linkage we add a mechanism that connects it to the spring/damper unit. This mechanism transmits tire forces to the spring/damper unit using a tensile member and a bellcrank (Fig. 2.2). This mechanism in combination with the 4-bar linkage is commonly called the pullrod suspension, by virtue of the tensile link. The pullrod suspension is generally found on purpose-built race cars and is rare on road-going vehicles. It provides advantageous tunability of force-displacement non-linearities, low unsprung weight and low aerodynamic drag. The main advantage of the pullrod suspension is that the mechanical advantage of the system can

be designed to decrease with wheel travel, giving a spring stiffening characteristic. The rising rate helps prevent suspension or chassis bottoming during bump travel and braking. The drawbacks are that the additional complexity of this system leads to packaging problems and increased cost [30].

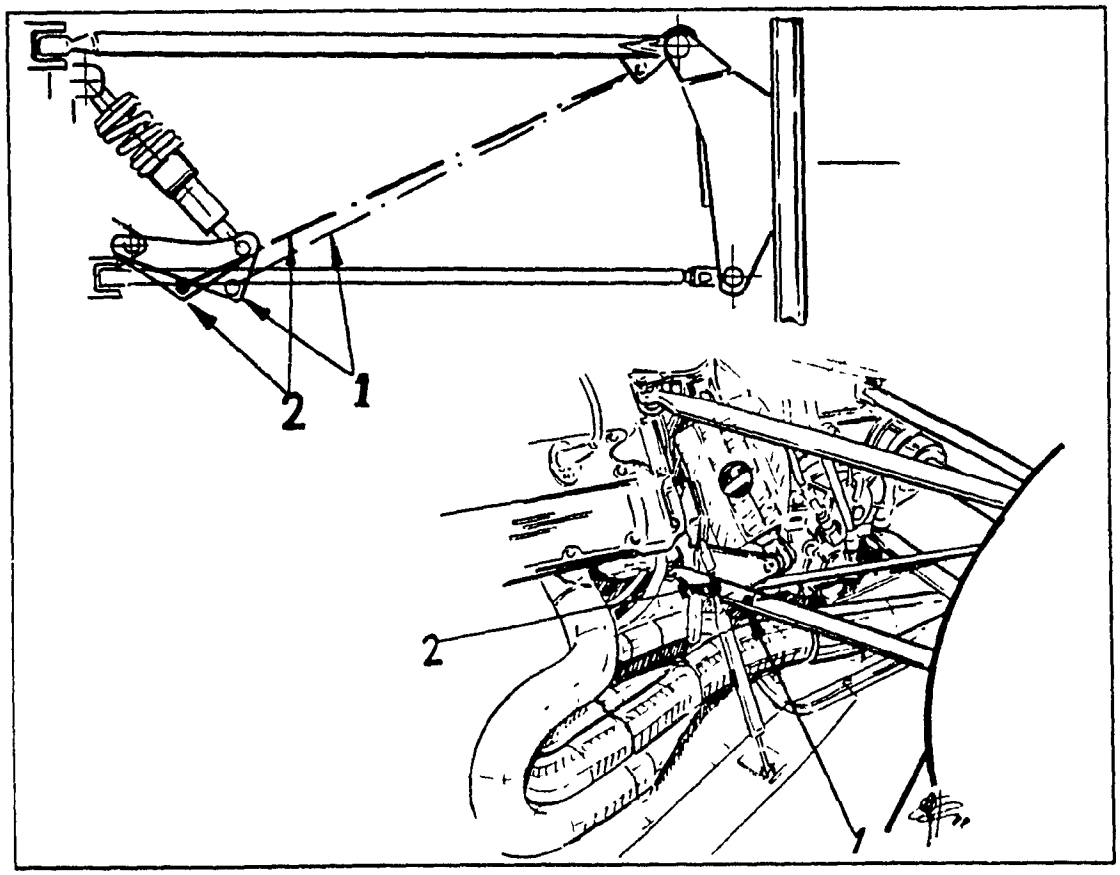

Fig. 2.1 Pullrod Rear Suspension on 1988 Williams FW12 Formula 1 Car [28]

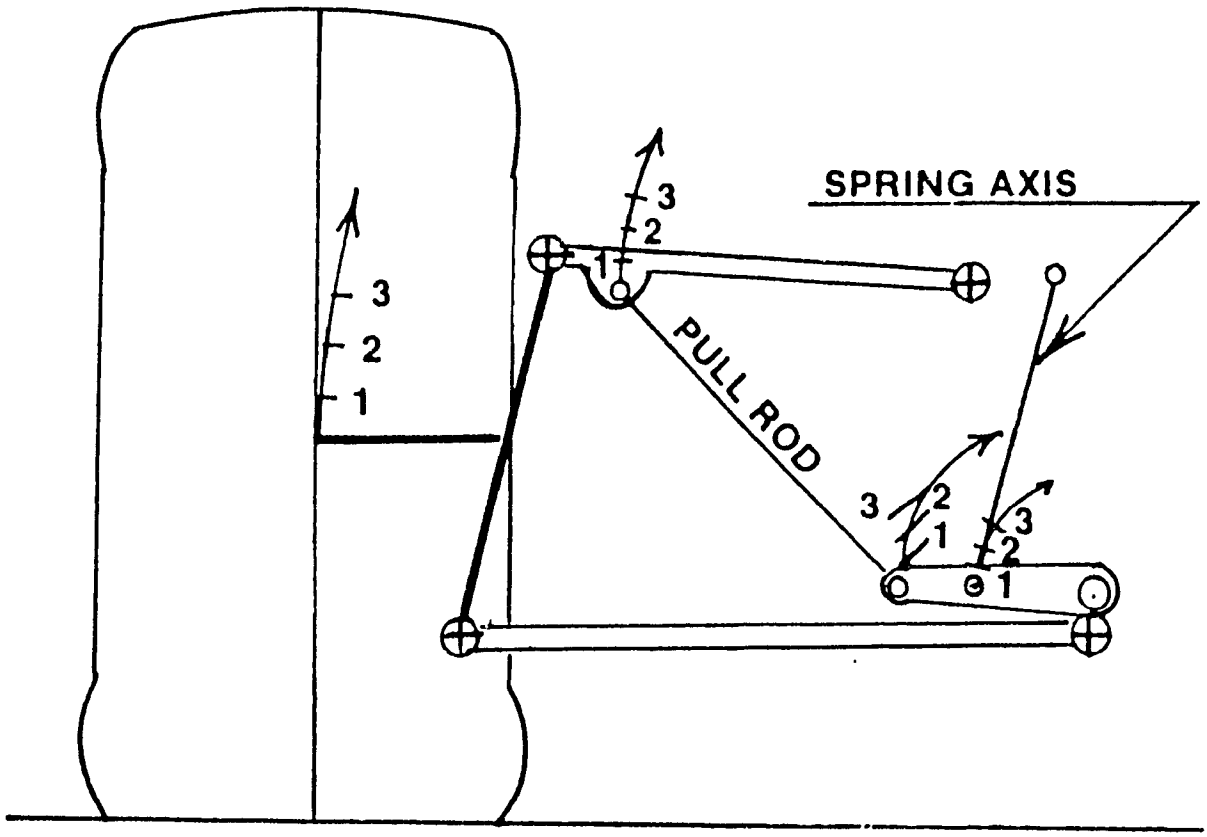

Fig. 2.2 Pullrod Suspension System Schematic [29]

2.3 Tires

The pneumatic tire is the most important design component. It plays the major role in the control, handling and stability of the vehicle. It is important to understand how the tire interacts with the road surface, and to be aware of the options and constraints of selecting a tire for a particular vehicle design [31].

The tire generates cornering force when the tire's contact patch travels at an angle to the wheel it is mounted on [32]. The tire's control, handling and stability characteristics are determined by the elastic behaviour of the tire in allowing the contact patch to move relative to the rim, along with the adhesion between the contact patch and the road surface.

For road-going vehicles, the designer would normally choose a radial-ply tire, since it can meet a wider range of service requirements when compared to bias- or cross-ply tires. For race cars, with their more narrowly-defined operating conditions, the designer has a choice of bias-ply and radial-ply tires [32].

For a given vehicle design, a tire must be selected to meet dimensional, load-carrying, limit-state performance, and economic requirements. An important dimensional consideration is the tire aspect ratio, which is the ratio of the height of the tire's cross-section to its width. For light vehicles, the trend is towards lower aspect ratio tires, because

cornering stability is improved. Judicious use of low aspect ratio tires yields a larger contact patch and space for larger brakes [32].

Ideally, a tire should be designed in parallel with the vehicle it is intended for [33]. This is only possible for an automobile manufacturer who is dealing with a tire manufacturer; in other cases existing tires must be used. Otherwise, it is difficult to obtain very detailed tire data. Tire companies are reluctant to release information which could be of use to their competitors.

For the purposes of this thesis, the Pacejka sinusoidal model will be used. The Pacejka model was described in section 1.2.1 [13]. It is a steady-state model which features four coefficients that describe the tire's cornering stiffness, peak force, and curvature. The Pacejka tire formulas used in this work calculate side force and self aligning torque. The variables used in the formulas are normal load, slip angle, and camber angle. The advantages of this model in comparison to the polynomial model mentioned in the previous chapter are that camber effects can be modelled, and that more accurate representation of tire forces and moments are provided. The disadvantage of this model is that only one type of tire is modelled. The side force and self aligning torque versus slip angle characteristics of the Pacejka tire model can be seen in Figures 2.3 and 2.4. Camber change characteristics are seen in Figures 2.5 and 2.6.

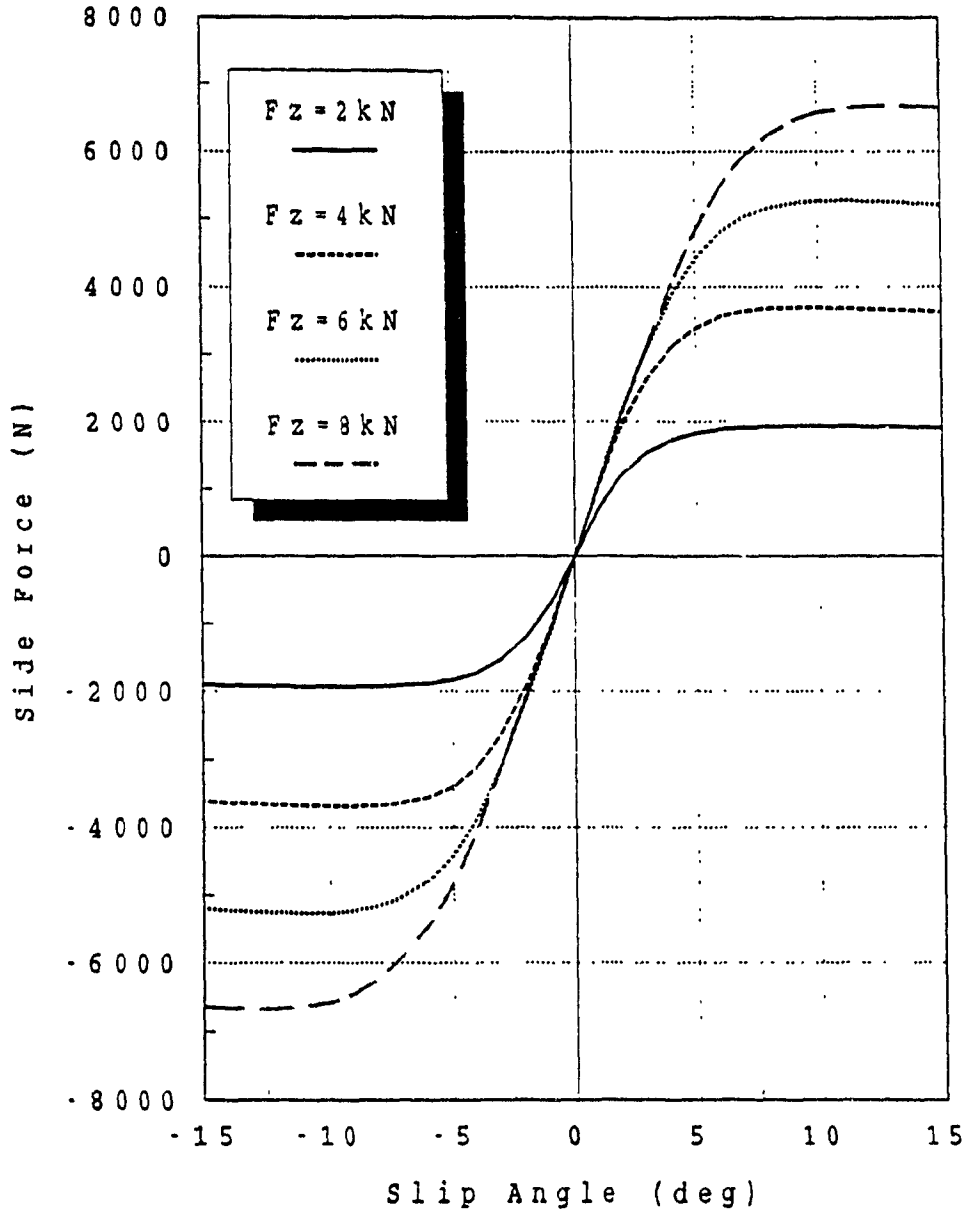

Fig. 2.3 Pacejka Sinusoidal Tire Side Force vs. Slip Angle at Zero Camber Angle [13]

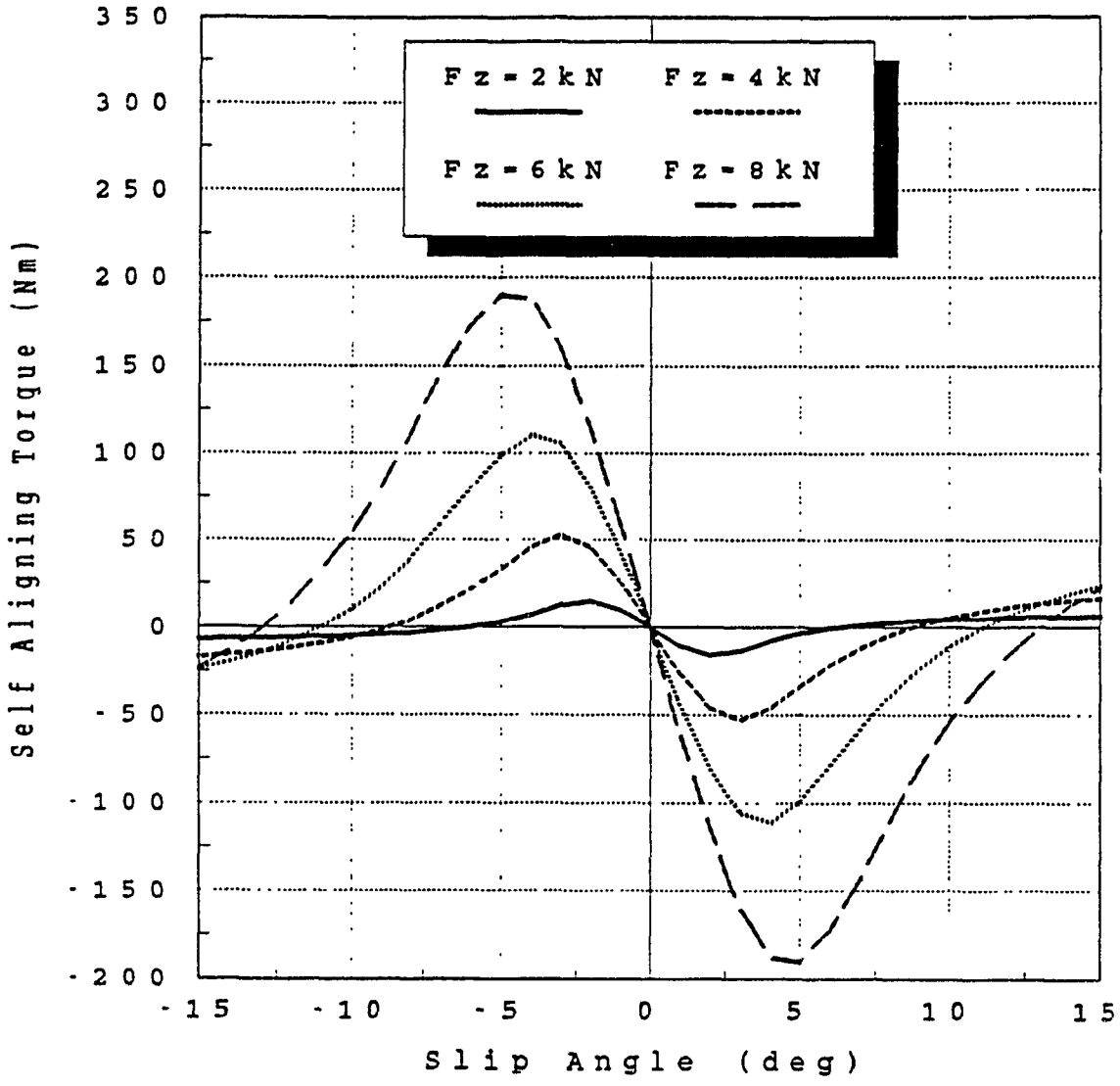

Fig. 2.4 Pacejka Sinusoidal Tire Self Aligning Torque vs. Slip Angle at Zero Camber Angle [13]

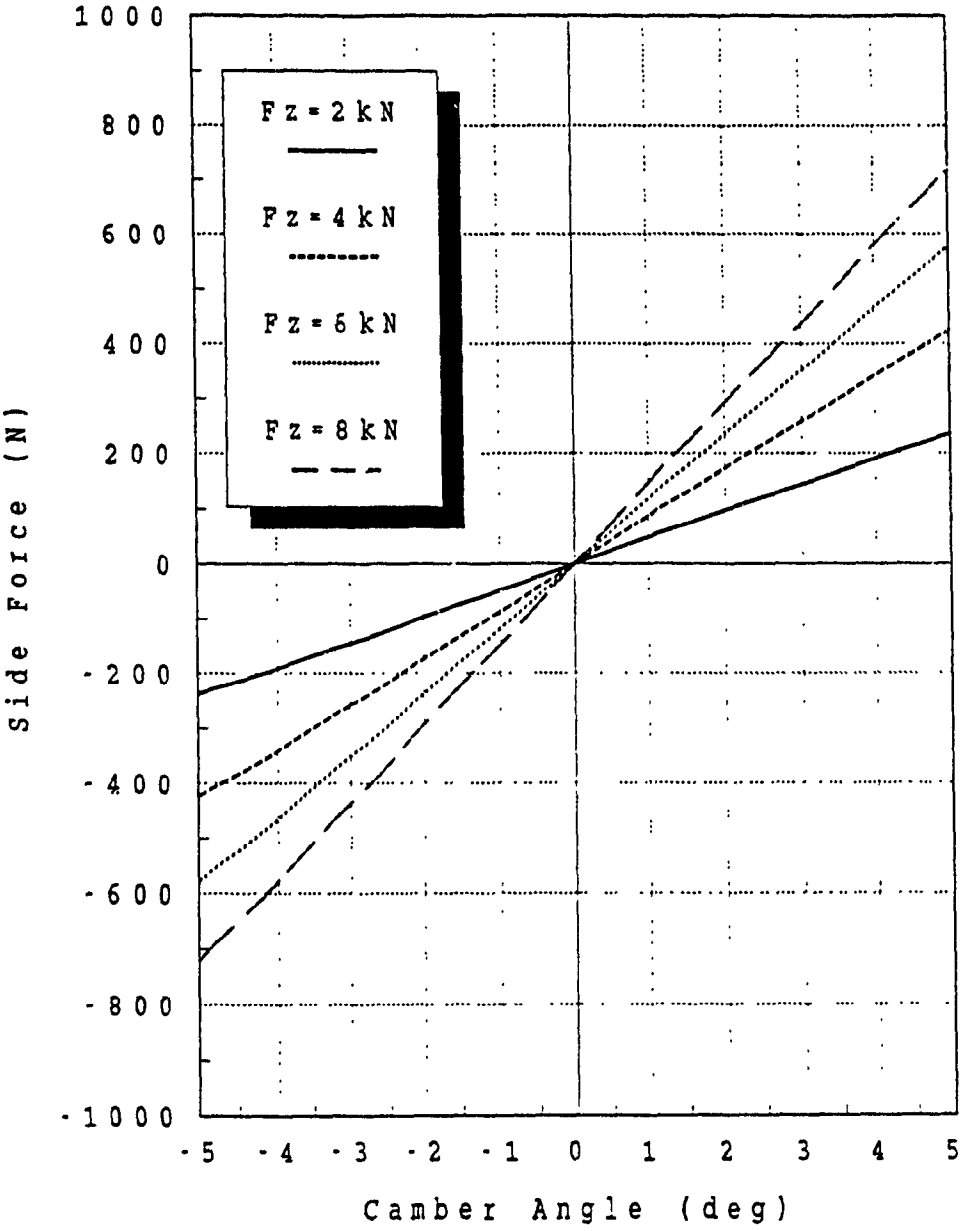

Fig. 2.5 Pacejka Sinusoidal Tire Side Force vs. Camber Angle at Zero Slip Angle [13]

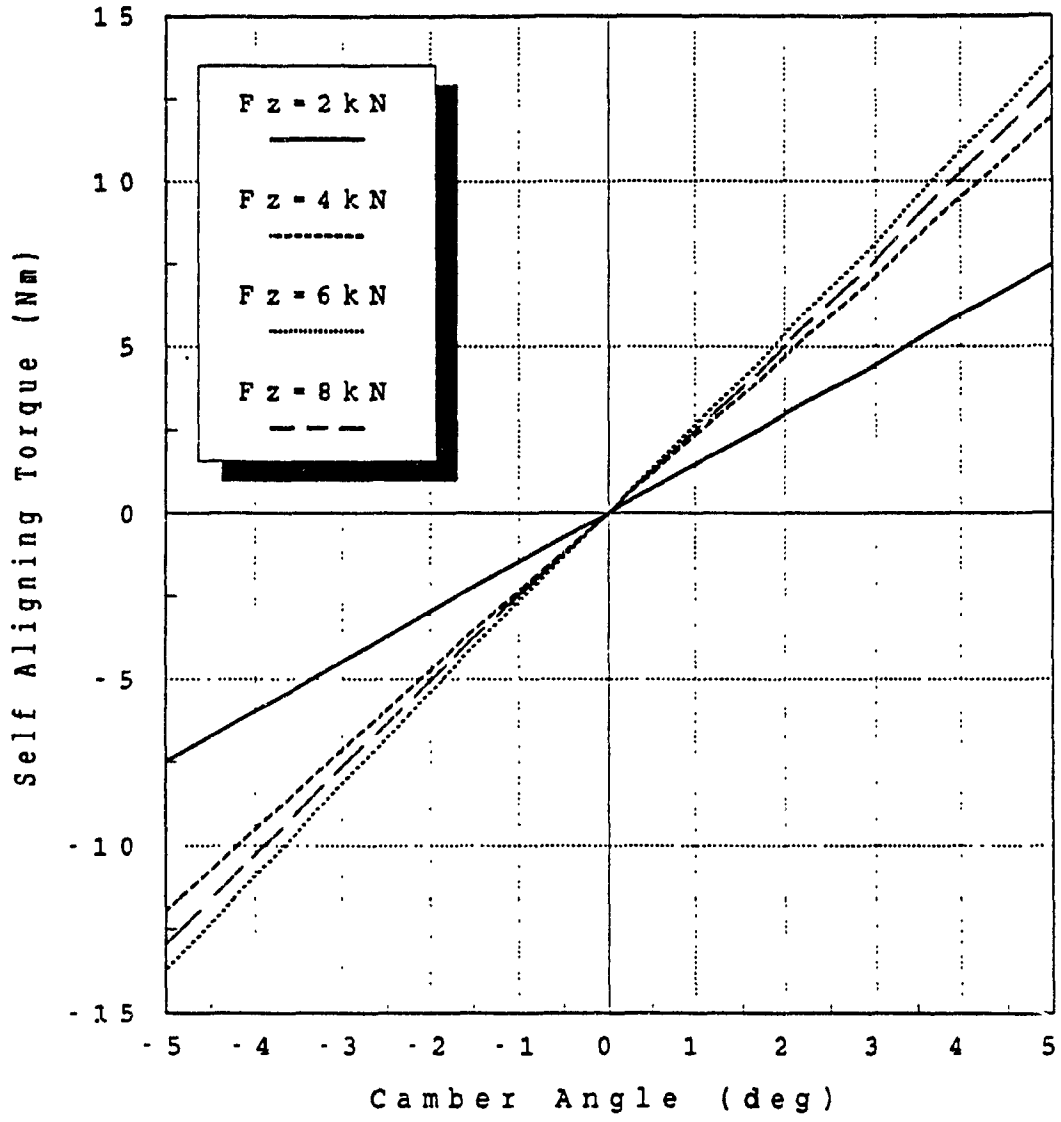

Fig. 2.6 Pacejka Sinusoidal Tire Self Aligning Torque vs. Camber Angle at Zero Slip Angle [13]

2.4 Springs

The spring portion of the pullrod suspension serves to store the energy of the moving wheel, transmitted by the pullrod and rocker. The most common spring in current automotive use is the helical coil spring (Fig. 2.7). The advantages of the coil spring are compactness, good material utilization, no wear, and no maintenance [32].

Before describing the spring stiffness selection process, the distinction between wheel rate and spring rate will be made. The SAE definition of spring rate is "the change of load of a spring per unit deflection, taken as a mean between loading and unloading at a specified load." Thus, spring rate refers to the force-deflection characteristics of a coil spring along its centerline. The SAE definition of wheel rate is "the change of wheel load, at the center of tire contact, per unit vertical displacement of the sprung mass relative to the wheel at a specified load" [35].

This distinction is made because of the design sequence. This design procedure uses the work of Thompson [36], who developed equations for the optimum spring and damper rates in passive car suspensions. These equations are based on the minimisation of the mean-squared tire forces or deflections on random roads (white noise) and take into account the body inertial coupling ratio $DI=i^2/ab$. Fig. 2.8 shows the 4DOF half-car model used; the pitch and bounce modes are modelled, and both unsprung masses vibrate vertically on the tires [36].

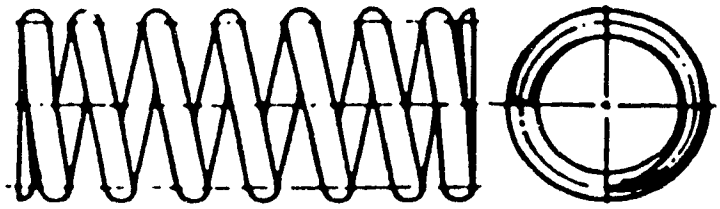

Fig. 2.7a Helical Coil Spring With Closed and Ground Ends (Race Car Applications) [34]

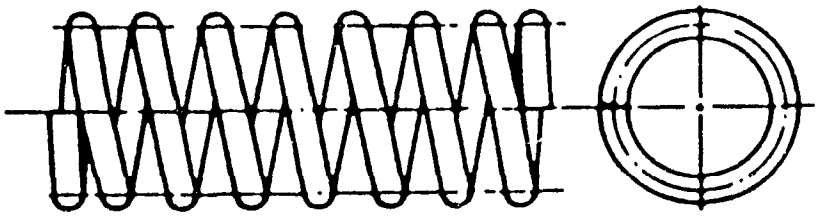

Fig. 2.7b Helical Coil Spring With Closed Ends (Passenger Car Applications) [34]

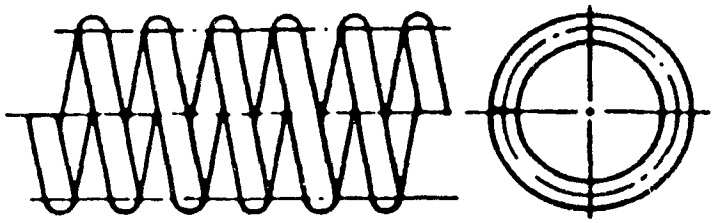

Fig. 2.7c Helical Coil Spring With Plain Ends (Passenger Car Applications) [34]

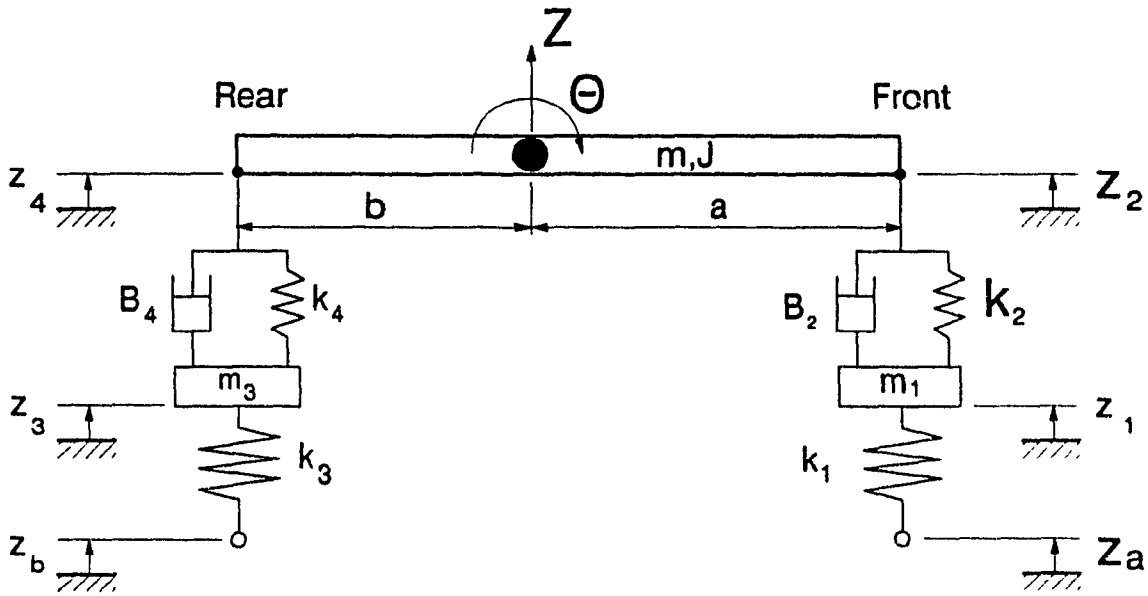

Fig. 2.8 4DOF Half Car Model [36]

The first step is to determine the equivalent front and rear dynamic body masses m_2 and m_4 [36]:

$$m_2 = \frac{DIm}{DI + (a/b)} \tag{2.1}$$

$$m_4 = \frac{DIm}{DI + (b/a)} \tag{2.2}$$

The wheel rates are then tuned according to the tire radial rates [36]:

$$k_2 = \frac{k_1 m_1 m_2}{(m_1 + m_2)^2} \tag{2.3}$$

$$k_1 = \frac{k_3 m_3 m_4}{(m_3 + m_4)^2} \tag{2.4}$$

It is important to note that the roll stiffness of each axle is the sum of the roll stiffness due to the suspension springs and of that provided by the anti-roll bar. The relative roll stiffness of the front and rear axles has a fundamental effect on the handling and stability of the vehicle, by apportioning the roll moment-induced weight transfer. Thus the spring-induced roll stiffness must be considered as part of the total roll stiffness.

2.5 Dampers

The energy stored in the suspension spring must be dissipated in order to avoid sustained oscillations. This is accomplished by a damper or shock absorber (Fig. 2.9). The damper dissipates energy in the form of heat by forcing oil through a series of orifices; heat being dissipated by convection. The damper shown in Fig. 2.9 is of the De Carbon type; this is a single-tube damper with a charged accumulator which accommodates the changes in oil volume over both stroke directions, and reduces the likelihood of cavitation. Variations of this basic design, with adjustability for different piston speeds, form the state-of-the-art in passive dampers [38].

Damper rates may be selected according to driver assessments, or through simulations. It may be advantageous to tune the dampers for a specific section of roadway such as an area of heavy braking or a bumpy corner leading onto a straight. This would require the measurement of vertical inputs at the wheels for the particular stretch of roadway. One possible simulation approach would be to assume a random road and to minimize the mean-squared tire forces, using the reference [36] of Thompson as in section 2.4. Equations are presented for the damper rate, taken at the wheel. Linkage kinematics must still be considered before the damper rate itself can be obtained.

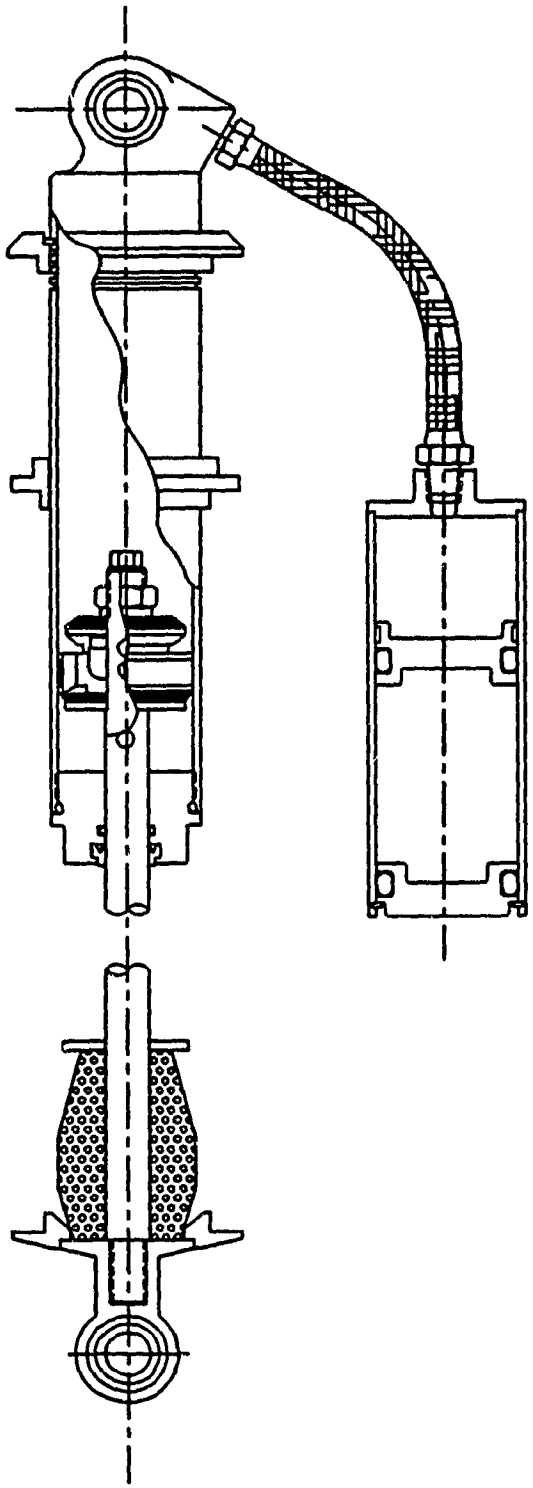

Fig. 2.9 De Carbon Damper [37].

The optimum linear damping rates are given by [36]:

$$B_2 = \sqrt{k_1 m_1 \left[\left(\frac{m_2}{m_2 + m_1} - \frac{k_2}{k_1} \right)^2 + \frac{m_2}{m_1} \left(\frac{k_2}{k_1} \right)^2 \right]} \qquad (2.5)$$

$$B_4 = \sqrt{k_3 m_3 \left[\left(\frac{m_4}{m_4 + m_3} - \frac{k_4}{k_3} \right)^2 + \frac{m_4}{m_3} \left(\frac{k_4}{k_3} \right)^2 \right]} \qquad (2.6)$$

Since the physical damper shown in Fig. 2.9 is a non-linear device, the linear damper rates B_2 and B_4 do not apply directly.

2.6 Anti-Roll Bars

The anti-roll bar is a spring device used to add roll stiffness, control the sprung mass roll angle and alter the front/rear roll stiffness distribution, thus changing the vehicle's handling and stability. Fig. 2.10 illustrates a typical anti-roll bar installation.

The anti-roll bar configuration is limited only by the designer's imagination. A typical anti-roll bar, however, consists of a torsion bar mounted laterally on the vehicle chassis. The bar has cranked ends that are connected to the suspension A-arms or to the hub carriers, either directly or by intermediate links. The torsion bar is mounted to the chassis by revolute bearings, so that the vehicle is free in bounce or pitch and will receive roll resistance from the bar

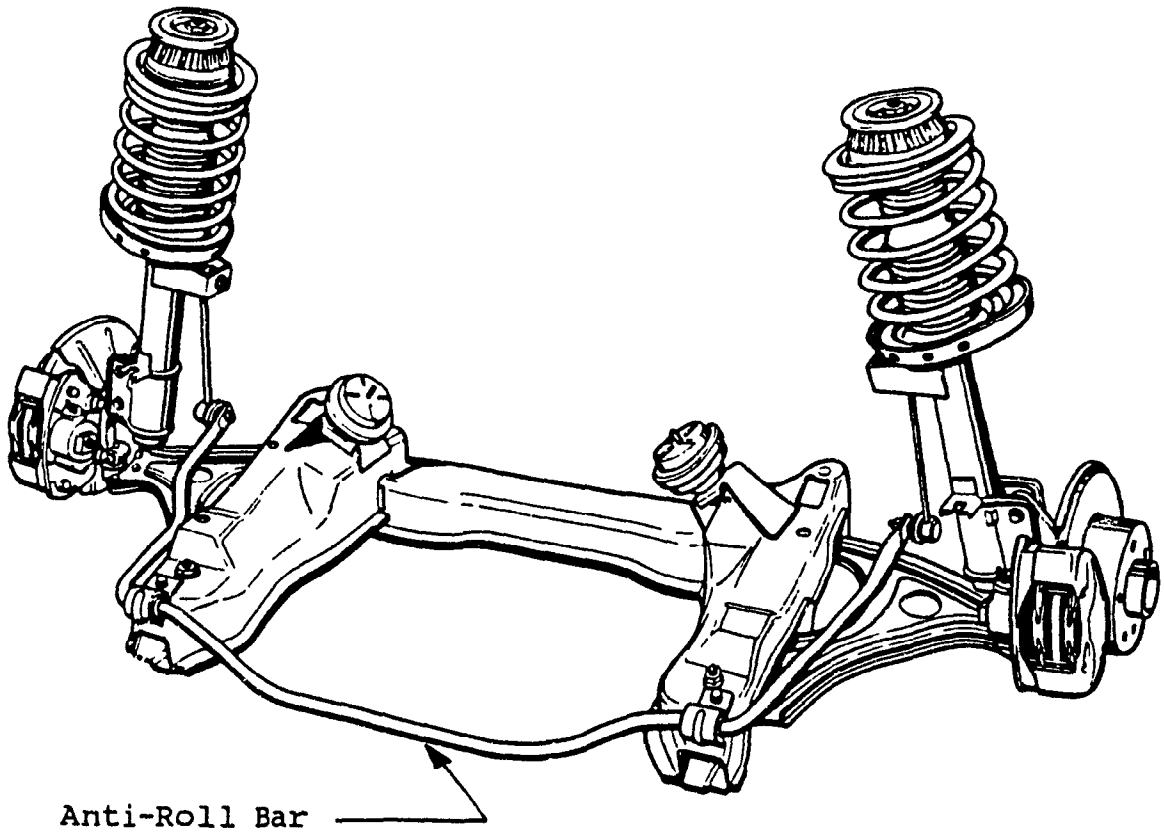

Fig. 2.10 Typical Anti-Roll Bar Installation on MacPherson Front Suspension [39]

only when there is relative motion between the left and right suspension systems.

Depending on the vehicle design, an anti-roll bar may be used on only one of the two axles. However, on high-quality passenger cars and competition cars, anti-roll bars are usually used on both the front and the rear axles [40].

2.7 Summary

In this chapter, the vehicle suspension system components are described. The qualitative effect of each component on vehicle handling has been discussed. Selection methods based on analytical techniques presented in the literature were presented for the tires, springs and dampers.

CHAPTER 3

Vehicle Handling and Stability: Mathematical Modeling, Analysis, and Design Synthesis

3.1 General

This chapter describes the various steps involved in the design synthesis of a vehicle with pullrod A-arm suspension linkages. From the point of view of vehicle handling, each step of the procedure is described in detail.

In the previous chapter, the physical components which comprise the vehicle system are described. These components are the tires, suspension linkages, springs, dampers, and anti-roll bars. They are connected together by the vehicle chassis, which has dimensional properties (wheelbase) as well as inertial properties (mass, C.G. position, moments and products of inertia).

The various steps involved in the design synthesis are:

1. Mathematical modeling of the vehicle motion for investigations into the vehicle dynamics behaviour (vehicle handling and stability).
2. Analysis to evaluate the vehicle dynamic response and stability for both steady-state and transient motions for steering inputs.
3. Kinematic and kineto-static analysis of suspension linkages and its implementation in the vehicle dynamics analysis.

4. A sequential design synthesis procedure which includes the aforementioned three steps in its scheme.

The first two steps involving vehicle dynamic analysis for handling and stability are outlined in Section (3.2). Steps 3 and 4 are described in Sections (3.3) and (3.4), respectively.

The MATLAB language is used to perform the computations of the vehicle design synthesis. MATLAB is an interactive computer-aided engineering language whose basic data element is an automatically-dimensioned matrix. Many matrix math and numerical problem-solving methods are intrinsic functions in MATLAB, and other solutions can be easily and quickly added in subroutine form. The graphics capabilities of MATLAB allow rapid and clear interpretation of results [41].

Figure 3.1 depicts the procedure for vehicle design synthesis. The required inputs are the vehicle inertial properties, the wheelbase, the initial positions of the dependent variables for the front and rear suspension linkages, the constants for the front and rear suspension linkages, the initial and final positions of the independent linkage variables, the lower and upper bounds of the percent CG position, a/L%, the estimated front and rear roll center heights and roll stiffnesses, the front and rear tire characteristics, and the performance criteria.

Next the center of gravity position is estimated. This calculation is made using the initial estimate of front and rear roll center heights and roll stiffnesses. The CG estimate is used to compute the sprung mass distribution in preparation for the calculation of the front and rear chassis spring rates.

The next step is to select the data for the front axle. The front chassis spring rate is computed. The linkage data and chassis spring rates are transferred to the kineto-static analysis, where incremental lateral forces are applied to the center of gravity, up to the rollover threshold. As a result, the linkage-induced nonlinearities of roll center heights and roll stiffness are tabulated. This procedure to obtain the nonlinear roll center heights and roll stiffness is repeated for the rear axle.

The roll center heights and roll stiffness nonlinearity tables are transferred to a second CG-finding iteration, to verify or modify the center of gravity position. Finally, the nonlinear dynamic analysis of the vehicle is carried out. In this step, the transient response is found and the steady-state response as estimated in the CG-finding procedure can be verified. If the vehicle's response meets the performance requirement, the vehicle layout is frozen, otherwise another design iteration is needed. The next section will define the 3DOF mathematical model of the vehicle in preparation for the detailed description of "vehicle design for handling".

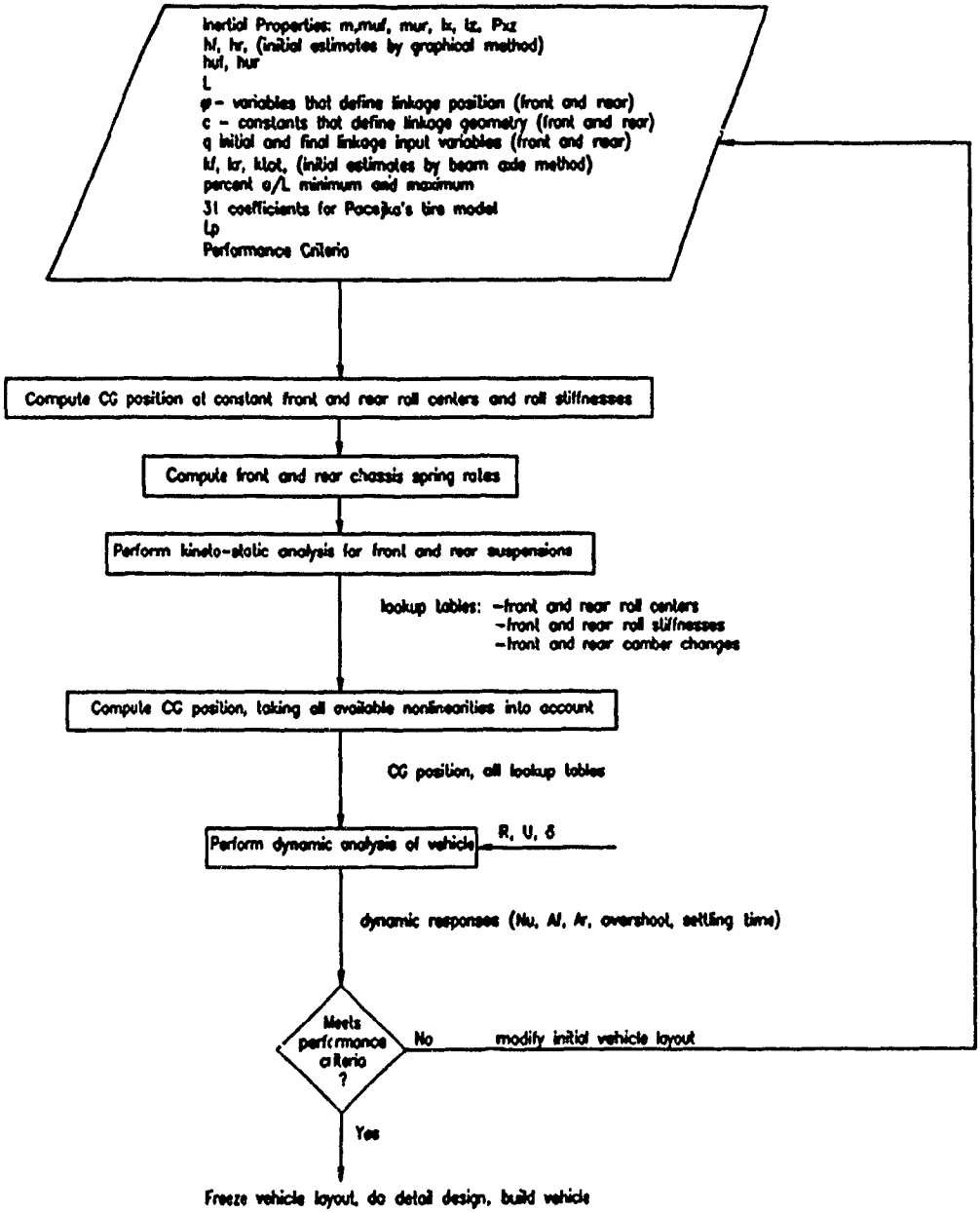

Fig. 3.1 Schematic of the Design Synthesis Procedure

3.2 A 3DOF Mathematical Vehicle Dynamic Model

3.2.1 Vehicle Axis System and Basic Configuration

The simulations performed in this thesis use a 3DOF nonlinear model of a vehicle with provision for sprung mass roll. Tire and suspension linkage nonlinearities are included. The equations of motion are based on a fixed control vehicle travelling on a smooth, level road. It is assumed that a fixed-control vehicle which travels on a smooth, level road at a constant forward speed will not experience bouncing and pitching movements. Thus the available vehicle motions will be yaw, sideslip, and sprung mass roll.

Fig. 3.2 depicts the directional control axis system of a 3DOF vehicle. Fig. 3.3 shows the tire axis system. The SAE axis convention system according to SAE J670e is used [35].

Neglecting camber steer and roll steer effects, the front and rear slip angles are [15]:

$$\alpha_f = \delta - \frac{V + ar}{U}$$
$$\alpha_r = \frac{br - V}{U} \qquad (3.1)$$

Consider now the case of a vehicle moving forward with constant U, with a constant sideslip velocity V in the negative direction, and without yaw velocity. According to the rear slip angle equation, the slip angle on the left rear tire will have positive magnitude.

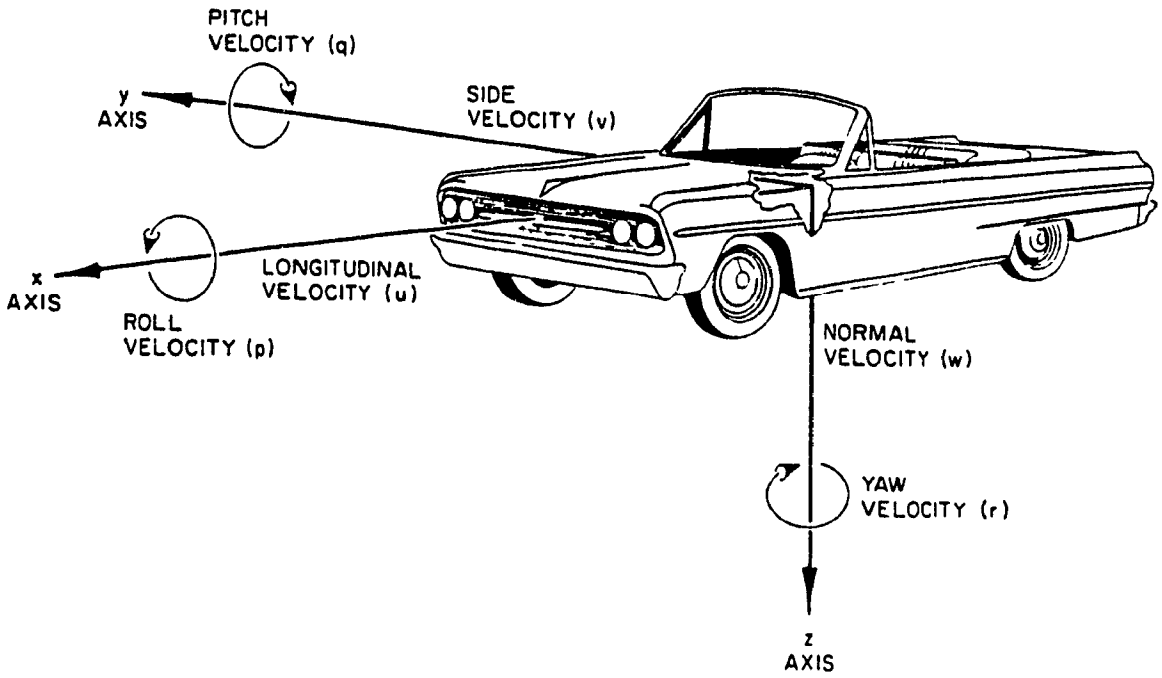

Fig. 3.2 SAE Vehicle Axis System [35]

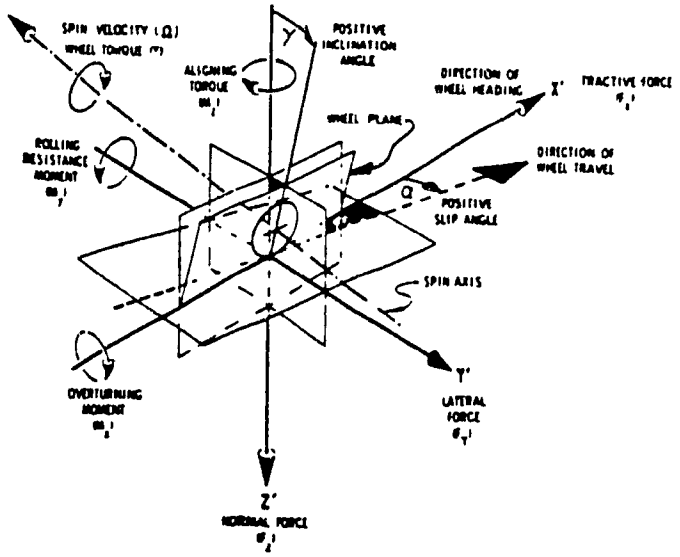

Fig. 3.3 SAE Tire Axis System [35]

From Fig. 3.3, this will create a lateral tire force in the positive direction, balancing the inertia force in the negative direction.

Now suppose that the left rear tire has a camber angle such that its top is inclined in towards the center of the chassis. Such a camber angle would commonly be considered a negative camber angle in the jargon of the automotive field. However, the SAE sign convention for camber angle is as shown in Fig. 3.3. According to SAE convention, positive camber angle provides an additional tire force in the positive Y direction. This is in agreement with the prevalent tire theory which states that a tire that is cambered towards the direction of its side force will have a small additional side force of the same sense [42].

In summary, the SAE vehicle and tire sign conventions as shown in Figs. 3.2 and 3.3 must be precisely followed in order to attain a correct mathematical vehicle simulation.

3.2.2 Equations of Motion

Fig. 3.4 shows the forces at the tires when slip angles are impressed on them. Fig. 3.5 shows the roll axis and pitch plane representations of a vehicle. The tire forces in the ground plane ultimately create a vehicle side force and yawing moment. Roll moments due to roll displacement and roll

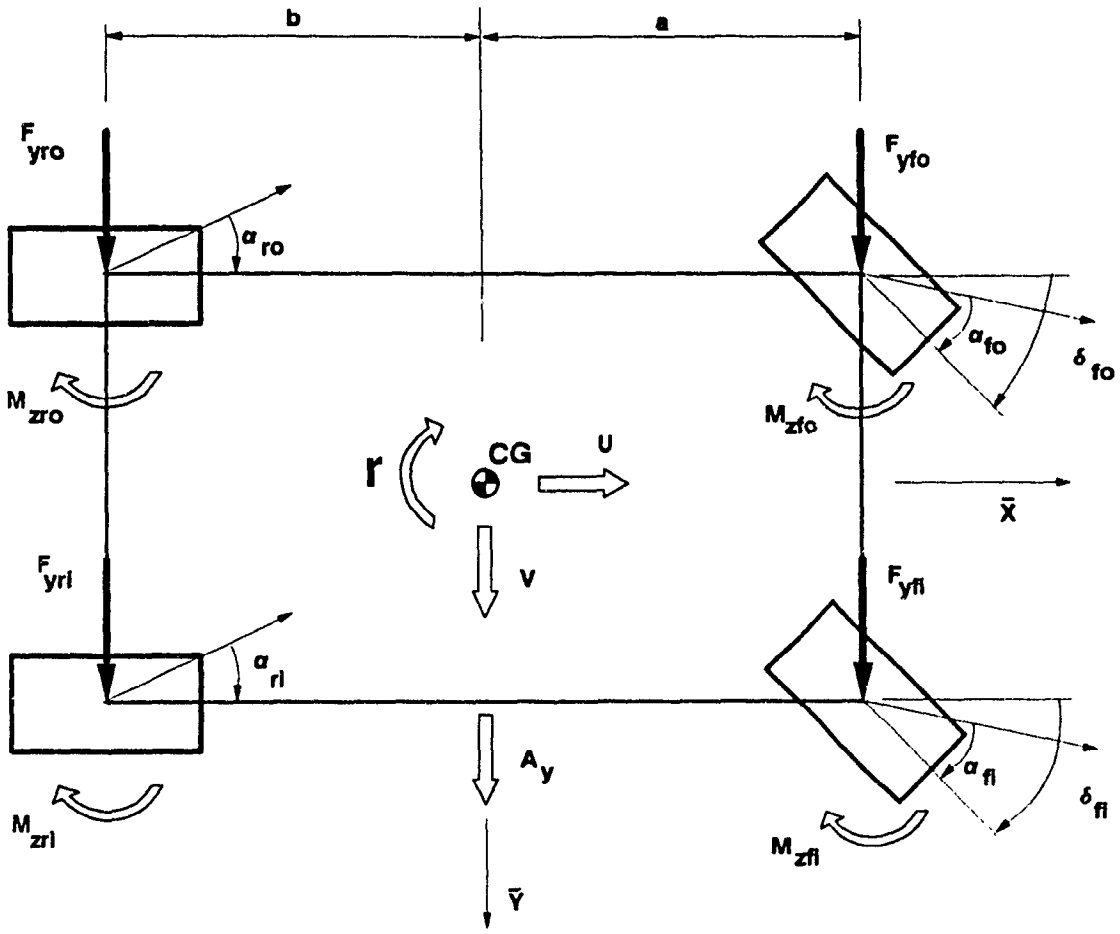

Fig. 3.4 Vehicle Yaw Plane With Tire Forces and Moments

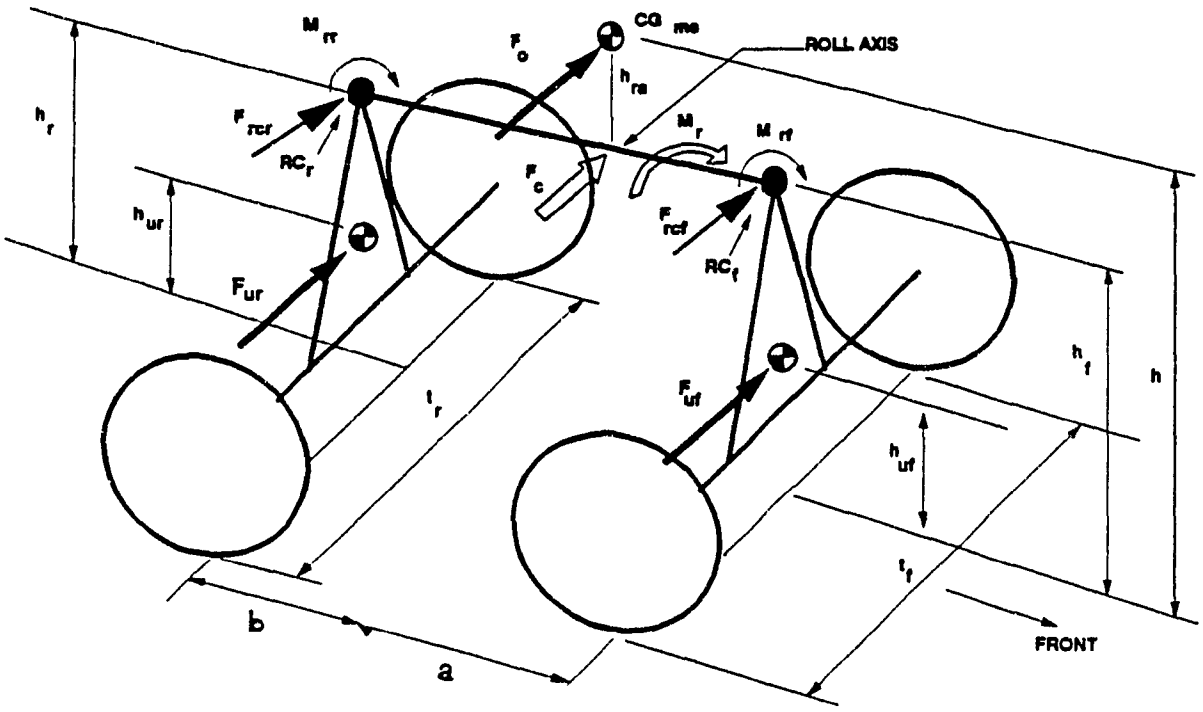

Fig. 3.5a Roll Axis Representation of Vehicle

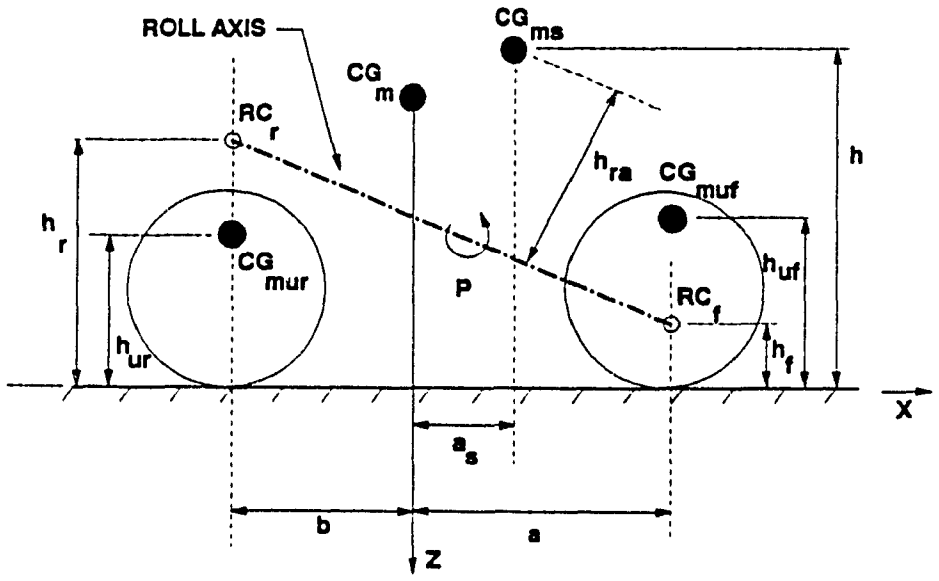

Fig. 3.5b Pitch Plane Representation of Vehicle

velocity add to the forces imparted by the tires. These roll moments are produced by the suspension roll stiffnesses and by the dampers. Forces and moments are combined, and the following equations are written in Newton-Euler form, in a non-inertial reference system:

Side Forces

$$\Sigma Y - m(\dot{V}+Ur) + m_s h_{ra}\dot{p}$$

Yawing Moment

$$\Sigma N - I_z\dot{r} - P_{xz}\dot{p} - P_{yz}pr - P_{xy}p^2 + (M_s a_s + M_{uf}a - M_{ur}b)(\dot{V}+Ur) \qquad (3.2)$$

Rolling Moment for Sprung Mass

$$\Sigma L_s - I_x\dot{p} - P_{xz}\dot{r} - P_{xy}pr + I_{yz}r^2 + m_s h_{ra}(\dot{V}+Ur)$$

where ΣY, ΣN, and ΣL_s are external forces and moments.

The following assumptions simplify the equations:

(1) The terms $P_{yz}pr$ and $P_{xy}p^2$ are negligible.

(2) The vehicle is symmetrical about the x-z plane, therefore $P_{xz}=0$.

(3) Distance a_s is negligible (i.e. the projections of the sprung mass C.G. and vehicle C.G. on the X-Y plane coincide).

(4) $m_{uf}a = m_{ur}b$.

The equations (3.2) are rewritten as follows:

$$\begin{aligned} &\Sigma Y - m(\dot{V}+Ur) + m_s h_{ra}\dot{p} \\ &\Sigma N - I_z\dot{r} \\ &\Sigma L - I_x\dot{p} + m_s h_{ra}(\dot{V}+Ur) \end{aligned} \qquad (3.3)$$

3.2.3 External Forces and Moments

The external cornering forces, yaw moments, and sprung mass roll moments are now described in detail. The Pacejka sinusoidal tire model provides tire lateral forces and self aligning torques as a function of normal load, slip angle, and camber angle, as seen in Figs. 2.3 - 2.6. The tire side force and self-aligning torque formulae for Pacejka's sinusoidal model follow [13]:

SIDE FORCE:

$$F_y = D\sin(C\arctan(B\phi)) + \Delta S_v$$

where

$$\begin{aligned}
\phi &= (1-E)(\alpha+\Delta S_h) + (E/B)\arctan(B(\alpha+\Delta S_h)) \\
D &= a_1F_z^2 + a_2F_z \\
C &= 1.30 \\
B &= \left(\frac{a_3\sin(a_4\arctan(a_5F_z))}{CD}\right)(1-a_{12}|\gamma|) \\
E &= a_6F_z^2 + a_7F_z + a_8 \\
\Delta S_h &= a_9\gamma \\
\Delta S_v &= (a_{10}F_z^2 + a_{11}F_z)\gamma
\end{aligned}$$

SELF ALIGNING TORQUE: (3.4)

$$M_z = D\sin(C\arctan(B\phi)) + \Delta S_v$$

where

$$\begin{aligned}
\phi &= (1-E)(\alpha+\Delta S_h) + (E/B)\arctan(B(\alpha+\Delta S_h)) \\
D &= a_1F_z^2 + a_2F_z \\
C &= 2.40 \\
B &= \left(\frac{a_3F_z^2 + a_4F_z}{CDe^{a_5F_z}}\right)(1-a_{12}|\gamma|) \\
E &= \frac{(a_6F_z^2 + a_7F_z + a_8)}{(1-a_{13}|\gamma|)} \\
\Delta S_h &= a_9\gamma \\
\Delta S_v &= (a_{10}F_z^2 + a_{11}F_z)\gamma
\end{aligned}$$

where a's are coefficients listed in Table 3.1.

TABLE 3.1a

Coefficients for tire formula (with load influence)

F_z(kN)

	a_1	a_2	a_3	a_4
F_y	-22.1	1011	1078	1.82
M_z	-21.3	1144	49.6	226

TABLE 3.1b

Coefficients for tire formula (with load influence)

F_z(kN)

	a_5	a_6	a_7	a_8
F_y	0.208	0.000	-0.354	0.707
M_z	0.069	-0.006	0.056	0.486

TABLE 3.1c

Coefficients for tire formula (with camber influence)

γ(deg.)

	a_9	a_{10}	a_{11}	a_{12}	a_{13}
F_y	0.028	0.000	14.8	0.022	0.000
M_z	0.015	-0.066	0.945	0.030	0.070

Applying equation (3.4) the external forces and moments are written from Figs. 3.4 and 3.5 as follows:

$$\begin{aligned} \Sigma Y &= F_{yfo}+F_{yfi}+F_{yro}+F_{yri} \\ \Sigma N &= a(F_{yfo}+F_{yfi})-b(F_{yro}+F_{yri})+M_{zfo}+M_{zfi}+M_{zro}+M_{zri} \\ \Sigma L_s &= (m_s g h_{ra}-k_{tot})\theta - L_p p \end{aligned} \quad (3.5)$$

3.2.4 Lateral Weight Transfer

During cornering, normal load is transferred laterally from the inside tires to the outside tires. The total magnitude of the lateral weight transfer depends solely on the CG height, track width, and mass of the vehicle. Adding a suspension system to the vehicle will not change the total lateral weight transfer. However, the suspension will influence the distribution of the total lateral weight transfer between the front and rear axles. This distribution affects the generation of tire cornering forces, and therefore the vehicle's stability is influenced.

Total lateral weight transfer is a sum of the weight transfer due to body roll, due to roll center height and sprung mass inertia force, and due to the inertia force of the unsprung masses [15].

$$\begin{aligned} W_{tf} &= W_{brf}+W_{rcf}+W_{uf} \\ W_{tr} &= W_{brr}+W_{rcr}+W_{ur} \end{aligned} \quad (3.6)$$

The weight transfer due to body roll is now calculated for the front and rear axles [15]:

$$W_{brf} = m_s A_y h_{ra} \cos\theta \frac{k_f}{k_{tot}} \frac{1}{t_f}$$
$$W_{brr} = m_s A_y h_{ra} \cos\theta \frac{k_r}{k_{tot}} \frac{1}{t_r} \qquad (3.7)$$

The weight transfer due to the sprung mass inertia force is applied at the front and rear roll centers as follows:

$$W_{rcf} = m_s A_y \frac{b}{L} \frac{h_f}{t_f}$$
$$W_{rcr} = m_s A_y \frac{a}{L} \frac{h_r}{t_r} \qquad (3.8)$$

The third component of the lateral weight transfer is due to the inertia forces of the unsprung masses:

$$W_{uf} = m_{uf} A_y \frac{h_{uf}}{t_f}$$
$$W_{ur} = m_{ur} A_y \frac{h_{ur}}{t_r} \qquad (3.9)$$

For small roll angles, and when the front and rear track widths are similar, the phenomenon of lateral weight transfer is classified in two ways: first, the total magnitude of weight transfer, determined solely by track width, vehicle mass and CG height; secondly, the proportional distribution of the total weight transfer between the front and rear axles.

The height dimension h affects the total lateral weight transfer. Raising the center of gravity (increasing h) will increase the total lateral weight transfer; lowering it does the opposite. Since the tires are sensitive to normal load, it is desired to keep the vehicle center of gravity as low as possible.

3.3 Kinematic and Kineto-Static Analysis of Suspension Linkages

This section will explain the kinematic and kineto-static analysis of suspension linkages used in the design synthesis scheme. The method of velocity coefficients [44] is used to analyze the A-arm pullrod linkage suspension as it undergoes large deflections. The application of the method of velocity coefficients solves the suspension linkage position, determines the rate of change of certain kinematic variables with respect to the suspension travel, characterizes the forces, and finds chassis spring rates, roll center heights and roll stiffnesses [44].

The mathematical definition of velocity coefficients will be given shortly. The basic idea of velocity coefficients is that they relate the independent variables of the suspension linkage (in the case of the pullrod suspension: bounce, roll and lateral sprung mass positions) to the dependent linkage variables (angles between revolute-jointed links, spring-damper unit compressed lengths, and tire carcass lateral displacements). The velocity coefficients are functions of position only and fully describe the instantaneous positions and velocities of all suspension links. The velocity coefficients are calculated for a particular position of the linkage, and must be recalculated for every instantaneous position [45].

When the sprung mass is placed in a certain bounce-roll-sideslip position, the kinematic analysis finds the position of the A-arms, the pullrod mechanism, and the tire contact patch. The kineto-static analysis finds the generalized forces created by the springs and dampers in the linkage for a given linkage position by equating the external and effective forces acting on the linkage.

The velocity coefficients solution used in this work is based on simplifications of the suspension system analysis software (GENKAD: GENeral purpose Kinematic Analysis and Design) presented in the Ph.D. thesis of Alanoly [44]. In the following sections the solution procedure is detailed.

3.3.1 Kinematic Solution

The pullrod suspension mechanism being solved has been described in section (2.2). All links, revolute and slider joints, and springs are identified in Figure 3.6. The position loop equations are of the form [45]:

$$f_i(\Omega_1, \Omega_2, \ldots, \Omega_n) = 0 \qquad (i = 1, 2, \ldots, m) \qquad (3.10)$$

where the set of Lagrangian coordinates is denoted by Ω_i . If the system has ℓ degrees of freedom, that many variables can be selected as generalized coordinates or inputs. The generalized coordinates are designated by $q_1, q_2, \ldots, q_\ell$. The rest of the coordinates are dependent variables of the set $\phi_1, \phi_2, \ldots, \phi_m$.

The equations (3.10) are then rewritten as:

$$f_i(\phi_1,\ldots,\phi_m;q_1,\ldots,q_j) = 0 \qquad (i=1,2,\ldots,m) \quad (3.11)$$

For kinematic position analysis, the independent variables q_i's are specified. The m algebraic equations (3.11) are then solved for the m unknown position variables $\phi_1,\phi_2,\ldots,\phi_m$ [45].

For the pullrod linkage in question, the independent loops, constants that define the geometry, c_i, dependent variables ϕ and independent variables q are shown in Fig. 3.6 and Table 3.1. Equations 3.12 are the loop-closure equations for the pullrod linkage and are as follows:

$$f_1 = c_5\cos(\phi_5) + c_7\cos(\phi_{10}) - c_6\cos(\phi_6) - c_4\cos(q_3 + c_{11}) = 0$$

$$f_2 = c_5\sin(\phi_5) + c_7\sin(\phi_{10}) - c_6\sin(\phi_6) - c_4\sin(q_3 + c_{11}) = 0$$

$$f_3 = \phi_3 + c_{10}\cos(c_1) - c_8\cos(\phi_{10} + c_{12}) - c_5\cos(\phi_5) - c_{22}\cos(q_3 + c_{27}) - q_1\cos(c_1) - (q_2 + c_9)\cos(c_2) = 0$$

$$f_4 = (q_2 + c_9)\sin(c_2) + c_{22}\sin(q_3 + c_{27}) + c_5\sin(\phi_5) + c_8\sin(\phi_{10} + c_{12}) + q_1\sin(c_1) - (\phi_3 + c_{10})\sin(c_1) = 0$$

$$f_5 = -(\phi_1 + c_{13})\cos(\phi_{11}) + c_{21}\cos(\phi_8 + c_{29}) + c_{19}\cos(\phi_7) - c_{20}\cos(\phi_6 + c_{31} - c_6\cos(\phi_6) + c_{14}\cos(q_3 + c_{15}) = 0$$

$$f_6 = -(\phi_1 + c_{13})\sin(\phi_{11}) + c_{21}\sin(\phi_8 + c_{29}) + c_{19}\sin(\phi_7) - c_{20}\sin(\phi_6 + c_{31} - c_6\sin(\phi_6) + c_{14}\sin(q_3 + c_{15}) = 0$$

$$f_7 = c_{17}\cos(q_3 + c_{16}) + c_{18}\cos(\phi_8) + (\phi_1 + c_{13})\cos(\phi_{11}) - c_{14}\cos(q_3 + c_{15}) - c_4\cos(c_{11} + q_3) = 0$$

$$f_8 = c_{17}\sin(q_3 + c_{16}) + c_{18}\sin(\phi_8) + (\phi_1 + c_{13})\sin(\phi_{11}) - c_{14}\sin(q_3 + c_{15}) - c_4\sin(c_{11} + q_3) = 0$$

...cont'd

$$f_9 = -c_7\cos(\phi_{16}) + c_6\cos(\phi_{13}) + c_4\cos(q_3 + c_{24}) - c_5\cos(\phi_9) = 0$$

$$f_{10} = -c_7\sin(\phi_{16}) + c_6\sin(\phi_{13}) + c_4\sin(q_3 + c_{24}) - c_5\sin(\phi_9) = 0$$

$$f_{11} = -(\phi_4 + c_{10})\cos(c_3) + (q_1)\cos(c_1) + c_{22}\cos(q_3 + c_{28}) + c_5\cos(\phi_9) + c_8\cos(\phi_{16} + c_{26}) + (q_2 + c_9)\cos(c_2) = 0$$

$$f_{12} = (q_2 + c_9)\sin(c_2) + c_{22}\sin(q_3 + c_{28}) + c_5\sin(\phi_9) + c_8\sin(\phi_{16} + c_{26}) + q_1\sin(c_1) - (\phi_4 + c_{10})\sin(c_3) = 0$$

$$f_{13} = -(\phi_2 + c_{13})\cos(\phi_{12}) + c_{21}\cos(\phi_{15} + c_{30}) + c_{19}\cos(\phi_{14}) - c_{20}\cos(\phi_{13} + c_{32}) - c_6\cos(\phi_{13}) + c_{14}\cos(q_3 + c_{25}) = 0$$

$$f_{14} = -(\phi_2 + c_{13})\sin(\phi_{12}) + c_{21}\sin(\phi_{15} + c_{30}) + c_{19}\sin(\phi_{14}) - c_{20}\sin(\phi_{13} + c_{32}) - c_6\sin(\phi_{13}) + c_{14}\sin(q_3 + c_{25}) = 0$$

$$f_{15} = -c_4\cos(q_3 + c_{24}) + c_{17}\cos(q_3 + c_{23}) + c_{18}\cos(\phi_{15}) + (\phi_2 + c_{13})\cos(\phi_{12}) - c_{14}\cos(q_3 + c_{25}) = 0$$

$$f_{16} = -c_4\sin(q_3 + c_{24}) + c_{17}\sin(q_3 + c_{23}) + c_{18}\sin(\phi_{15}) + (\phi_2 + c_{13})\sin(\phi_{12}) - c_{14}\sin(q_3 + c_{25}) = 0$$

(3.12)

LEGEND:
DOT = REVOLUTE JOINT
ARC = RIGID CONNECTION
SQUARE = EDGE NUMBER
ARROW = EDGE DIRECTION
PARALLEL LINES = SLIDER JOINT
DOTTED LINES = IMAGINARY LINKS

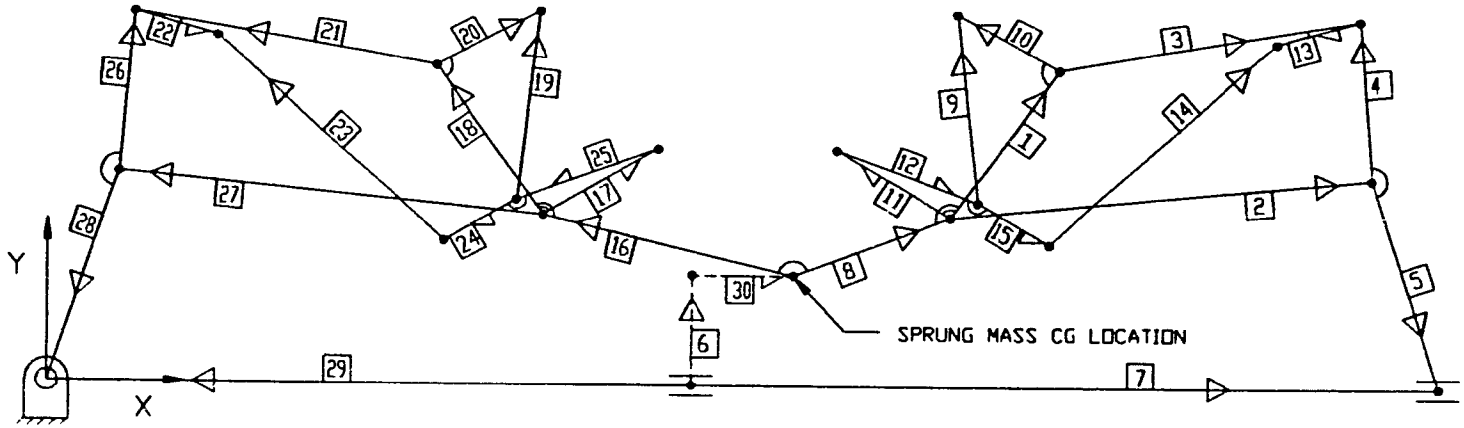

FIG. 3.6 PLANAR PULLROD SUSPENSION LINKAGE: EDGE AND LOOP SCHEMATIC

TABLE 3.1 - Pullrod Linkage Constants and Variables

EDGE #	length variable	length constant	angle variable	angle constant
1	0	c_4	q_3	c_{11}
2	0	c_5	ϕ_5	0
3	0	c_6	ϕ_6	0
4	0	c_7	ϕ_{10}	c_{31}
5	0	c_8	ϕ_{10}	c_{12}
6	q_2	c_9	0	c_2
7	ϕ_3	c_{10}	0	c_1
8	0	c_{22}	q_3	c_{27}
9	$\dot{\psi}_1$	c_{13}	ϕ_{11}	0
10	0	c_{14}	q_3	c_{15}
11	0	c_{17}	q_3	c_{16}
12	0	c_{18}	ϕ_8	0
13	0	c_{20}	ϕ_6	c_{31}
14	0	c_{19}	ϕ_7	0
15	0	c_{21}	ϕ_8	c_{29}
16	0	c_{22}	q_3	c_{28}
17	0	c_{17}	q_3	c_{23}
18	0	c_4	q_3	c_{24}
19	ϕ_2	c_{13}	ϕ_{12}	0
20	0	c_{14}	q_3	c_{25}
21	0	c_6	ϕ_{13}	0
22	0	c_{20}	ϕ_{13}	c_{32}
23	0	c_{19}	ϕ_{14}	0
24	0	c_{21}	ϕ_{15}	c_{30}
25	0	c_{18}	ϕ_{15}	0
26	0	c_7	ϕ_{16}	0
27	0	c_5	ϕ_9	0
28	0	c_8	ϕ_{16}	c_{26}
29	ϕ_4	c_{10}	0	c_3
30	q_1	0	0	c_1

The loop-closure equations are solved for the unknown solution vector ϕ as follows (see also flowchart Fig. 3.7):

1. An estimate of the linkage solution vector is made. The initial estimate of the solution vector is denoted by ϕ^i.
2. Evaluate the m×m Jacobian matrix **A** for the values ϕ^i.

$$\mathbf{A} = [A_{ij}] = \left[\frac{\partial f_i}{\partial \phi_j}\right] \qquad \begin{matrix} i=1,m \\ j=1,1 \end{matrix} \qquad (3.13)$$

3. Evaluate the residual vector $\mathbf{f}^i$ at the point $\phi = \phi^i$.
4. Solve the correction vector $\Delta\phi$ using the Newton-Raphson algorithm which gives the linear equation

$$\Delta\phi^i = -\mathbf{A}^{-1}\mathbf{f}^i \qquad (3.14)$$

5. Make an improved estimate ϕ^{i+1} of the solution vector of the form

$$\phi^{i+1} = \phi^i + \Delta\phi^i \qquad (3.15)$$

6. Check the soundness of estimated solution ϕ^{i+1} by checking the residual vector; if $|\mathbf{f}^{i+1}-\mathbf{f}^i|$ is within a desired tolerance ftol, the new linkage position has been found, otherwise continue iterating.

$$|f_{i+1} - f_i| \le ftol \qquad (i = 1,2,\ldots,m) \qquad (3.16)$$

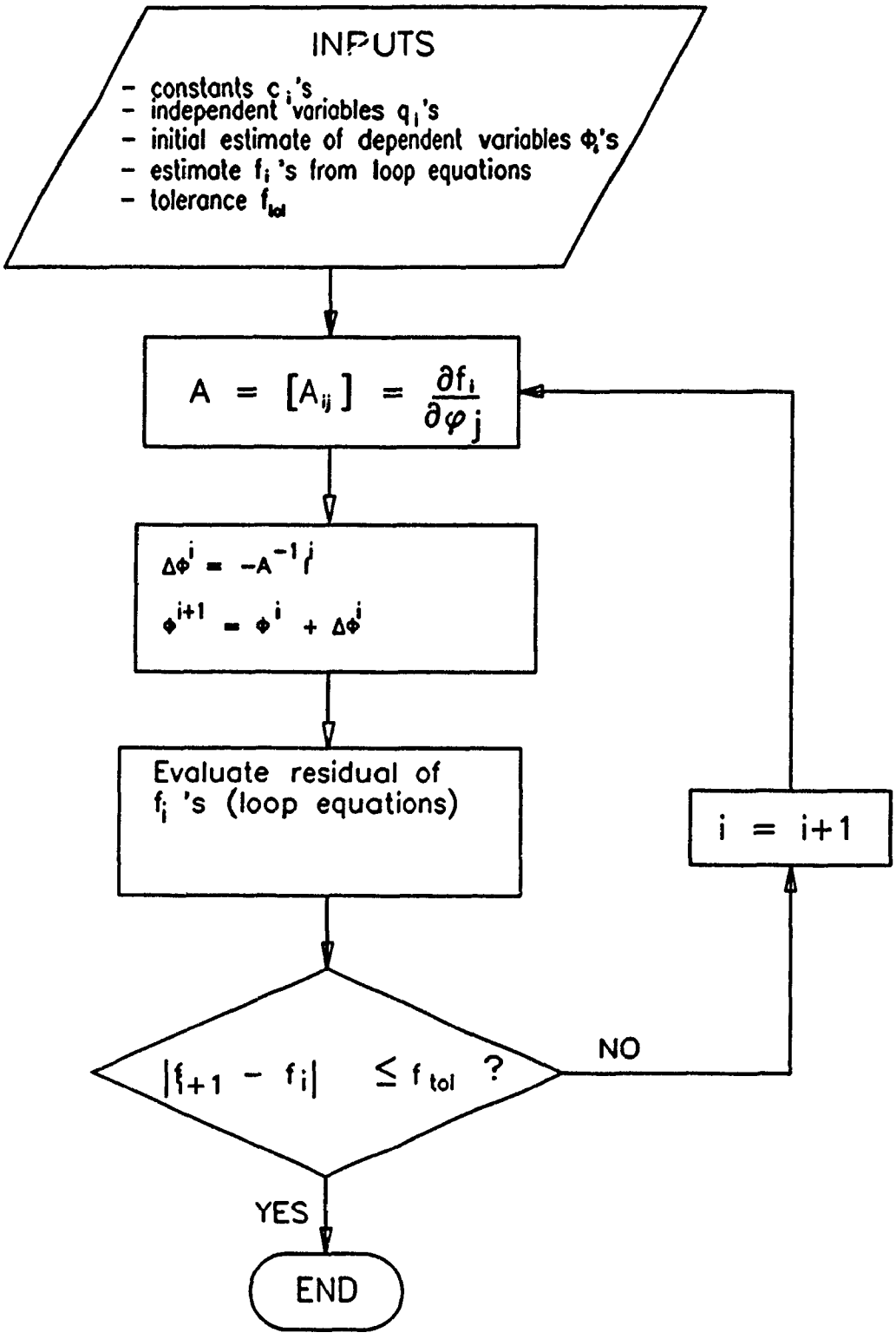

Fig. 3.7 Kinematic Position Analysis Flowchart

When a feasible pullrod linkage is analyzed, convergence is usually rapid. However, if convergence does not occur, a counter limits the number of iterations. Non-convergence is usually due to an initial guess which was too far from the true solution, an error in specifying system constants, or a system that is near singularity [45]. This concludes the description of the Newton-Raphson iterative kinematic solution.

In preparation for the kineto-static solution, the velocity coefficients and absolute sensitivities of velocity coefficients to the independent variables are now described. The equation (3.11) can be written as [44]:

$$\sum_{i=1}^{m} \frac{\partial f_k}{\partial \phi_i} d\phi_i = -\sum_{j=1}^{l} \frac{\partial f_k}{\partial q_j} dq_j, \quad k = 1,2,\ldots,m \tag{3.17}$$

or

$$\boldsymbol{A}\, d\boldsymbol{\phi} = -\boldsymbol{B}\, d\boldsymbol{q} \tag{3.18}$$

in matrix form, where

$$\boldsymbol{A} = [A_{ij}] = \left[\frac{\partial f_i}{\partial \phi_j}\right], \text{ an } m \times m \text{ Jacobian matrix.}$$

$$\boldsymbol{B} = [B_{ij}] = \left[\frac{\partial f_i}{\partial q_j}\right], \text{ an } m \times l \text{ matrix.}$$

From equation (3.18),

$$d\boldsymbol{\phi} = -\boldsymbol{A}^{-1}\boldsymbol{B}\, d\boldsymbol{q} = \boldsymbol{K}\, d\boldsymbol{q} \tag{3.19}$$

where the elements of the matrix $\mathbf{K}=-\mathbf{A}^{-1}\mathbf{B}$ are the velocity coefficients of the mechanism [45]. The velocity coefficients relate the dependent variables ϕ_i to the independent variables q_j as follows:

$$d\phi_i = \sum_{j=1}^{l} K_{ij}\, dq_j = \sum_{j=1}^{l} \frac{\partial \phi_i}{\partial q_j} dq_j \tag{3.20}$$

Before calculating the wheel rate, the derivative of velocity coefficients $\mathbf{K}$ with respect to independent variables $\mathbf{q}$ must be calculated. The derivative of $\mathbf{K}$ with respect to $\mathbf{q}$ is also called the absolute sensitivity of velocity coefficients $\mathbf{K}$ to independent variables $\mathbf{q}$:

$$\boldsymbol{K} = -\boldsymbol{A}^{-1}\boldsymbol{B} \tag{3.21}$$

$$\boldsymbol{A}\boldsymbol{K} = -\boldsymbol{B} \tag{3.22}$$

$$\frac{d}{dq_i}(\boldsymbol{A}\boldsymbol{K}) = -\frac{d}{dq_i}(\boldsymbol{B}) \tag{3.23}$$

$$\frac{d\boldsymbol{A}}{dq_i}\boldsymbol{K} + \boldsymbol{A}\frac{d\boldsymbol{K}}{dq_i} = -\frac{d\boldsymbol{B}}{dq_i} \tag{3.24}$$

$$\boldsymbol{A}\frac{d\boldsymbol{K}}{dq_i} = -\frac{d\boldsymbol{B}}{dq_i} - \frac{d\boldsymbol{A}}{dq_i}\boldsymbol{K} \tag{3.25}$$

$$\frac{d\boldsymbol{K}}{dq_i} = -\boldsymbol{A}^{-1}\left[\frac{d\boldsymbol{A}}{dq_i}\boldsymbol{K} + \frac{d\boldsymbol{B}}{dq_i}\right] \tag{3.26}$$

Solving individual terms, and since $\mathbf{A}=\mathbf{A}(\mathbf{q},\boldsymbol{\phi})$,

$$\frac{d\mathbf{A}}{dq_i} = \frac{\partial \mathbf{A}}{\partial q_i} + \frac{\partial \mathbf{A}}{\partial \boldsymbol{\phi}} \frac{d\boldsymbol{\phi}}{dq_i} \tag{3.27}$$

$$\frac{d\mathbf{A}}{dq_i} = \frac{\partial \mathbf{A}}{\partial q_i} + \frac{\partial \mathbf{A}}{\partial \boldsymbol{\phi}} \mathbf{K}_i \tag{3.28}$$

where $\mathbf{K}_i$ is the ith column of $\mathbf{K}$

$$\frac{d\mathbf{A}}{dq_i} = \frac{\partial \mathbf{A}}{\partial q_i} + \sum_{k=1}^{m} \frac{\partial \mathbf{A}}{\partial \phi_k} \frac{\partial \phi_k}{\partial q_i} \tag{3.29}$$

and since $\mathbf{B}=\mathbf{B}(\mathbf{q},\boldsymbol{\phi})$,

$$\frac{d\mathbf{B}}{dq_i} = \frac{\partial \mathbf{B}}{\partial q_i} + \sum_{k=1}^{m} \frac{\partial \mathbf{B}}{\partial \phi_k} \frac{\partial \phi_k}{\partial q_i} \tag{3.30}$$

Combining terms,

$$\frac{d\mathbf{K}}{dq_i} = -\mathbf{A}^{-1}\left[\left(\frac{\partial \mathbf{A}}{\partial q_i} + \sum_{k=1}^{m} \frac{\partial \mathbf{A}}{\partial \phi_k} \frac{\partial \phi_k}{\partial q_i}\right)\mathbf{K} + \left(\frac{\partial \mathbf{B}}{\partial q_i} + \sum_{k=1}^{m} \frac{\partial \mathbf{B}}{\partial \phi_k} \frac{\partial \phi_k}{\partial q_i}\right)\right] \tag{3.31}$$

3.3.2 Kineto-Static Solution

For the kineto-static solution, the force/displacement characteristics of the suspension linkage must be examined. From the principle of virtual work [44],

$$\partial W = \sum_{i=1}^{p} F_i \partial \phi_i \tag{3.32}$$

$$\partial W = \sum_{i=1}^{p}\left[F_i \sum_{j=1}^{l} K_{ij}\partial q_j\right] = \sum_{j=1}^{l}\left(\sum_{i=1}^{p} F_i K_{ij}\right)\partial q_j \qquad (3.33)$$

and from the second term of equation (3.33), the generalized forces $\mathbf{Q}$ corresponding to the generalized coordinates $\mathbf{q}$ are:

$$Q_j = \sum_{i=1}^{p} F_i K_{ij} \qquad (3.34)$$

If all force generators are passive elements,

$$F_i = F_i\left(\phi_i, \frac{d\phi_i}{dt}\right) \qquad (3.35)$$

and since

$$\begin{aligned} d\phi_i &= \sum_{j=1}^{l} K_{ij} dq_j \qquad (i = 1,2,\ldots,m) \\ \frac{d\phi_i}{dt} &= \sum_{j=1}^{l} K_{ij}\dot{q}_j \end{aligned} \qquad (3.36)$$

thus,

$$Q_j = Q_j(\mathbf{q}, \dot{\mathbf{q}}) \qquad (3.37)$$

Furthermore, for the passive planar A-arm linkage, where the linearized linkage position is denoted by superscript o, the displacement from the linearized linkage position is expressed by $(\phi_i - \phi_i^{\circ})$ and the forces due to each of the p force generator (spring and damper) elements in the linkage are

$$F_i = k_i(\phi_i - \phi_i^{\circ}) + C_i \sum_{j=1}^{l} K_{ij}\dot{q}_j \qquad (3.38)$$

therefore the generalized forces in the linkage are

$$Q_j = \sum_{i=1}^{p} K_{ij}\left\{k_i(\phi_i - \phi_i^o) + C_i\sum_{j=1}^{l} K_{ij}\dot{q}_j\right\} \tag{3.39}$$

Equation (3.37) states that the generalized force matrix **Q** is a function of **q** and $\dot{\mathbf{q}}$. Accordingly, the linearized kinetic characteristics of the pullrod A-arm suspension linkage are written in terms of constant-coefficient stiffness and damping matrices, **K** and **C**, as [44]:

$$\mathbf{Q} = \mathbf{K}\mathbf{q} + \mathbf{C}\dot{\mathbf{q}} \tag{3.40}$$

If there are s force generators, then equation (3.39) becomes:

$$Q_i = \sum_{s=1}^{p} K_{si}\left\{k_s(\phi_s - \phi_s^o) + C_s\sum_{i=1}^{l} K_{si}\dot{q}_i\right\} \tag{3.41}$$

The stiffness is derived:

$$\mathbf{K}_{ij} = \frac{\partial Q_i}{\partial q_j}\Big|_{\mathbf{q}=\mathbf{q}^o} = \frac{\partial}{\partial q_j}\left(\sum_{s=1}^{p} K_{si}\left\{k_s(\phi_s - \phi_s^o) + C_s\sum_{i=1}^{l} K_{si}\dot{q}_i\right\}\right)\Big|_{\mathbf{q}=\mathbf{q}^o} \tag{3.42}$$

$$= \frac{\partial}{\partial q_j}\left(\sum_{s=1}^{p} K_{si}\left\{k_s(\phi_s - \phi_s^o)\right\}\right)\Big|_{\mathbf{q}=\mathbf{q}^o} \tag{3.43}$$

$$= \sum_{s=1}^{p}\left\{K_{si}k_s\frac{\partial}{\partial q_j}(\phi_s - \phi_s^o) + k_s(\phi_s - \phi_s^o)\frac{\partial K_{si}}{\partial q_j}\right\}\Big|_{\mathbf{q}=\mathbf{q}^o} \tag{3.44}$$

$$\mathbf{K}_{ij} = \sum_{s=1}^{p} k_s \left\{ K_{sj} K_{si} + (\phi_s - \phi_s^o) \frac{\partial K_{si}}{\partial q_j} \right\} \Big|_{q=q^o} \tag{3.45}$$

The damping is derived:

$$\mathbf{C}_{ij} = \frac{\partial Q_i}{\partial \dot{q}_j} \Big|_{q=q^o} = \frac{\partial}{\partial \dot{q}_j} \left(\sum_{s=1}^{p} K_{si} \left\{ k_s (\phi_s - \phi_s^o) + C_s \sum_{i=1}^{l} K_{si} \dot{q}_i \right\} \right) \Big|_{q=q^o} \tag{3.46}$$

$$= \frac{\partial}{\partial \dot{q}_j} \left(\sum_{s=1}^{p} K_{si} C_s \sum_{i=1}^{l} K_{si} \dot{q}_i \right) \Big|_{q=q^o} \tag{3.47}$$

$$= \sum_{s=1}^{p} K_{si} C_s \frac{\partial}{\partial \dot{q}_j} \left(\sum_{i=1}^{l} K_{si} \dot{q}_i \right) \Big|_{q=q^o} \tag{3.48}$$

$$= \sum_{s=1}^{p} K_{si} C_s \left(\sum_{i=1}^{l} K_{si} \frac{\partial}{\partial \dot{q}_j} \dot{q}_i \right) \Big|_{q=q^o} \tag{3.49}$$

$$\text{since } \frac{\partial \dot{q}_i}{\partial \dot{q}_j} = 0 \quad \text{for } i \neq j$$
$$= 1 \quad \text{for } i = j$$

$$\mathbf{C} = \sum_{s=1}^{p} K_{si} K_{sj} C_s \tag{3.50}$$

Static equilibrium is reached when the generalized forces balance the external forces. This means that the suspension linkage moves until the forces from the springs, expressed as generalized forces **Q**, balance the external forces **R**. The condition for static equilibrium is expressed as [44]:

$$g(q) = Q - R = 0$$

$$\text{where } Q = \text{generalized forces} \quad R = \text{external forces} \quad g = \text{static equilibrium vector} \tag{3.51}$$

Equation (3.51) is a set of 1 simultaneous nonlinear equations in 1 unknowns, and can be solved using the Newton-Raphson method. The estimated solution vector is [44]:

$$q^{i+1} = q^i - (\mathbf{K}^{-1})^i g^i \tag{3.52}$$

where the stiffness matrix $\mathbf{K}$ for linear springs is given in equation (3.45).

Fig. 3.8 shows a flowchart of the kineto-static solution procedure. This procedure consists of two nested Newton-Raphson procedures. The inner loop solves an incremental linkage position within a specified kinematic tolerance. The outer loop checks whether the generalized forces Q balance the external forces R which are applied along the generalized coordinates q. A specified kinetic tolerance must be met.

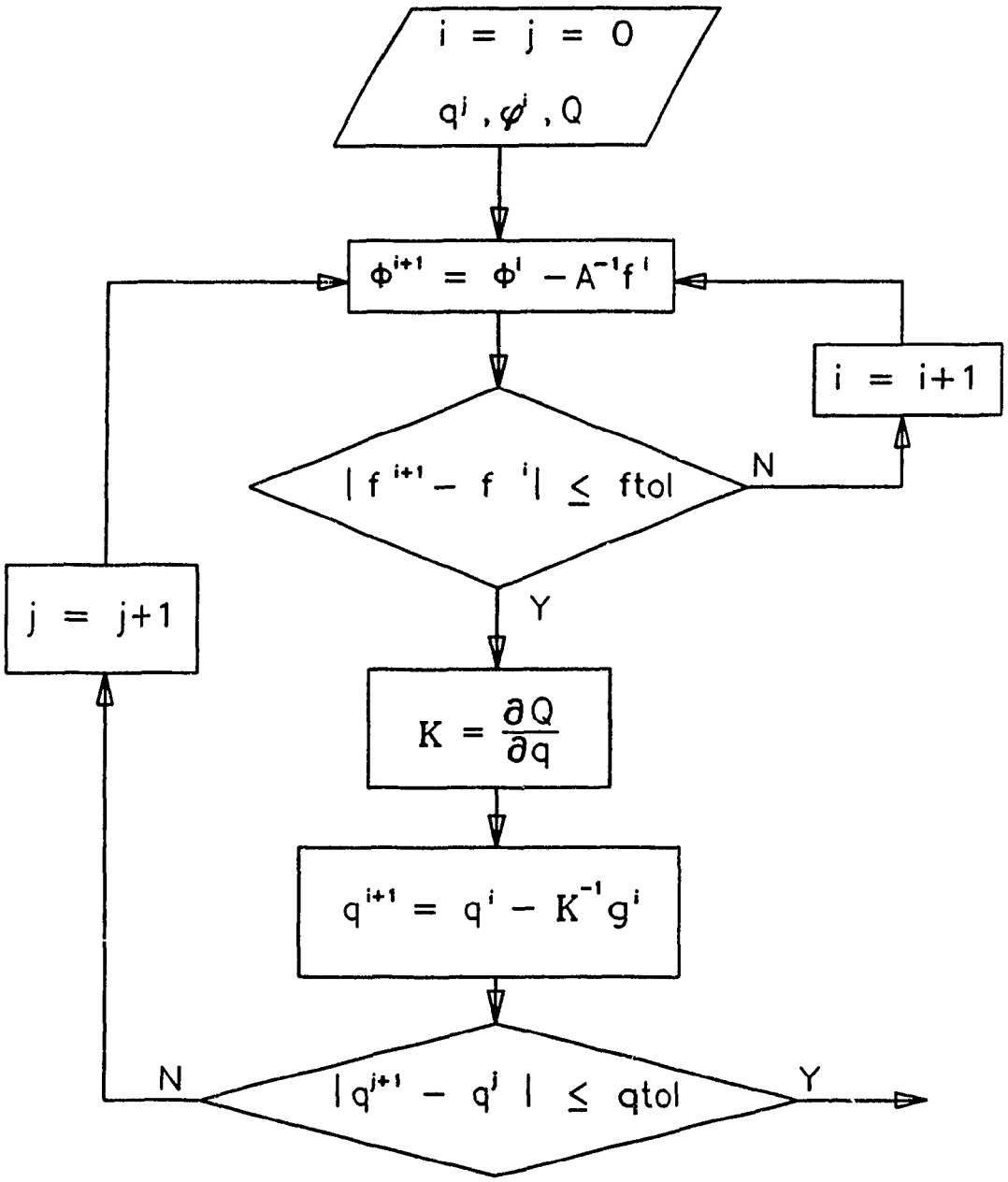

Fig. 3.8 Kineto-Static Analysis Procedure [44]

3.4 Vehicle Design Synthesis

3.4.1 Performance Index

Final understeer or oversteer is quantified by the understeer number N_u as defined by Dixon [47]:

$$N_u = \frac{A_r}{A_f} - 1 \qquad (3.53)$$

When the understeer number is zero, the vehicle exhibits neutral handling at its limit of adhesion. In general, the steady-state handling of a light vehicle at its limit of adhesion should be neutral, however, it is essential that the vehicle transient response be considered as well. Vehicle design synthesis based solely on steady-state conditions can yield disastrously unstable transient response [42].

Even if a non-zero understeer number is desired, its magnitude should be low [47]. A light vehicle with final neutral handling will be very sensitive to small changes in tires, suspension, and aerodynamic characteristics [46]. Minor alterations in the last three areas will provide the desired understeer number absolute value.

3.4.2 Procedure for Finding the Vehicle Center of Gravity

At the conceptual stage of the design synthesis, the vehicle chassis and suspension can be visualized according to the roll axis representation as seen in Fig. 3.5. The center of gravity is located by the variables a, b, h, and h_{ra}, where the wheelbase L = a+b. It is assumed that the wheelbase L has been fixed. The ratio a/L is the nondimensional distance from the front axle to the center of gravity position, in the $\overline{X}$-$\overline{Y}$ plane. We now ask, what should be the magnitudes of a and h? Using the center of gravity finding procedure, we will answer this question.

The values a and h influence the lateral weight transfer of the vehicle, as discussed in section 3.2.4. The height dimension h affects the total lateral weight transfer. Raising the center of gravity (increasing h) will increase the total lateral weight transfer; lowering it does the opposite. Since the tires are normal load sensitive, it is desired to keep the vehicle center of gravity as low as possible. For the purposes of this work, it is assumed that the CG height h has been previously selected at its lowest practical value.

The values a and L determine how the weight transfer due to the sprung mass inertia force is proportioned between the front and rear axles, where F_{rcf} and F_{rcr} are lateral forces acting at the front and rear roll centers, respectively (see eqns. (3.8)):

$$F_{rcf} = m_s A_y \frac{b}{L}$$
$$F_{rcr} = m_s A_y \frac{a}{L} \qquad (3.54)$$

The lateral forces are coupled with the vehicle track and roll center height as follows [15]:

$$W_{rcf} = F_{CF} \frac{h_f}{t_f}$$
$$W_{rcr} = F_{CR} \frac{h_r}{t_r} \qquad (3.55)$$

The center of gravity finding procedure optimises the value of a for neutral handling (N_u=0) and maximum lateral acceleration. The procedure includes the effects of all weight transfer components discussed in section (3.2.4).

The effect of varying dimension a, considered along with the other weight transfer components, is quantified by comparing the lateral acceleration of the front axle against that of the rear axle. This comparison is made when the vehicle model is simulated under maximum steady-state cornering. Maximum steady-state cornering occurs at the hignest possible speed which will still allow vehicle control. For reasons of safety, it is important to consider the transient response as well, since a vehicle which is under control during steady-state cornering may be unstable in a transient maneuver. The transient response will be considered later in this thesis. The center of gravity location is fundamental to the handling and stability of the vehicle [46].

Thus, the center of gravity finding procedure has been created to obtain limit-state neutral handling for a particular tire-chassis-suspension combination.

Steady-State Response for CG Finding

The 3DOF vehicle equations of motion as given by eqns. (3.3) are written in the vehicle-fixed, non-inertial reference frame. The center of gravity finding procedure requires the 3DOF vehicle equations of motion in the inertial reference frame. We begin the conversion of the non-inertial equations by recalling eqns. (3.3):

$$\begin{aligned} \Sigma Y &= m(\dot{V}+Ur) + m_s h_{ra}\dot{p} \\ \Sigma N &= I_z \dot{r} \\ \Sigma L_s &= I_x \dot{p} + m_s h_{ra}(\dot{V}+Ur) \end{aligned}$$

Assuming the vehicle sprung mass roll velocity p and yaw velocity r to be constant, the sprung mass roll acceleration $\dot{p}$ and yaw acceleration $\dot{r}$ are equal to zero. Therefore the vehicle equations of motion can be reduced as follows:

$$\begin{aligned} \Sigma Y &= m(\dot{V}+Ur) \\ \Sigma N &= 0 \\ \Sigma L_s &= m_s h_{ra}(\dot{V}+Ur) \end{aligned} \qquad (3.56)$$

If equations (3.56) are converted to the inertial reference frame, the result is:

$$\begin{aligned} \Sigma Y &= mA_y \\ \Sigma L_s &= m_s h_{rs} A_y \end{aligned} \tag{3.57}$$

where $A_y = \frac{U^2}{R}$.

Center of Gravity Finding Algorithm

The center of gravity finding algorithm is based on the work of Dominy and Dominy [21]. The goal of this algorithm is to find the CG position variable "a" at which the maximum steady-state lateral acceleration of the front axle equals that of the rear axle. The CG position variable "a" is systematically varied for a constant wheelbase, L, until the front and rear axles develop the same maximum steady-state lateral accelerations. It is at this condition that the chassis and suspension will provide the best performance, subject to satisfactory transient behaviour (response) of the vehicle that was mentioned earlier in this section.

If the vehicle is being driven at the limit of adhesion, then the tire data need only be considered at peak slip angles. This requires that the tire cornering force versus normal load data at peak slip angles be accurate.

The flowchart for the center of gravity finding procedure is shown in Fig. 3.9.

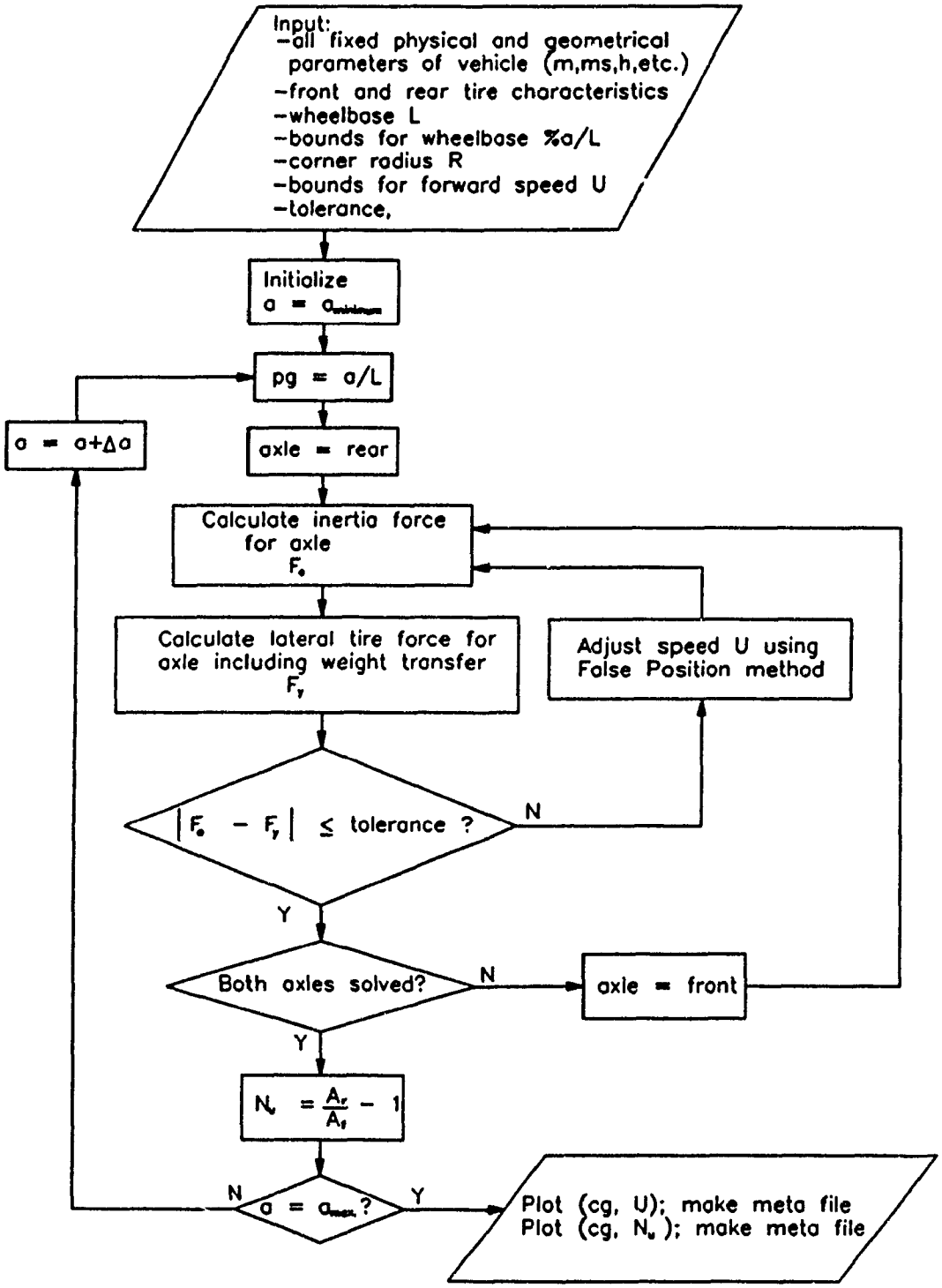

Fig. 3.9 Flowchart for Center of Gravity Finding Procedure

The simulation is started by selecting front and rear tire and chassis characteristics, as well as a corner radius. In addition, upper and lower bounds for the center of gravity location and forward speed must be set. The forward speed bounds must be set to bracket the limiting forward speed. The program is then initialized by setting the center of gravity position to the minimum "a" value, expressed in percent of wheelbase.

An iterative technique is used to solve the cornering speed. For the lowest speed bound the outward force on the rear of the vehicle is calculated. The lateral tire force corresponding to the peak slip angle is calculated. The process is repeated for the highest speed bound. The false-position numerical method is used to find the speed at which the outward vehicle forces and the lateral tire forces are in equilibrium. This speed is considered to be the maximum speed at which the rear of the vehicle can corner. The procedure is repeated for the front of the vehicle. The vehicle's handling is then characterized using the understeer number N_u.

The CG position variable "a" is then incremented and the understeer number N_u for that position is found. This procedure is repeated for entire wheelbase range. The CG position at which $N_u=0$ and the limiting speed is maximum is chosen to be the best value of "a".

3.4.3 Chassis Spring Rate Selection Procedure

Using the center of gravity finding procedure that was just described in the previous section, combined with the kinematic analysis of the tentative front and rear suspension linkages, an estimate of the required chassis spring rates is made. The spring stiffness values will be used in the kineto-static suspension analysis to find the nonlinear roll centers and roll stiffnesses.

The pullrod linkage is solved by increments from full droop to full bump position. For each linkage position, the velocity coefficients and absolute sensitivities are calculated. The information at the static ride height is then used to calculate the spring rate.

The wheel rate at static ride height is first calculated using the baseline procedure given in section 2.4. Recalling equation (3.45):

$$K_{22} = \frac{\partial Q_2}{\partial q_2} = \sum_{s=1}^{2} k_s \left\{ K_{sj} K_{si} + (\phi_s - \phi_s^o) \frac{\partial K_{si}}{\partial q_j} \right\} \Big|_{q=q^o} \qquad (3.58)$$

and assuming that the vehicle is symmetrical about the $\bar{X}$-$\bar{Y}$ plane and has identical chassis springs:

$$k_w(0) = k_s \left\{ K_{s2}(0)^2 + (\phi_s - \phi_s^o) \frac{\partial K_{s2}}{\partial q_2} \right\} \qquad (3.59)$$

where $K_{s2}(0)$ = velocity coefficient relating bounce motion spring displacement to q_2
$k_w(0)$ = wheel rate at static ride height
$\phi_s(0)$ = spring displacement at static ride height

From equation (3.39),

$$\phi_s - \phi_s^2 = \frac{m_s g}{K_{s2}(0)\, k_s} \tag{3.60}$$

since at static ride height the vertical load is the vehicle weight. The spring rate k_s is then determined by substituting equation (3.60) into equation (3.59) and solving for k_s:

$$k_s = \frac{k_w(0)}{(K_{s2}(0))^2} - \frac{m_s g \left(\frac{\partial K_{s2}}{\partial q_2}\right)}{(K_{s2}(0))^3} \tag{3.61}$$

3.4.4 Kineto-Static Linkage Analysis Procedure

The kineto-static linkage analysis procedure is performed as detailed in section 3.3 (Fig. 3.8). The kineto-static solution is used to find the roll centers and roll stiffnesses of the front and rear axles when acted upon by dynamic cornering forces. The change of the roll centers and roll stiffnesses as a function of lateral force is then applied to the center of gravity finding procedure to determine the vehicle's understeer number Nu, and to calculate the CG position "a".

From the equations of motion, it is apparent that the roll centers are used to find the lateral load transfer during steady-state cornering. Various definitions exist for the roll center. The kinematic roll centers, as defined by Ellis [31], are "kinematic centers of rotation of the suspension assuming that the wheels are rigid and do not move sideways on the road surface". The kinematic roll center procedure is based on the Kennedy-Aronhold theorem, which states that "relative instant centers associated with three moving planes lie on a straight line" [45]. The kinematic roll center procedure of Smith [48] is the same as Ellis', except that lateral movement of the contact patches is accommodated. The SAE definition of force roll center is the "point in the transverse vertical plane through any pair of wheel centers at which lateral forces may be applied to the sprung mass without producing suspension roll" [35].

Alanoly [44] has reviewed these roll center concepts and others, commenting on their various contradictions and shortcomings. Based on these observations, Alanoly's revised roll center definition is used in this work. The roll center is defined as the instantaneous center of rotation of the chassis, relative to the tire contact patches, for a lateral force applied to the center of gravity. Roll stiffness is defined as the rate of change of the roll moment with respect to the chassis roll angle.

Roll Center Calculation

The calculation of roll center location begins with selection of notation (Fig. 3.10). Note that the X-Y (inertial-fixed) coordinate system is centered at one of the tire contact patches. The three independent coordinates q_1, q_2, and q_3 are designated as X_{cg}, Y_{cg}, and θ, respectively. This gives the planar pullrod A-arm linkage three degrees of freedom. It is very important to realize that these planar linkage degrees of freedom are different from the dynamic vehicle degrees of freedom. The front and rear suspension linkages are individually analysed. The suspension analysis outputs are then used as "black boxes" in the dynamic vehicle analysis. The degrees of freedom referred to in this section apply exclusively to the planar pullrod A-arm linkage.

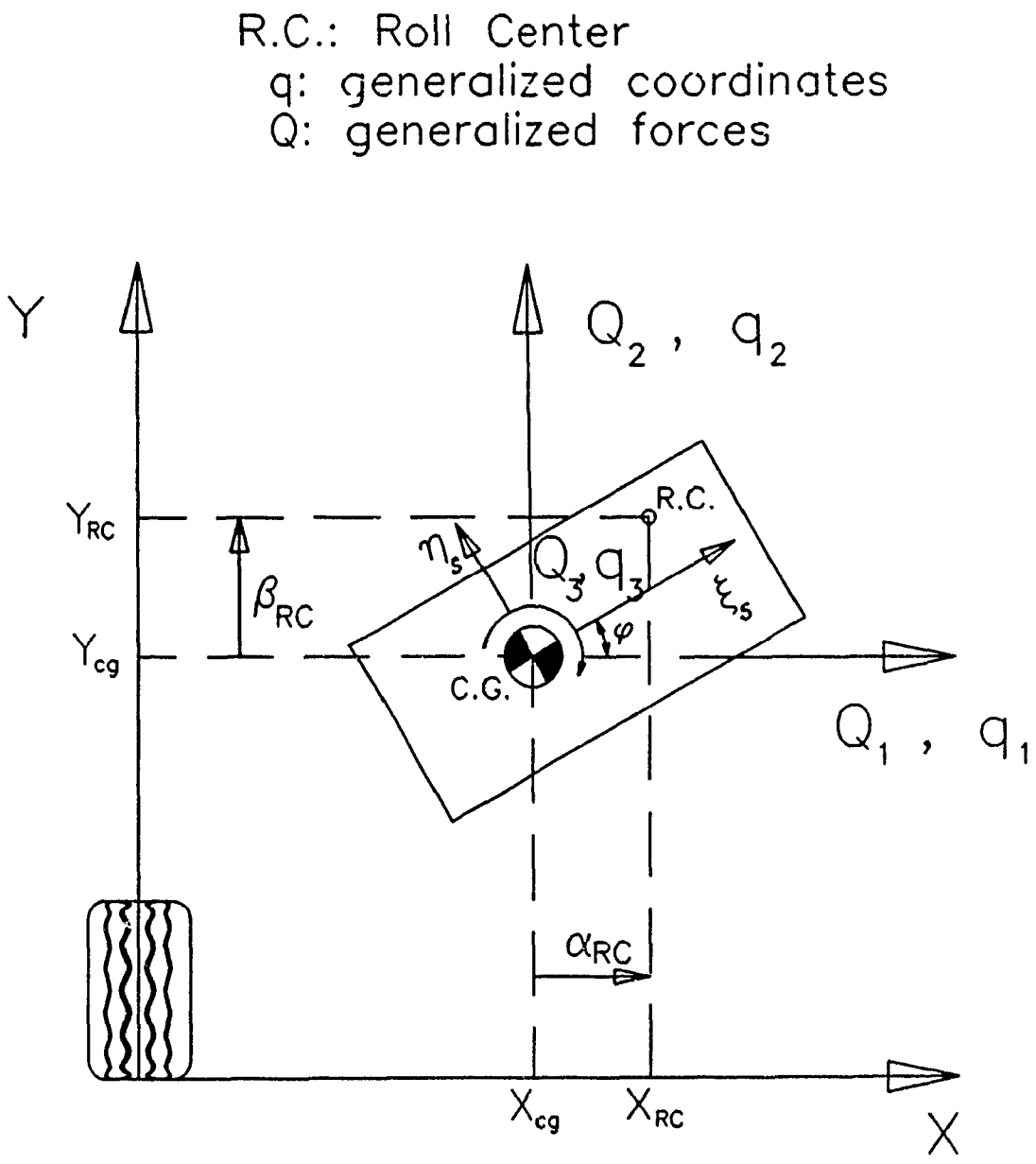

Fig. 3.10 Notation for Roll Center Calculation [44]

Based on the linearized force generation characteristics of the linkage suspension [44]:

$$\kappa_{ij} = \frac{\partial Q_i}{\partial q_j} \tag{3.62}$$

and for the planar pullrod A-arm linkage under scrutiny,

$$\begin{bmatrix} \delta Q_1 \\ \delta Q_2 \\ \delta Q_3 \end{bmatrix} = \begin{bmatrix} \kappa_{11} & \kappa_{12} & \kappa_{13} \\ \kappa_{21} & \kappa_{22} & \kappa_{23} \\ \kappa_{31} & \kappa_{32} & \kappa_{33} \end{bmatrix} \begin{bmatrix} \delta q_1 \\ \delta q_2 \\ \delta q_3 \end{bmatrix} \tag{3.63}$$

Based on the definition of roll center, an incremental lateral force, δQ_1, is applied to the center of gravity. By setting $\delta Q_2 = 0$ and $\delta Q_3 = 0$, the deflections [δq] are solved from Eqn. (3.63):

$$\begin{bmatrix} \delta q_1 \\ \delta q_2 \\ \delta q_3 \end{bmatrix} = \frac{\delta Q_1}{\Delta} \begin{bmatrix} \kappa_{22}\kappa_{33} - \kappa_{32}\kappa_{23} \\ \kappa_{31}\kappa_{23} - \kappa_{21}\kappa_{33} \\ \kappa_{21}\kappa_{32} - \kappa_{31}\kappa_{22} \end{bmatrix} \tag{3.64}$$

$$\text{where } \Delta = det \begin{bmatrix} \kappa_{11} & \kappa_{12} & \kappa_{13} \\ \kappa_{21} & \kappa_{22} & \kappa_{23} \\ \kappa_{31} & \kappa_{32} & \kappa_{33} \end{bmatrix}$$

Our goal is to write expressions for α_{RC} and β_{RC} (Fig. 3.10). Transforming the body-fixed coordinates ξ_s and η_s to the inertial-fixed X-Y coordinate system:

$$\alpha_{RC} = \xi_s \cos\theta - \eta_s \sin\theta$$
$$\beta_{RC} = \xi_s \sin\theta + \eta_s \cos\theta \qquad (3.65)$$

The inertial-fixed roll center coordinates X_{RC}, Y_{RC} can then be expressed as:

$$X_{RC} = X_{cg} + \alpha_{RC}$$
$$Y_{RC} = Y_{cg} + \beta_{RC} \qquad (3.66)$$

$$X_{RC} = X_{cg} + (\xi_s \cos\theta - \eta_s \sin\theta)$$
$$Y_{RC} = Y_{cg} + (\xi_s \sin\theta + \eta_s \cos\theta) \qquad (3.67)$$

By definition the instantaneous roll center has no translation, therefore :

$$\dot{X}_{RC} = 0 = \dot{X}_{cg} - (\xi_s \sin\theta + \eta_s \cos\theta)\dot{\theta}$$
$$i.e. \quad \beta_{RC} = \frac{\dot{X}_{cg}}{\dot{\theta}}$$
$$\dot{Y}_{RC} = 0 = \dot{Y}_{cg} + (\xi_s \cos\theta - \eta_s \sin\theta)\dot{\theta} \qquad (3.68)$$
$$i.e. \quad \alpha_{RC} = \frac{-\dot{Y}_{cg}}{\dot{\theta}}$$

Taking the time derivative of equation (3.64) and substituting into equation (3.68), and considering $\dot{q}_1 = \dot{x}_{CG}$, $\dot{q}_2 = \dot{y}_{CG}$ and $\dot{q}_3 = \dot{\theta}$ gives

$$\alpha_{RC} = \frac{\kappa_{21}\kappa_{33} - \kappa_{31}\kappa_{23}}{\kappa_{21}\kappa_{32} - \kappa_{31}\kappa_{22}} \qquad (3.69)$$

$$\beta_{RC} = \frac{\kappa_{22}\kappa_{33} - \kappa_{32}\kappa_{23}}{\kappa_{21}\kappa_{32} - \kappa_{31}\kappa_{22}} \qquad (3.70)$$

Roll Stiffness Calculation

Using the same notation as introduced in Fig. 3.10, the roll stiffness is calculated. The roll moment is defined as:

$$M_r = Q_1\beta_{RC} - Q_2\alpha_{RC} + Q_3 \tag{3.71}$$

Following the definition of roll stiffness as given in the beginning of this section:

$$K_r = \frac{\delta M_r}{\delta\theta} = \frac{\delta Q_1}{\delta\theta}\beta_{RC} + Q_1\frac{\delta\beta_{RC}}{\delta\theta} - \frac{\delta Q_2}{\delta\theta}\alpha_{RC} - Q_2\frac{\delta\alpha_{RC}}{\delta\theta} + \frac{\delta Q_3}{\delta\theta} \tag{3.72}$$

Assuming that only the lateral force is incremented, $\delta Q_2 = \delta Q_3 = 0$. Thus equation (3.72) reduces to:

$$K_r = \frac{\delta Q_1}{\delta\theta}\beta_{RC} + Q_1\frac{\delta\beta_{RC}}{\delta\theta} - Q_2\frac{\delta\alpha_{RC}}{\delta\theta} \tag{3.73}$$

Using eqn. (3.65):

$$K_r = \frac{\delta Q_1}{\delta\theta}\beta_{RC} + Q_1\alpha_{RC} + Q_2\beta_{RC} \tag{3.74}$$

Since

$$\frac{\delta Q_1}{\delta\theta} = \frac{\delta Q_1}{\delta q_3} \tag{3.75}$$

then from equation (3.64),

$$\frac{\delta Q_1}{\delta q_3} = \frac{\Delta}{\kappa_{21}\kappa_{32} - \kappa_{31}\kappa_{22}} \tag{3.76}$$

Substituting equation (3.76) into equation (3.74), the expression for the roll stiffness based on the kineto-static linkage analysis becomes:

$$K_r = \frac{\Delta}{(\kappa_{21}\kappa_{32} - \kappa_{31}\kappa_{22})} \frac{(\kappa_{22}\kappa_{33} - \kappa_{32}\kappa_{23})}{(\kappa_{21}\kappa_{32} - \kappa_{31}\kappa_{22})} + Q_1\alpha_{RC} + Q_2\beta_{RC}$$

$$K_r = \frac{\Delta\,(\kappa_{22}\kappa_{33} - \kappa_{32}\kappa_{23})}{(\kappa_{21}\kappa_{32} - \kappa_{31}\kappa_{22})^2} + Q_1\alpha_{RC} + Q_2\beta_{RC} \qquad (3.77)$$

Roll Damping Calculation

A simplified roll damping value has been used. A roll damping ratio of 0.3 is used, based on the total roll stiffness.

$$\frac{L_p}{L_{pcrit}} = 0.3$$

$$L_p = 0.3\,L_{pcrit} \qquad (3.78)$$

$$L_p = 0.6\sqrt{K_r I_x}$$

3.4.5 Transient Vehicle Dynamic Analysis

The nonlinear vehicle equations of motion are solved by taking the equations (3.3) and rearranging them:

$$\Sigma Y - mUr = m\dot{V} + m_s h_{ra}\dot{p}$$

$$\Sigma N = I_z\dot{r} \qquad (3.79)$$

$$\Sigma L_s - m_s h_{ra} Ur = m_s h_{ra}\dot{V} + I_x\dot{p}$$

Rewriting equation (3.79) in a matrix form:

$$\begin{Bmatrix} \Sigma Y - mUr \\ \Sigma N \\ \Sigma L_s - m_s h_{ra} Ur \end{Bmatrix} = \begin{bmatrix} m & 0 & m_s h_{ra} \\ 0 & I_z & 0 \\ m_s h_{ra} & 0 & I_x \end{bmatrix} \begin{Bmatrix} \dot{V} \\ \dot{r} \\ \dot{p} \end{Bmatrix} \qquad (3.80)$$

$$\begin{Bmatrix} \dot{V} \\ \dot{r} \\ \dot{p} \end{Bmatrix} = \begin{bmatrix} m & 0 & m_s h_{ra} \\ 0 & I_z & 0 \\ m_s h_{ra} & 0 & I_x \end{bmatrix}^{-1} \begin{Bmatrix} \Sigma Y - mUr \\ \Sigma N \\ \Sigma L_g - m_s h_{ra} Ur \end{Bmatrix} \tag{3.81}$$

After finding the inverse of the mass-inertia matrix, the adjoint of the matrix divided by its determinant, we are left with the following equations:

$$\begin{Bmatrix} \dot{V} \\ \dot{r} \\ \dot{p} \end{Bmatrix} = \frac{1}{\Delta} \begin{bmatrix} I_x I_z & 0 & -I_z m_s h_{ra} \\ 0 & I_x m - (m_s h_{ra})^2 & 0 \\ -I_z m_s h_{ra} & 0 & I_z m \end{bmatrix} \begin{Bmatrix} \Sigma Y - mUr \\ \Sigma N \\ \Sigma L - m_s h_{ra} Ur \end{Bmatrix} \tag{3.82}$$

where $\Delta = I_x I_z m - I_z (m_s h_{ra})^2$.

Equation (3.82) is now rewritten as a system of first order differential equations:

$$\begin{Bmatrix} \dot{y} \\ \dot{V} \\ \dot{\psi} \\ \dot{r} \\ \dot{\theta} \\ \dot{p} \end{Bmatrix} = \begin{Bmatrix} V \\ \dfrac{I_x I_z (\Sigma Y - mUr) - I_z m_s h_{ra} (\Sigma L - m_s h_{ra} Ur)}{m I_x I_z - I_z (m_s h_{ra})^2} \\ r \\ \dfrac{\Sigma N (I_x m - (m_s h_{ra})^2)}{m I_x I_z - I_z (m_s h_{ra})^2} \\ p \\ \dfrac{-I_z m_s h_{ra} (\Sigma Y - mUr) + I_z m (\Sigma L - m_s h_{ra} Ur)}{m I_x I_z - I_z (m_s h_{ra})^2} \end{Bmatrix} \tag{3.83}$$

The state-space equation (3.83) with the appropriate initial conditions is solved over a desired time step using the fourth-order Runge-Kutta numerical method. MATLAB provides a fourth-order Runge-Kutta solver as an intrinsic function. The MATLAB implementation of the fourth-order Runge-Kutta method was chosen because it is self-starting, provides automatic step size, and is efficient and reliable.

The output from the vehicle dynamic analysis consists of the body-fixed y-position, lateral velocity, yaw angle, yaw angular velocity, roll angle, and roll angular velocity. In addition, the body-fixed lateral acceleration, yaw angular acceleration, and roll angular acceleration can be extracted.

3.4.6 Handling Refinement and Design Procedure: Summary

This section has described the mathematical model and the algorithms used to design and refine a vehicle system for handling. The software implementation of these procedures will be described in the following section.

3.5 Vehicle Design Synthesis Software

Software has been written to implement the vehicle design synthesis for vehicle handling and stability, as described in this chapter. A flowchart of the software is seen in Fig. 3.11.

Complete vehicle parameters, front and rear linkage information, and performance criteria are entered. The center of gravity finding routine CGFIND (based on Section 3.4.2) then calculates the sprung mass distribution. The sprung mass distribution is read by the chassis spring rate finder SPRING which then computes the chassis spring rate for the front suspension (Section 3.4.3).

The kineto-static linkage solver KINSTAT (Section 3.4.4) then computes the non-linear roll centers and roll stiffnesses for the front suspension linkage and saves them as lookup tables. The SPRING-KINSTAT procedure is repeated for the rear suspension linkage. CGFIND then recomputes the center of gravity using all non-linearity tables for front and rear suspensions.

Vehicle dynamic solver DYNAMIC (Section 3.4.5) computes handling response using comprehensive data including lookup tables from KINSTAT, vehicle information including the new CG, and the initial conditions and forcing functions for the vehicle. The vehicle dynamic handling response is compared to the performance criteria.

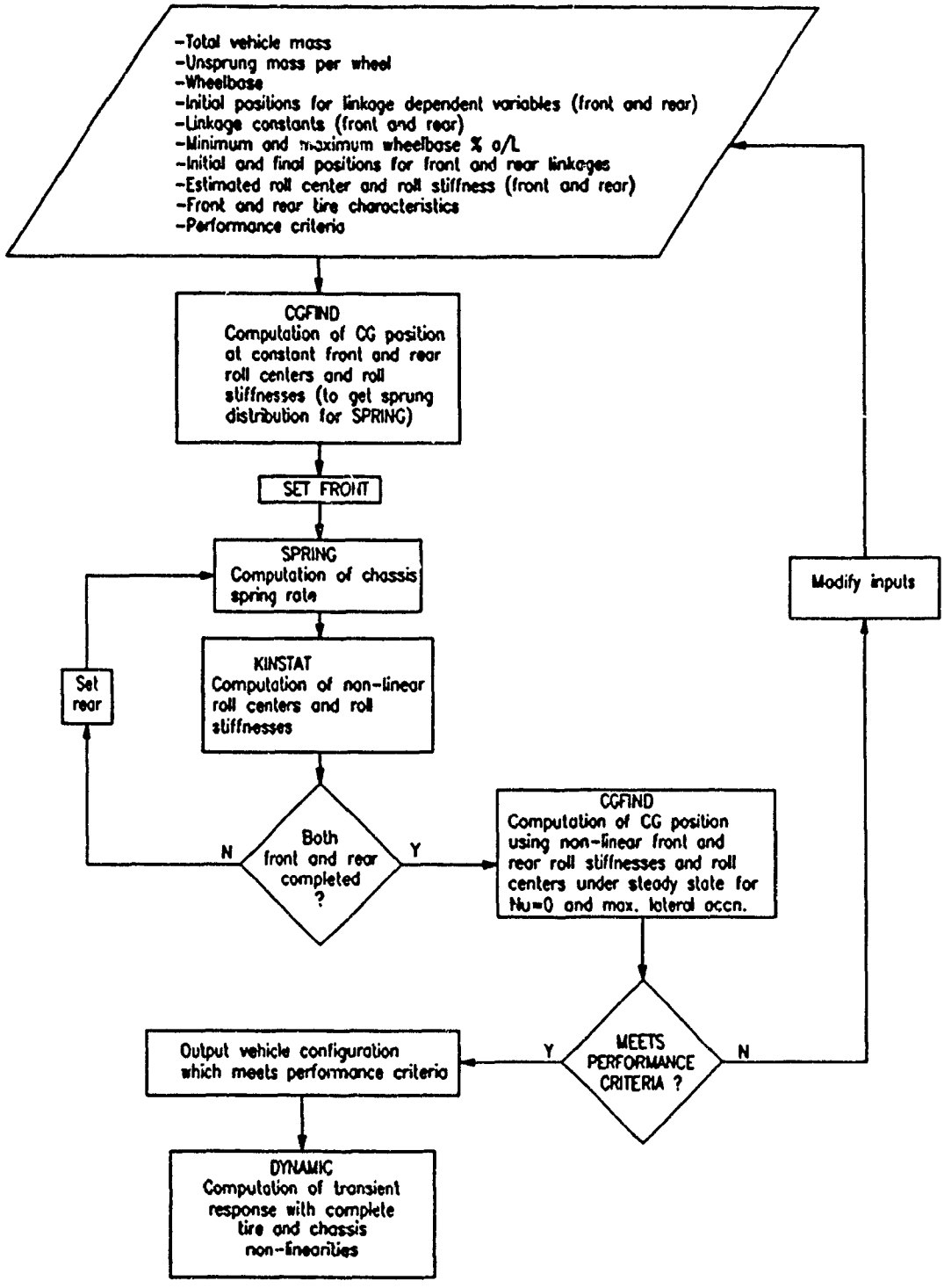

Fig. 3.11 Vehicle Design Synthesis Software Flowchart

3.5.1 Vehicle Synthesis Case Study

The results from a vehicle design synthesis are now described to illustrate the modeling, analysis, and design synthesis methods described in this chapter. The results are based on a steady-state analysis. Table 3.2 shows the parameters of the sample vehicle.

TABLE 3.2: Vehicle Parameters for Case Study

m=318 kg
ms=251 kg
muf=30.45 kg
mur=36.59 kg
kfaux=4000 Nm/rad
h=0.3048 m
huf=0.254 m
hur=0.0.2921 m
L=1.778 m
tf=1.257 m
tr=1.251 m
front tire: bias ply racing
rear tire: same as front, on wider rim

Front and rear chassis spring rates of 32.3 kN/m and 125 kN/m, respectively, are selected. The instantaneous roll center locations and roll stiffnesses for the front and rear suspensions are seen in Figs. 3.12 to 3.15. The results of the center of gravity finding procedure are seen in Figs. 3.16 and 3.17. It can be seen that the CG position for neutral handling gives the maximum limiting speed.

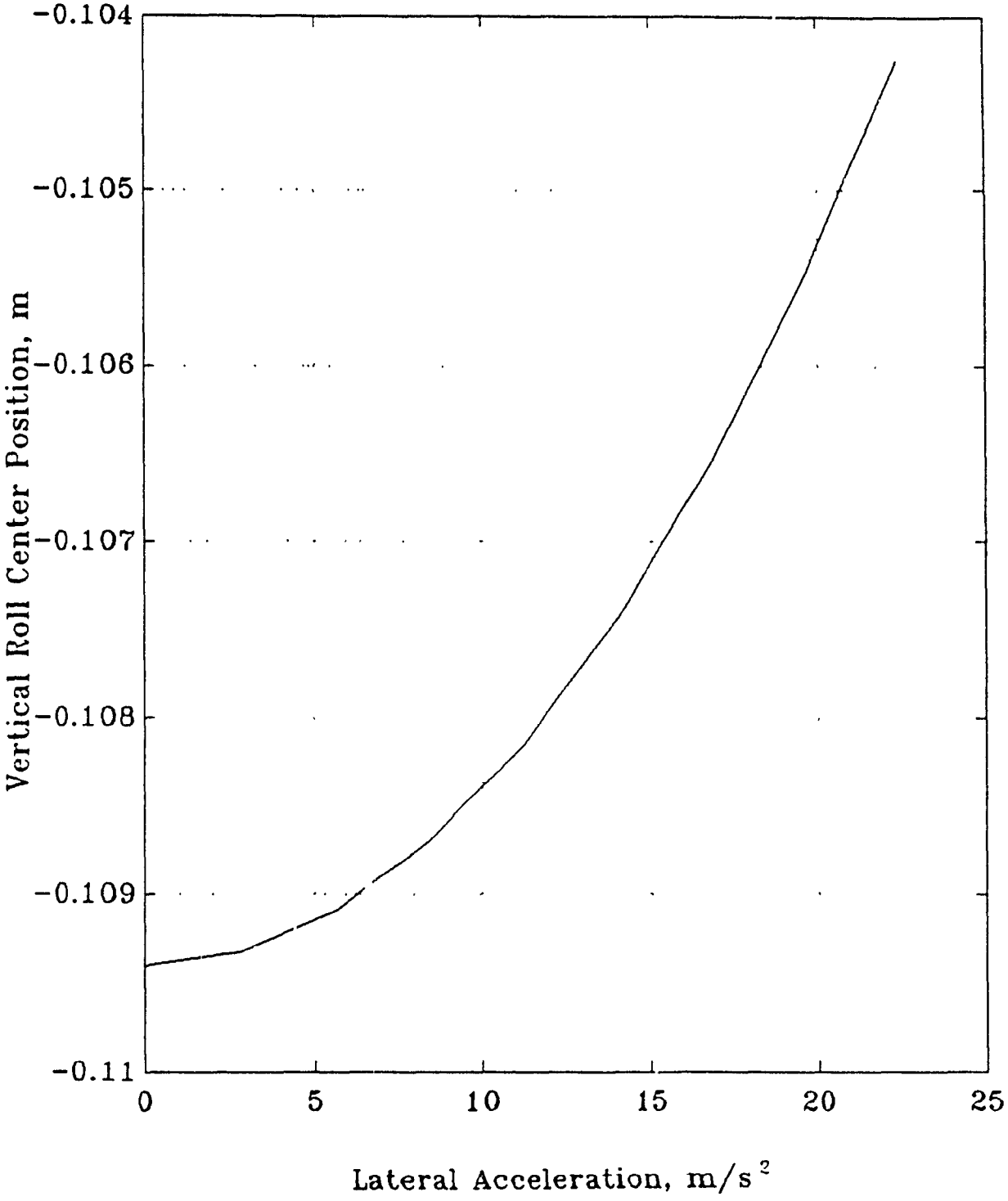

Fig. 3.12 Front Roll Center Height vs. Lateral Acceleration

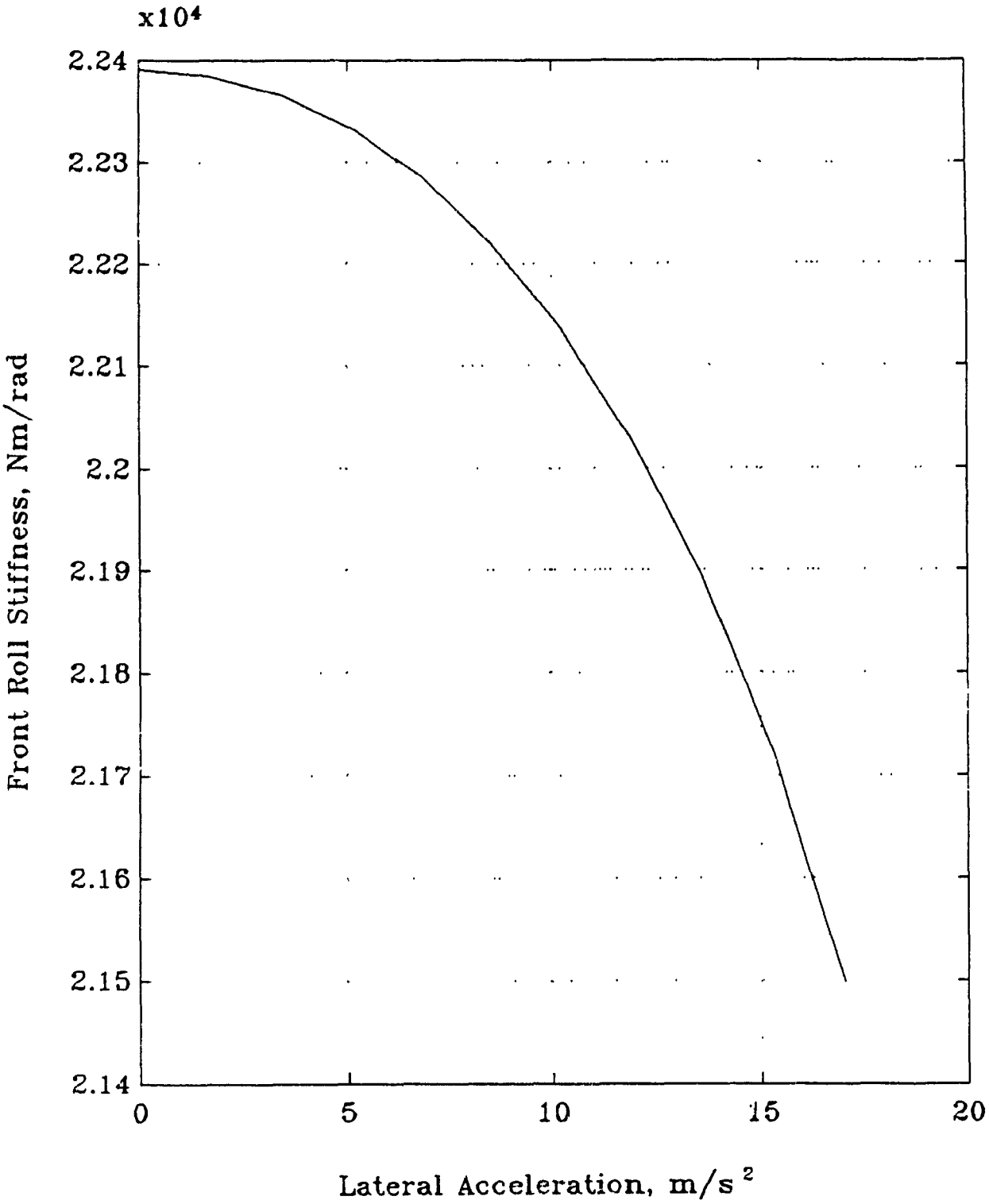

Fig. 3.13 Front Roll Stiffness vs. Lateral Acceleration

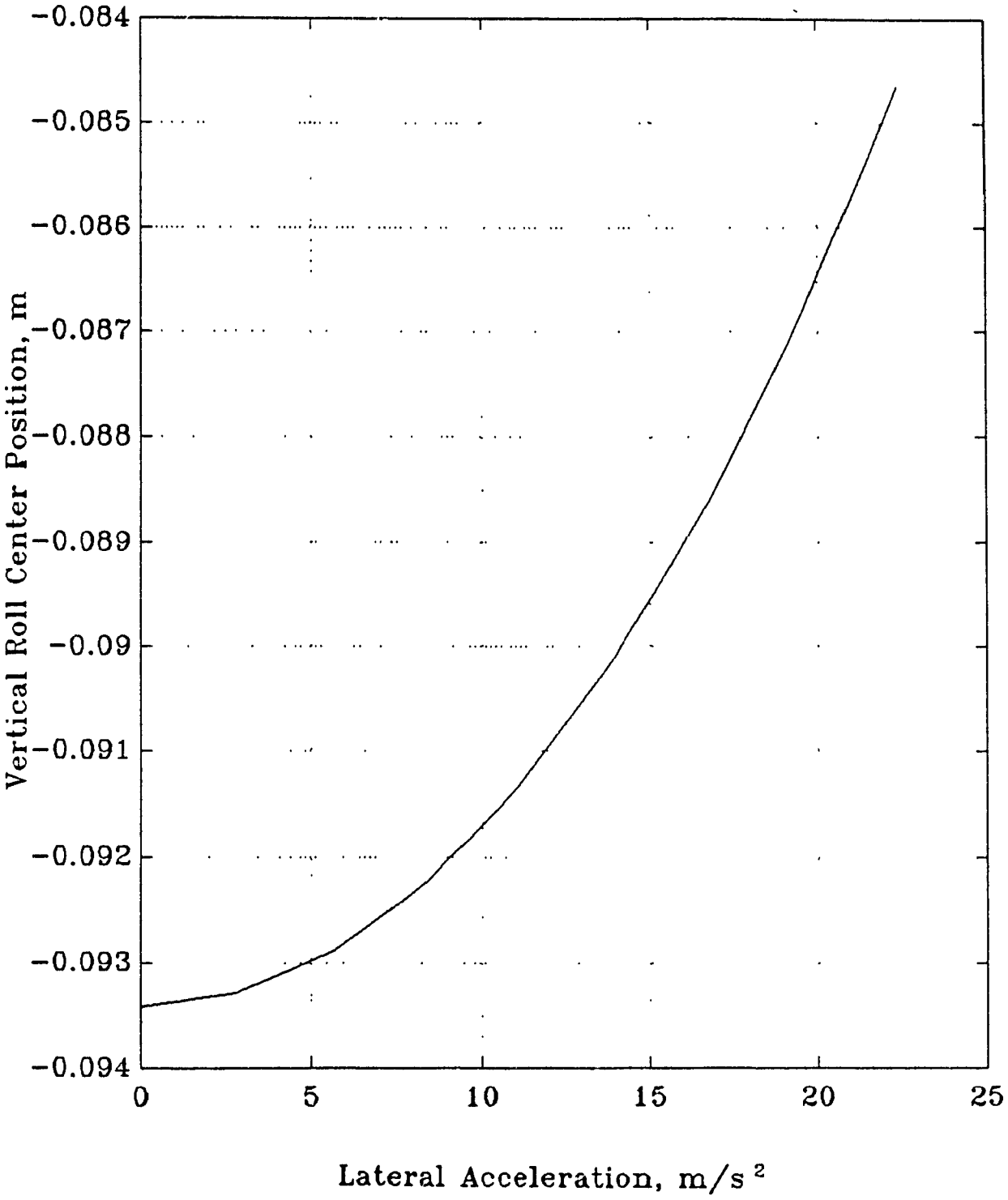

Fig. 3.14 Rear Roll Center Height vs. Lateral Acceleration

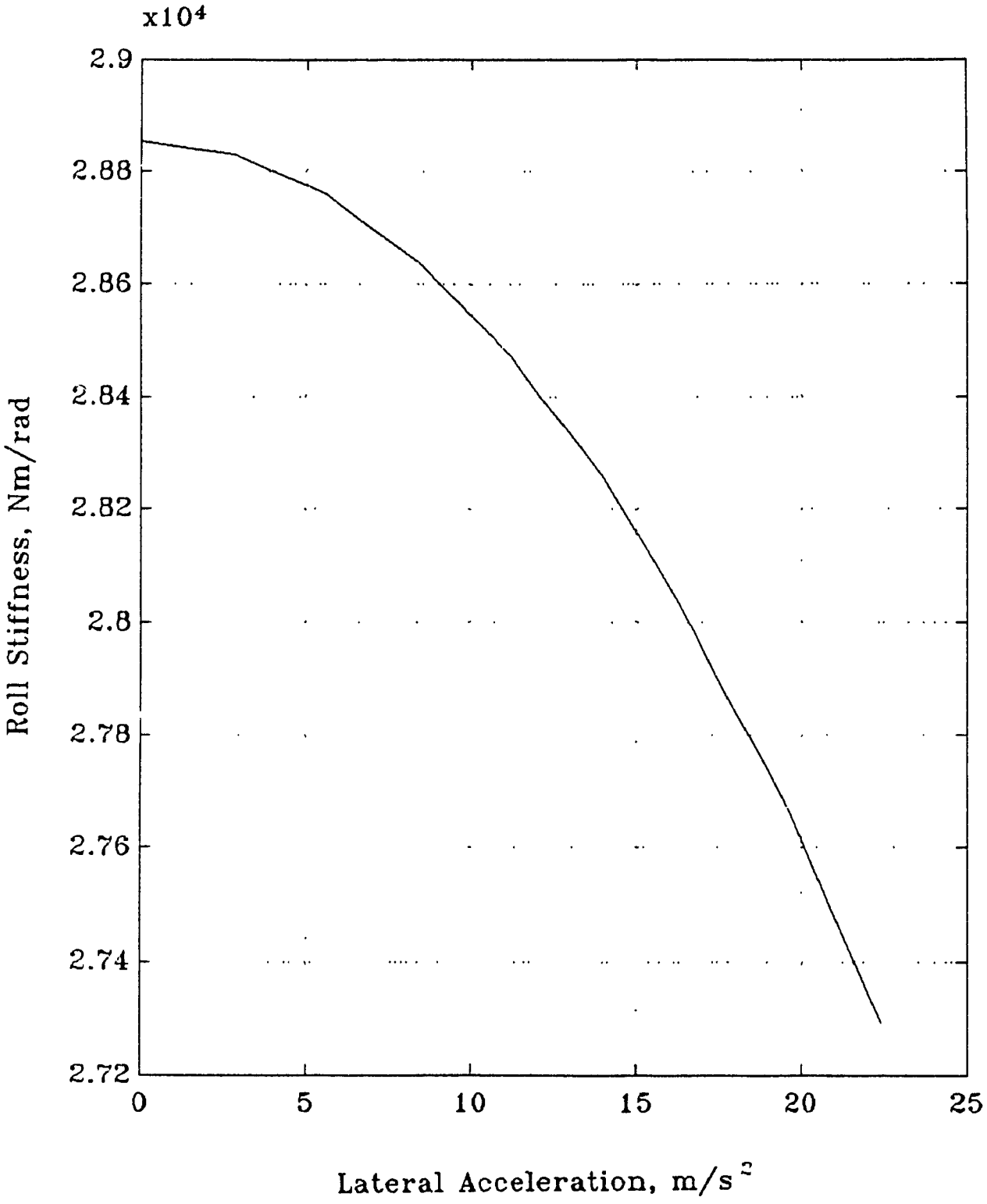

Fig. 3.15 Rear Roll Stiffness vs. Lateral Acceleration

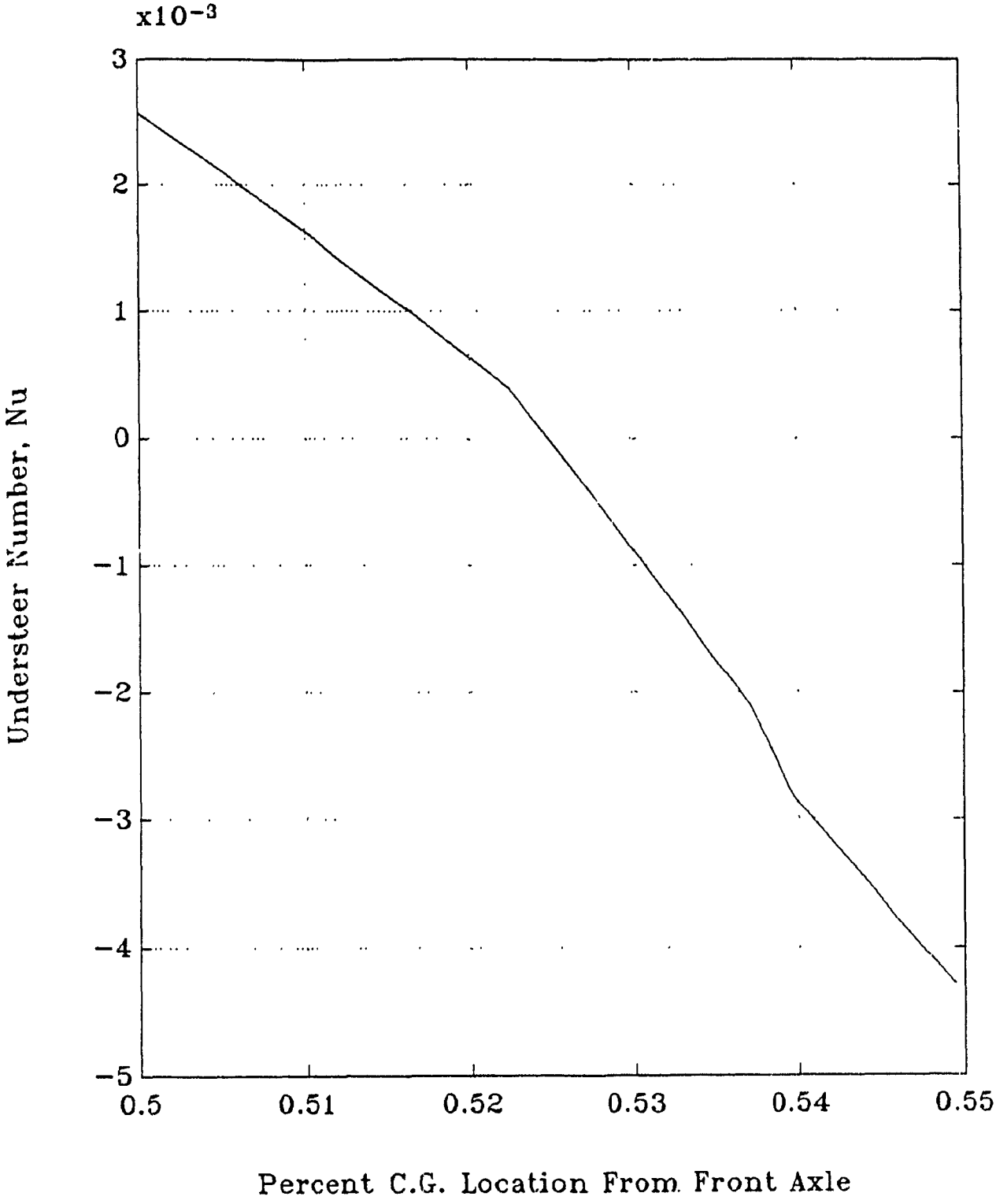

Fig. 3.16 Case Study: Understeer Number vs. CG Position

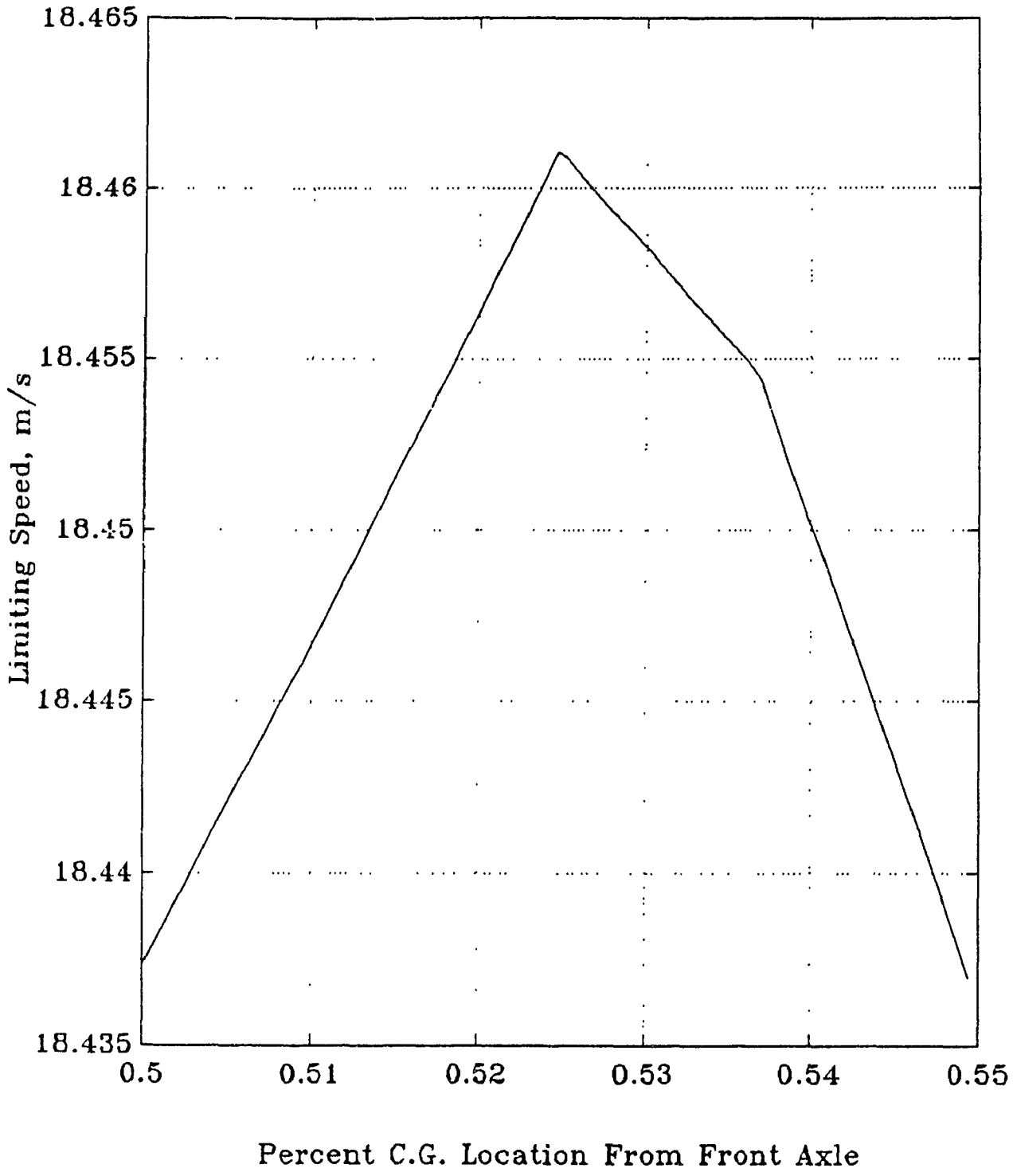

Fig. 3.17 Case Study: Limiting Speed vs. CG Position

3.6 Summary

This chapter has described the various stages of a design synthesis for the handling of a vehicle with pullrod A-arm suspension linkages. Each step of the procedure has been described in detail. The procedure is implemented as a MATLAB-based software. The software consists of four modules called CGFIND, SPRING, KINSTAT, and DYNAMIC. CGFIND computes the best center of gravity location. SPRING computes the chassis spring rates. KINSTAT computes the non-linear roll centers and roll stiffnesses. DYNAMIC computes the transient and steady-state handling response for the vehicle, taking into account the selected tire and chassis non-linearities.

CHAPTER 4

Case Studies of Vehicle Dynamic Analysis

4.1 General

A transient vehicle handling study is carried out in this chapter. The purpose of this study is to investigate transient response of a typical vehicle in order to gain confidence in the mathematical modeling, analysis, and design synthesis for handling and stability. A vehicle with typical parameters is selected, and the handling characteristics of such a vehicle are considered as the vehicle synthesis is carried out in steps.

The first step is to test the mathematical model. At this stage the handling model uses a linearized tire model.

The next step is to add the non-linear tire model to the vehicle handling model. This step will show how the handling response of a vehicle is influenced by a tire model that is a function of normal load, slip angle and camber angle.

The subsequent step is to carry out kinematic and kineto-static suspension analysis in order to evaluate velocity coefficients and to incorporate them in the calculation of non-linear roll centers and roll stiffnesses in the vehicle handling model.

The final step is to perform a parametric study using the fully developed vehicle handling model. Relevant design parameters are varied and the effects on the vehicle handling and stability responses are demonstrated.

4.2 Linear 3DOF Vehicle Model (CASE1)

This example is used to verify the mathematical model of the vehicle and the solution procedure of the equations of motion. The vehicle example, as specified in Table 4.1, is taken from Ellis [31]. In Ellis, the vehicle's steady-state response was solved by Laplace transforms. In CASE1, the same problem is solved as described in Section (3.4.5) and the results are compared.

TABLE 4.1: CASE1: VEHICLE MODEL PARAMETERS

m	= 874.2	kg
ms	= 773.5	kg
Ix	= 276.6	kg*m²
Iz	= 1027.6	kg*m²
Pxz	= -11.25	kg*m²
h	= 0.2987	m
hf	= 0.287	m
hr	= 0.116	m
a	= 1.28	m
b	= 0.817	m
ASTFf	= 769	Nm/rad
ASTFr	= 1242	Nm/rad
INSTFf	= 2349	N/rad
INSTFr	= 3932	N/rad
RCBRf	= 0.07	rad/rad
RCBRr	= 0.62	rad/rad
U	= 30.48	m/s
δ	= 0	rad
Cf	= -29089.9	N/rad
Cr	= -42700.8	N/rad
Lphi	= -30889.7	Nm/rad
Lp	= -2093.7	Nm/rad/s

where ASTFf = aligning stiffness of both front tires
ASTFr = aligning stiffness of both rear tires
INSTFf = inclination stiffness of both front tires
INSTFr = inclination stiffness of both rear tires
RCBRf = roll camber change of both front tires
RCBRr = roll camber change of both rear tires
Cf = cornering stiffness for both front tires
Cr = cornering stiffness for both rear tires
h = Z-distance from roll axis to sprung mass CG

The equations of motion used in this validation differ slightly from equations (3.3), in that the P_{xz} product of inertia is included [31]:

$$\begin{aligned} \Sigma Y &= m(\dot{V}+Ur)+m_s h\dot{p} \\ \Sigma N &= I_z\dot{r}-P_{xz}\dot{p} \\ \Sigma L_s &= m_s h(\dot{V}+Ur)-P_{xz}\dot{r}+I_x\dot{p} \end{aligned} \qquad (4.1)$$

A step input has been applied to the vehicle in the form of aerodynamic forces and moments representing a wind gust with initial conditions as zero. The inputs are as follows:

Lateral Aero Force = 786.4 N

Aero Yawing Moment = 366.6 Nm

Aero Rolling Moment = 503.1 Nm

These inputs are added to the external force and moment equations. The force and moment equations used here differ from those presented in equation (3.5):

$$\begin{aligned} \Sigma Y &= Y_v V+Y_r r+Y_\theta\theta+Y_\delta\delta+Lateral\ Aero\ Force \\ \Sigma N &= N_v V+N_r r+N_\theta\theta+N_\delta\delta+Aero\ Yawing\ Moment \\ \Sigma L_s &= L_\theta\theta+L_p p+Aero\ Rolling\ Moment \end{aligned} \qquad (4.2)$$

where

$$
\begin{aligned}
Y_v &= (Cf+Cr)/U \\
N_v &= (a*Cf-b*Cr+ASTFf+ASTFr)/U \\
Y_r &= (a*Cf-b*Cr)/U \\
N_r &= (a^2*Cf+b^2*Cr+a*ASTFf-b*ASTFr)/U \\
Y_\theta &= INSTFr*RCBRf+INSTFr*RCBRr \\
N_\theta &= a*INSTFf*RCBRf-b*INSTFr*RCBRr \\
L_\theta &= -30890 \\
Y_\delta &= -Cf \\
N_\delta &= -a*Cf \\
L_p &= -2093.7
\end{aligned}
\tag{4.3}
$$

It should be noted that the aerodynamic inputs representing a wind gust remain the same throughout the simulation. This implies that the wind direction relative to the car remains the same as the car is yawing, which means that the wind direction has the same yaw velocity as the car. While this is not a physically realistic case, the example was used for comparison purposes.

Figures 4.1, 4.2, and 4.3 compare the calculated results to the published results. The solid lines represent the numerically-obtained response, whereas the dotted line is Ellis' response. The offset evident between the numerical solution and Ellis' solution is due to the selection of zero initial conditions for the numerical solution. The numerical solution was repeated with initial conditions identical to Ellis' solution and the transient response in both cases

agreed more closely. More specifically, the transient response for the lateral velocity and the yaw angular velocity agreed very closely. The peak transient response for the sprung mass roll angle was lower by approximately 10 percent for CASE1 when compared to the reference response. The steady-state solutions for the revised initial conditions continued to have a difference of 8 percent, 2 percent and 7 percent, respectively, for the lateral velocity, yaw velocity, and roll angle.

It is clear that the trends for both sets of responses are the same, and that the agreement of the results is generally good. It can be concluded that the solution procedure for the 3DOF mathematical vehicle dynamic model is valid.

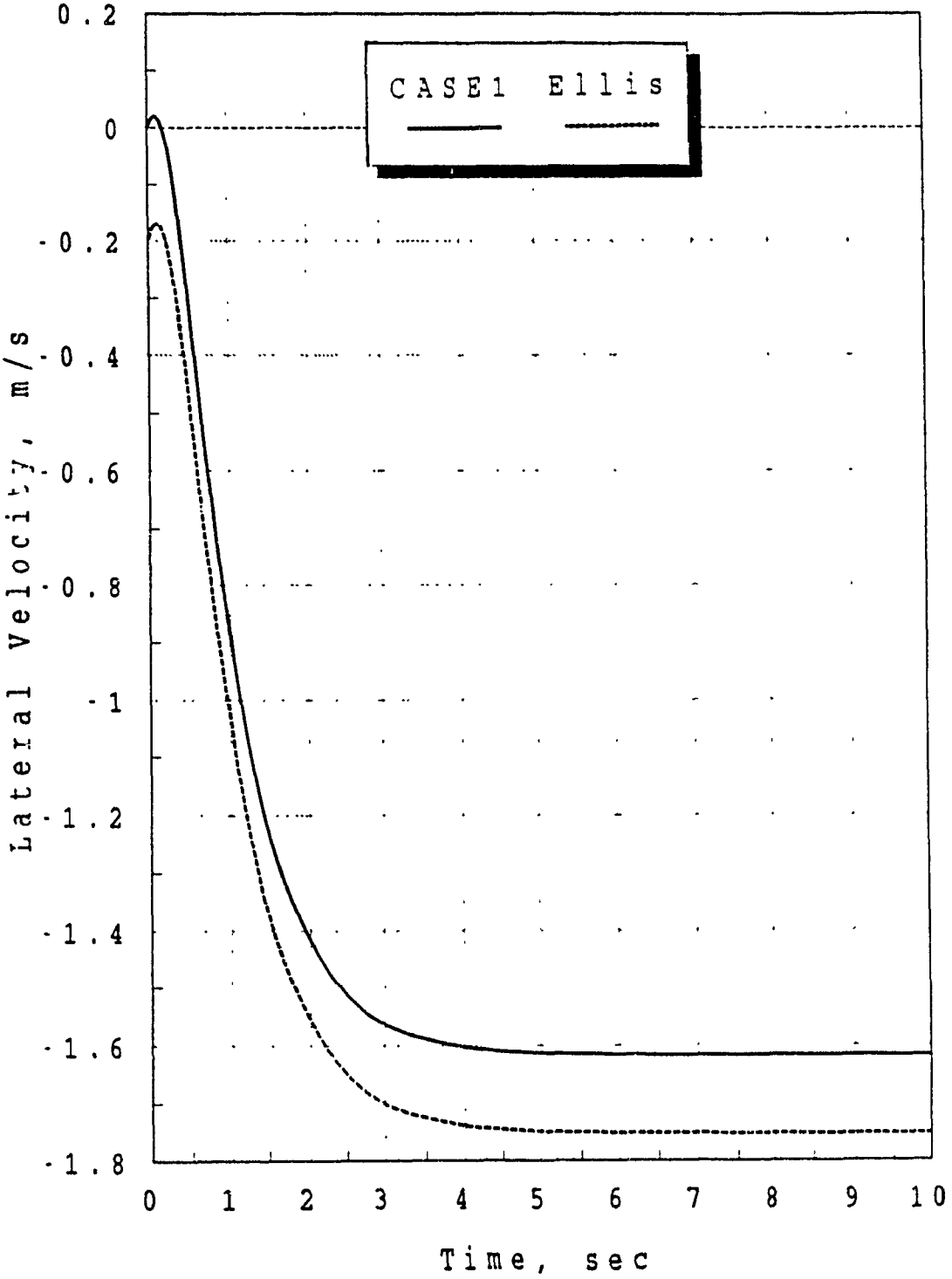

Fig. 4.1 CASE1 Lateral Velocity vs. Time

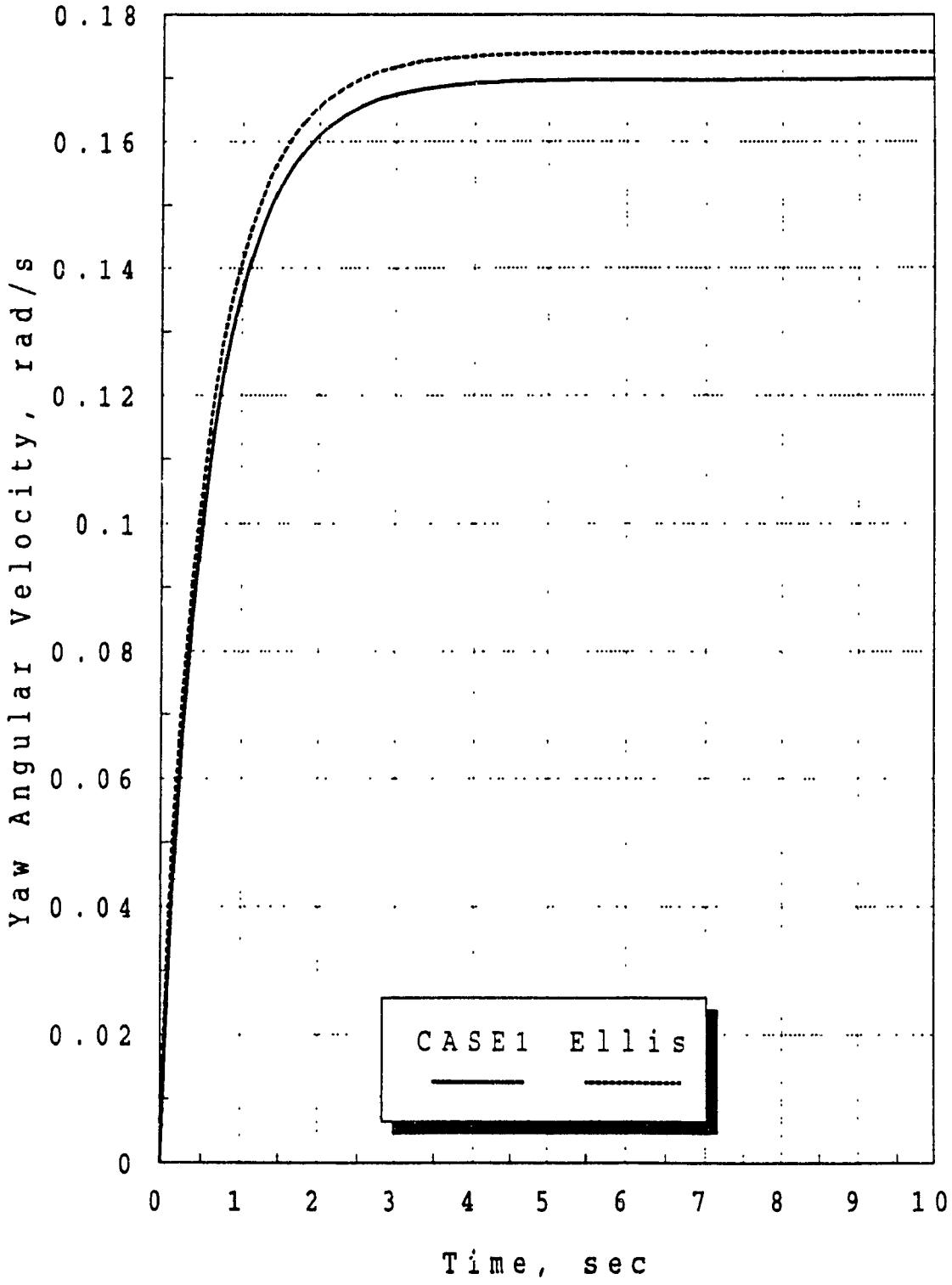

Fig. 4.2 CASE1 Yaw Angular Velocity vs. Time

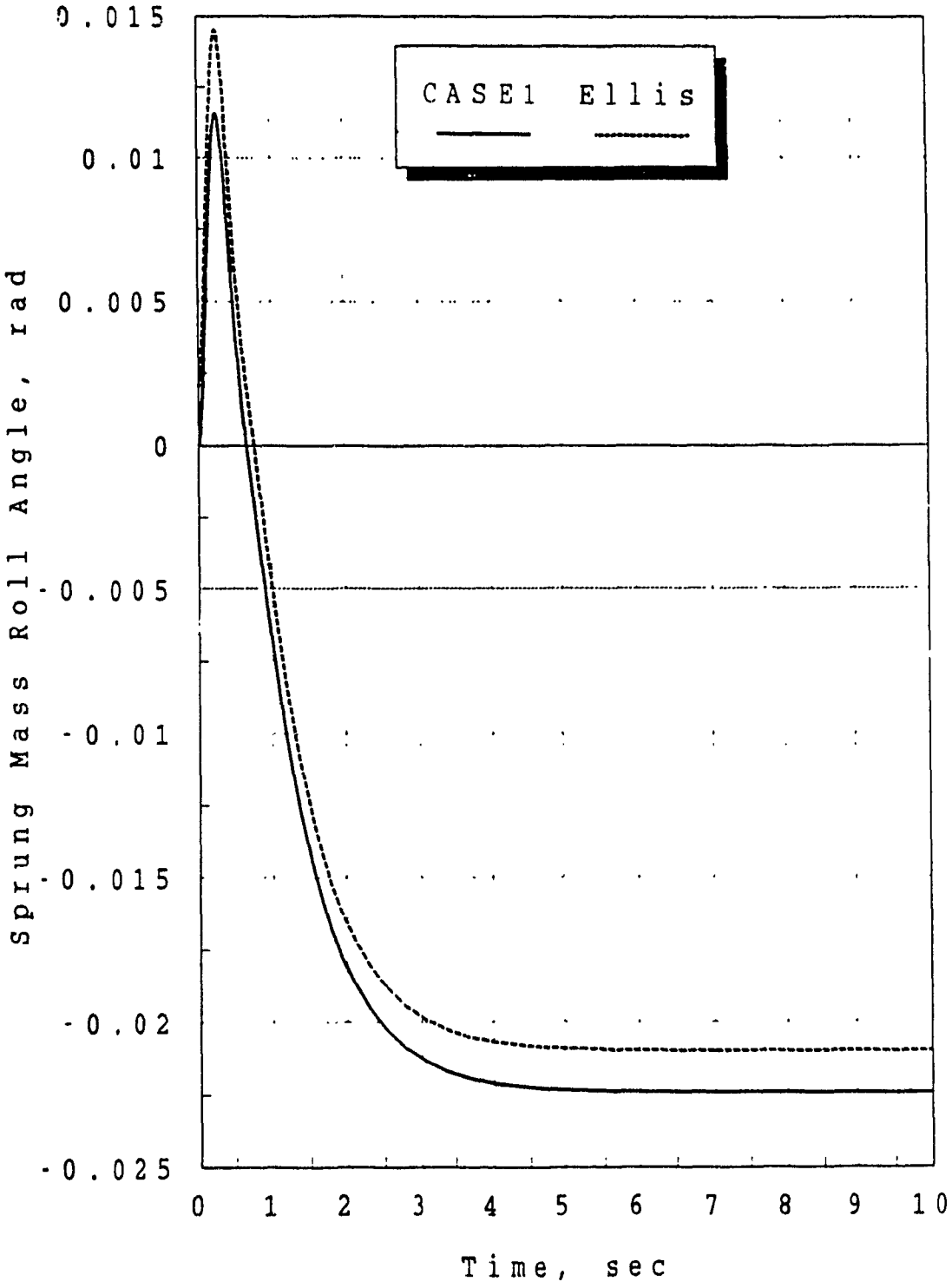

Fig. 4.3 CASE1 Sprung Mass Roll Angle vs. Time

4.3 3DOF Vehicle Model With Nonlinear Tire (CASE2)

This section will demonstrate the vehicle handling model incorporating the non-linear tire. The linear tire coefficients used in the previous section are replaced by Pacejka's tire model. The camber angle has been fixed at zero. Full lateral weight transfer has been included. Table 4.2 shows the changes in the vehicle model parameters.

TABLE 4.2: CASE2: VEHICLE MODEL PARAMETERS

m	= 874.2	kg
ms	= 773.5	kg
muf	= 45.0	kg
mur	= 55.7	kg
Ix	= 276.6	kg*m²
Iz	= 1027.6	kg*m²
Pxz	= -11.25	kg*m²
h	= 0.4813	m
hra	= 0.2987	m
huf	= 0.3048	m
hf	= 0.287	m
hur	= 0.3048	m
hr	= 0.116	m
a	= 1.28	m
b	= 0.817	m
tf	= 1.257	m
tr	= 1.251	m
ASTFf	= 769	Nm/rad
ASTFr	= 1242	Nm/rad
INSTFf	= 2349	N/rad
INSTFr	= 3932	N/rad
RCBRf	= 0.07	rad/rad
RCBRr	= 0.62	rad/rad
U	= 30.48	m/s
δ	= 0	rad
kf	= 15445	Nm/rad
kr	= 15445	Nm/rad
Lphi	= -30889.7	Nm/rad
Lp	= -2093.7	Nm/rad/s

The external forces differ from equations (4.2) and (4.3) as follows:

$$\begin{aligned}
\Sigma Y &= (INSTFf*RCBRf + INSTFr*RCBRr)\,p \\
&\quad + F_{yfo} + F_{yfi} + F_{yro} + F_{yri} \\
\Sigma N &= (a*INSTFf*RCBRf - b*INSTFr*RCBRr)\,\theta \\
&\quad + \delta*ASTFf \\
&\quad + a(F_{yfo} + F_{yfi}) - b(F_{yro} + F_{yri}) \\
&\quad + M_{zfo} + M_{zfi} + M_{zro} + M_{zri} \\
\Sigma L_s &= L_\theta\theta + L_p p
\end{aligned} \tag{4.4}$$

The step aerodynamic input of CASE1 was used again with zero initial conditions . The response of the 3DOF vehicle model to the aerodynamic input is found in Figs. 4.4 to 4.9. The solid lines refer to the Pacejka tire-shod vehicle, while the dotted lines are the responses from CASE1.

It is apparent that the 3DOF vehicle with the non-linear tire is less sensitive to the wind disturbance. The steady-state y-position and the yaw and roll angles are smaller, and the vehicle with the non-linear tire is quicker to reach a steady-state in sideslip, yaw and roll. A possible explanation for this is that the Pacejka tire model includes saturation of lateral force and self aligning torque, whereas the cornering stiffness and aligning stiffness constants used in Ellis' example do not account for saturation. In addition, the Pacejka tire is much stiffer in its linear range than the tire cornering stiffness used by Ellis.

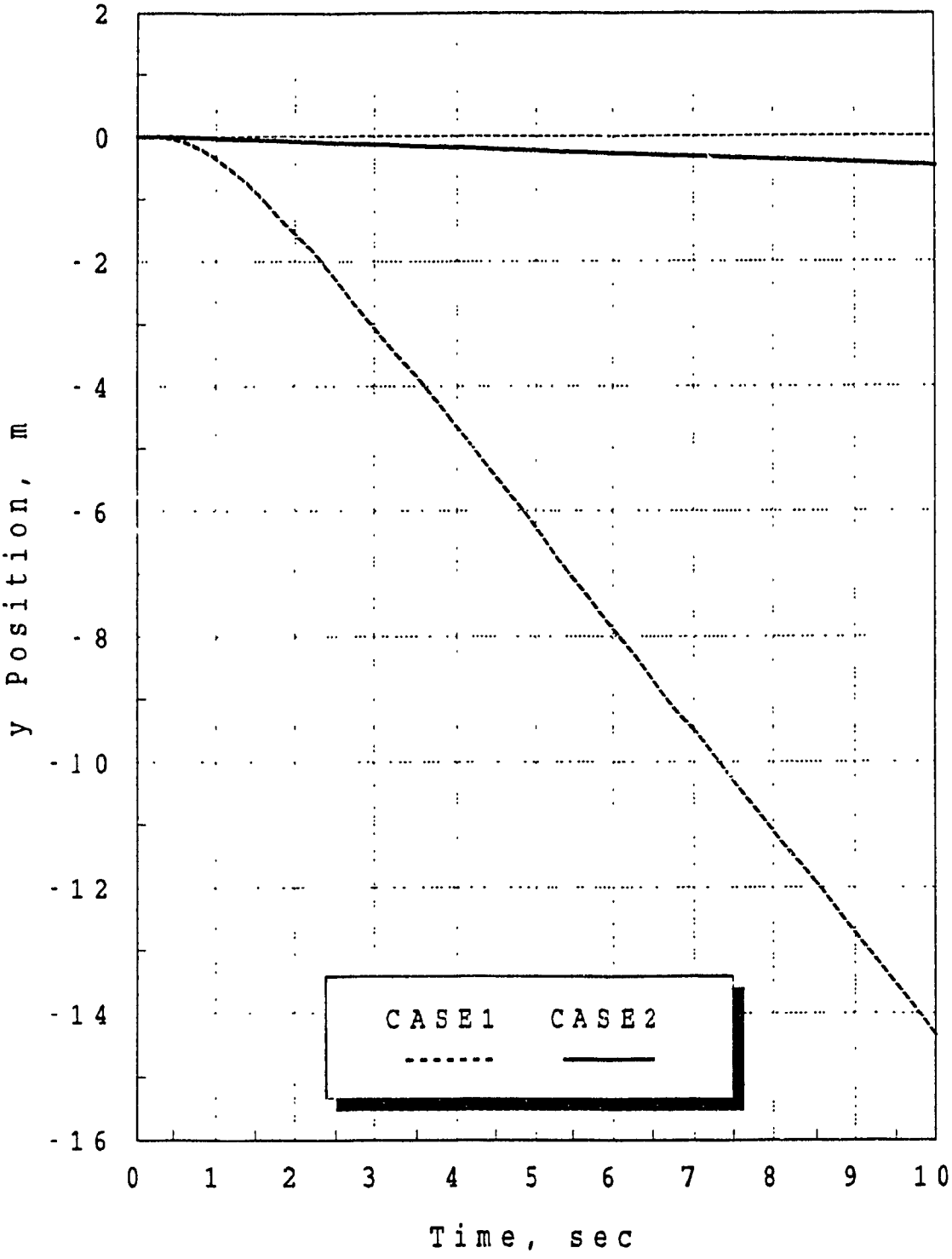

Fig. 4.4 CASE2 y Position vs. Time

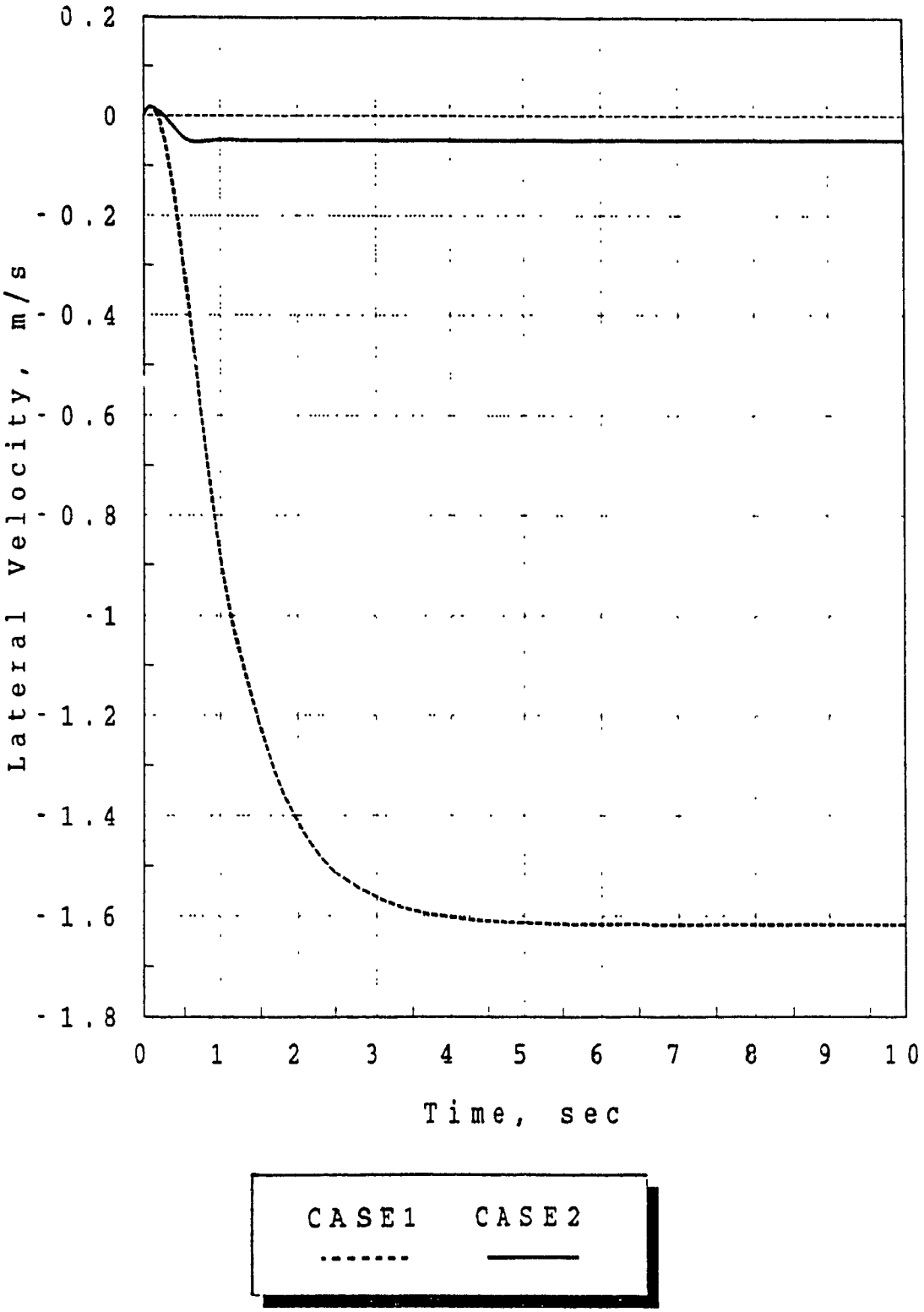

Fig. 4.5 CASE2 Lateral Velocity vs. Time

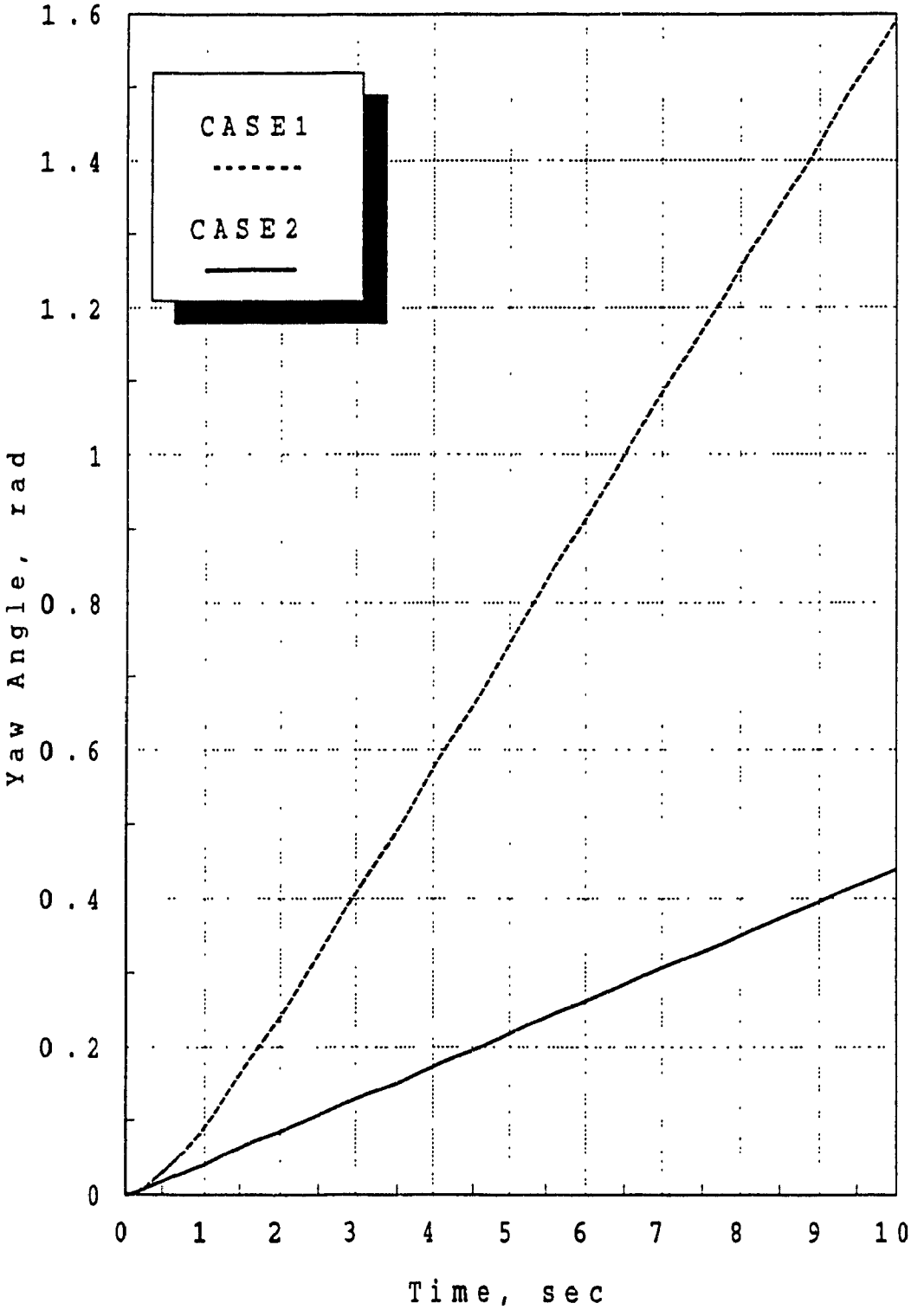

Fig. 4.6 CASE2 Yaw Angle vs. Time

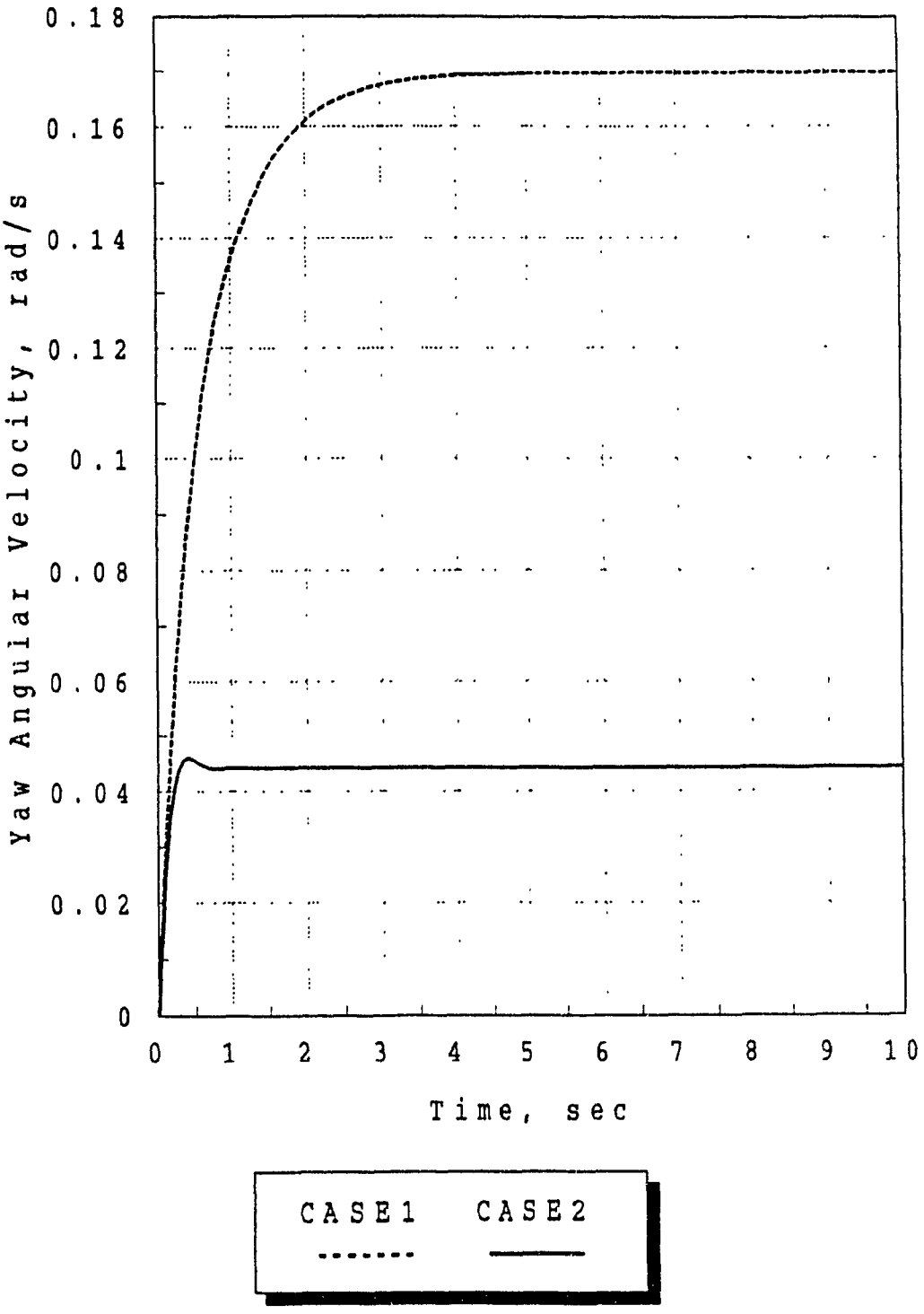

Fig. 4.7 CASE2 Yaw Angular Velocity vs. Time

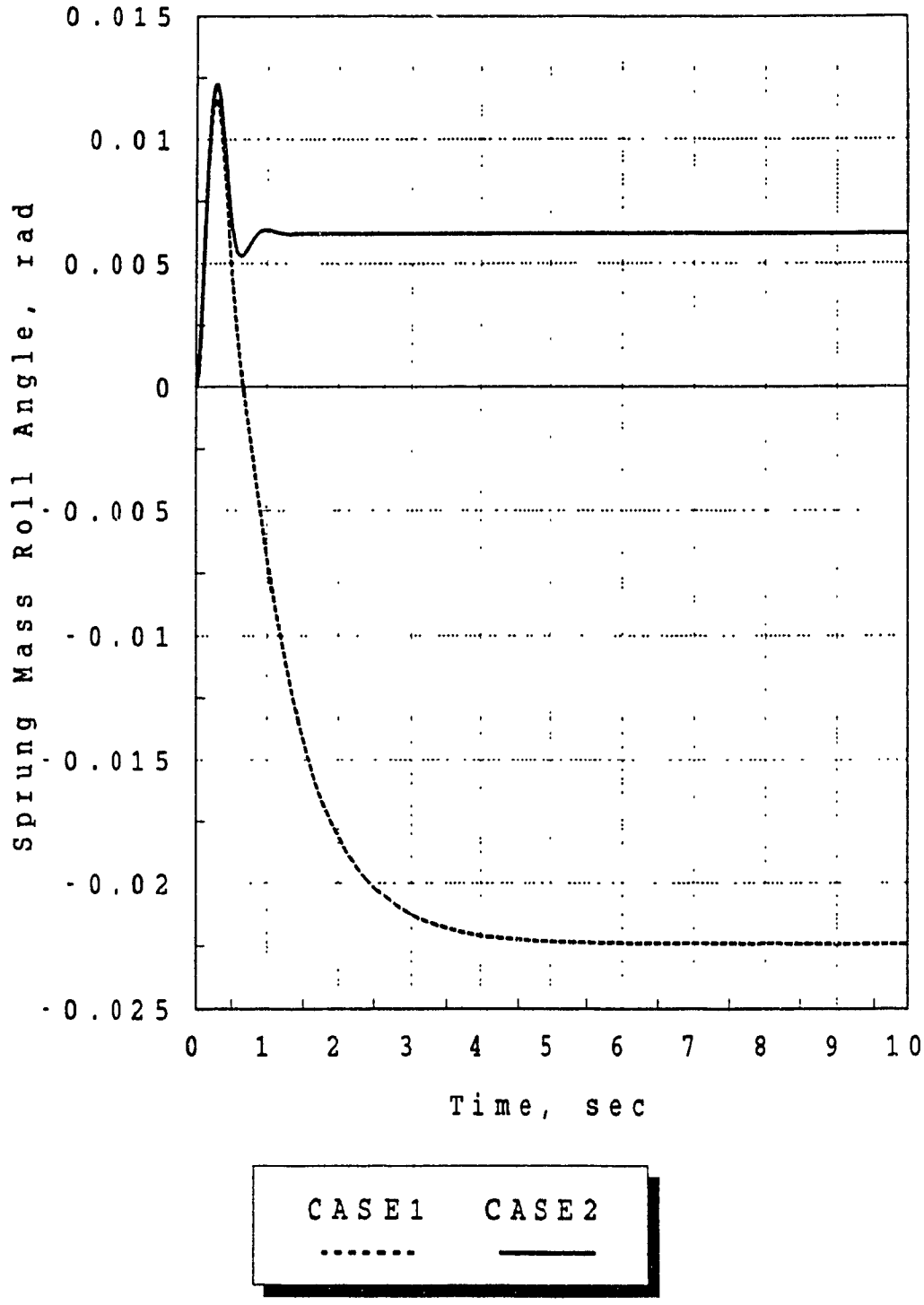

Fig. 4.8 CASE2 Sprung Mass Roll Angle vs. Time

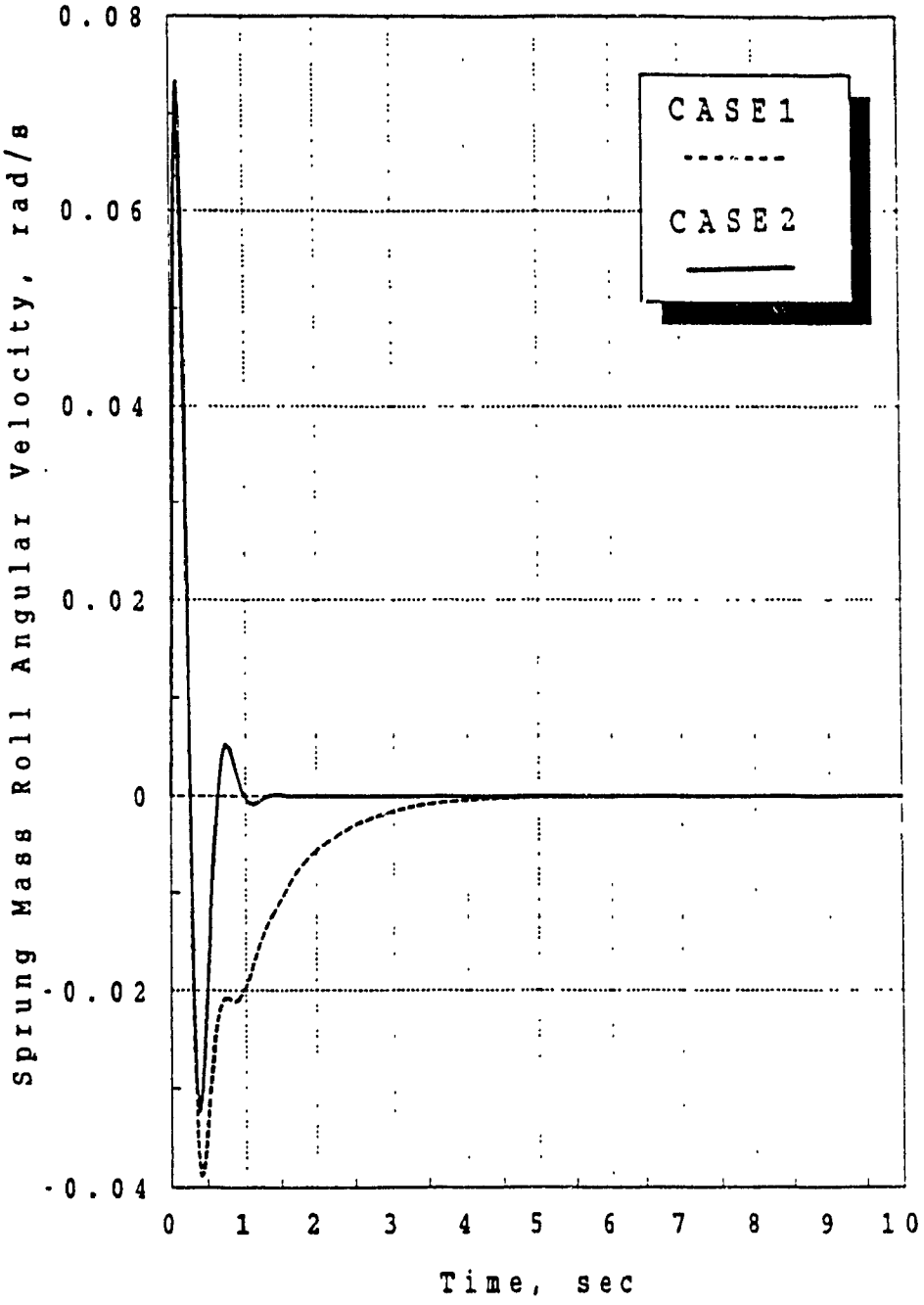

Fig. 4.9 CASE2 Sprung Mass Roll Angular Velocity vs. Time

4.4 3DOF Vehicle Model With Camber Change (CASE3)

Camber change effects are now included in the 3DOF vehicle model with a nonlinear tire. The 3DOF vehicle model used in this case is identical to the one used in CASE2. The nonlinear tire model is the same Pacejka sinusoidal model as used in CASE2, with the exception that the tire lateral force and self aligning torque is now a function of normal load, slip angle and camber angle.

The characteristics of the sprung mass roll angle vs. wheel camber change were found by performing a kineto-static analysis using KINSTAT. The kineto-static analysis results for the front and rear suspensions are found in Figs. 4.10 to 4.13.

Comparing the new vehicle response (solid lines) to that of CASE2 (dotted lines) in Figs. 4.14 to 4.19, it can be seen that the vehicle model used here is sensitive to camber change. The handling response in terms of number of oscillations and the time to reach steady-state is similar. However, the transient and steady-state response magnitudes for CASE3 are considerably higher than those of CASE2. A vehicle handling and stability analysis that neglected camber change would underestimate vehicle performance, especially lateral acceleration, path followed, and yaw response.

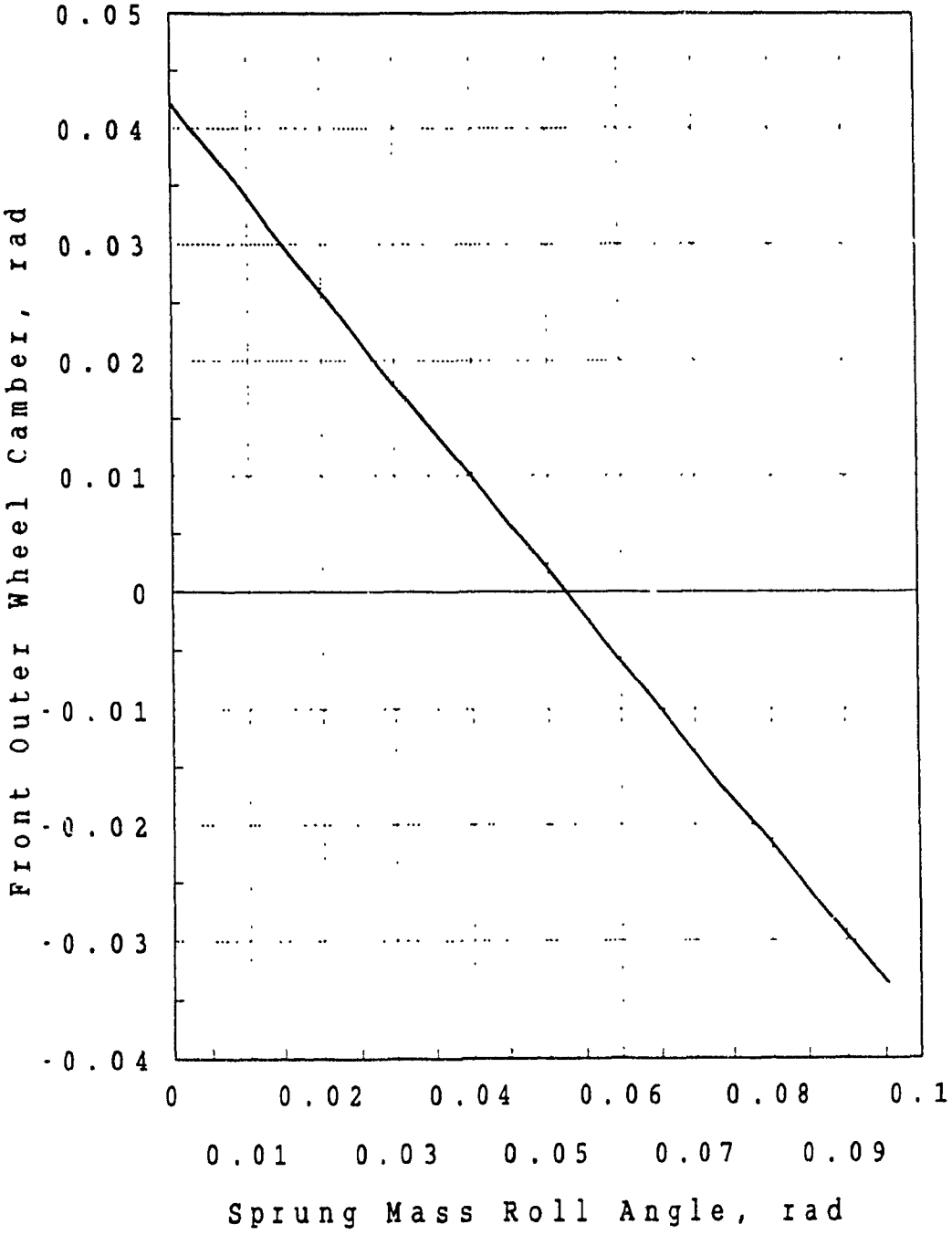

Fig. 4.10 Sprung Mass Roll Angle vs. Front Outer Camber

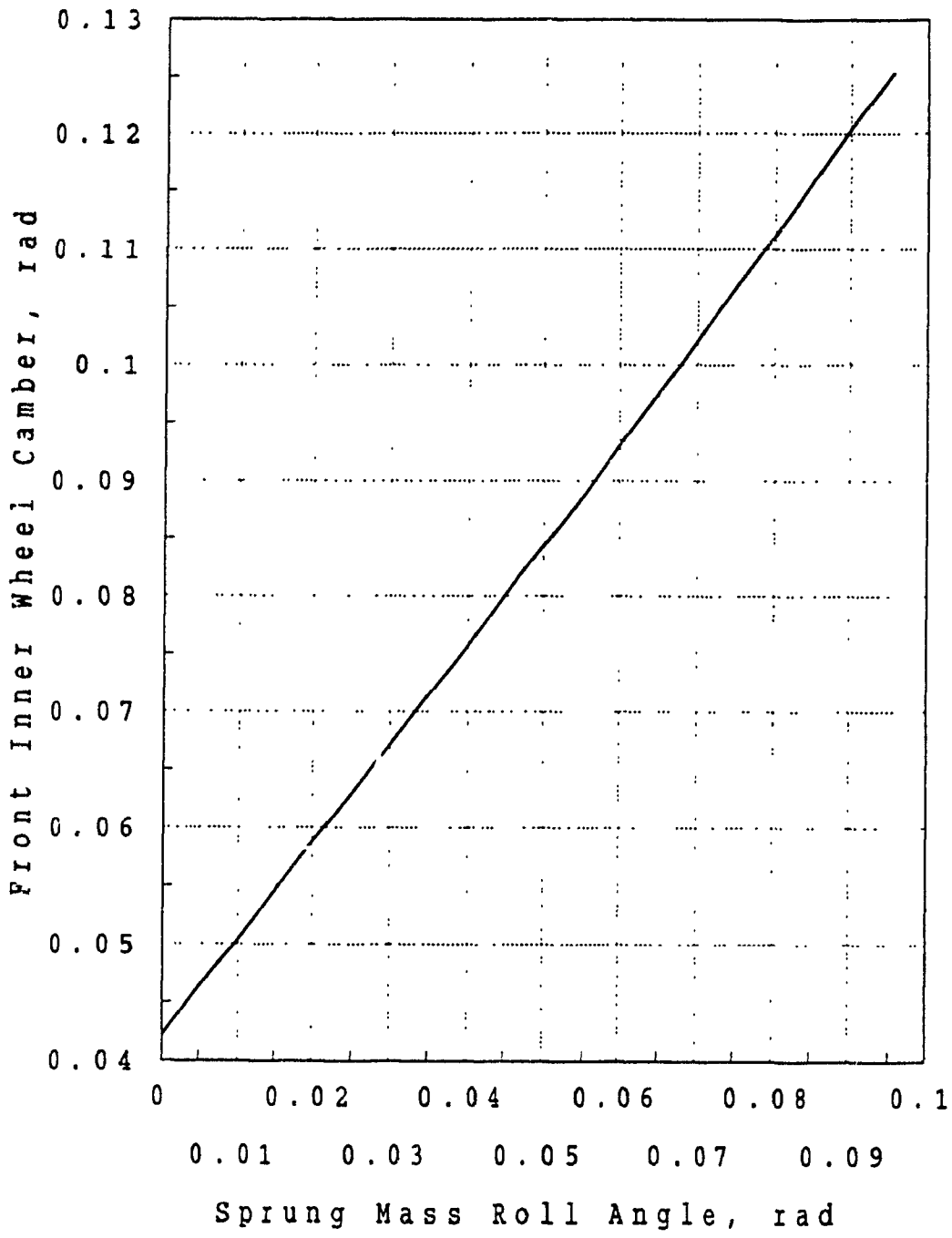

Fig. 4.11 Sprung Mass Roll Angle vs. Front Inner Camber

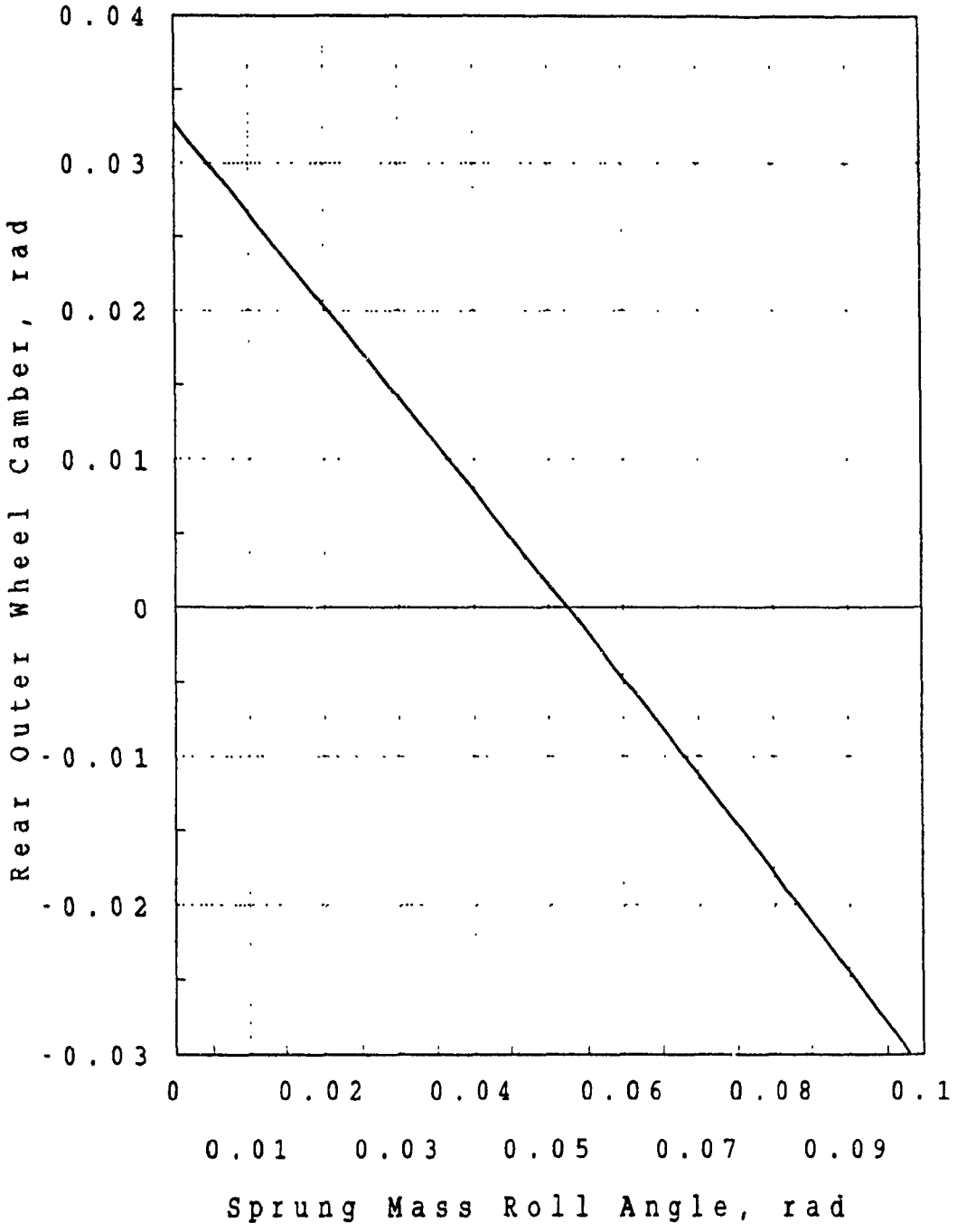

Fig. 4.12 Sprung Mass Roll Angle vs. Rear Outer Camber

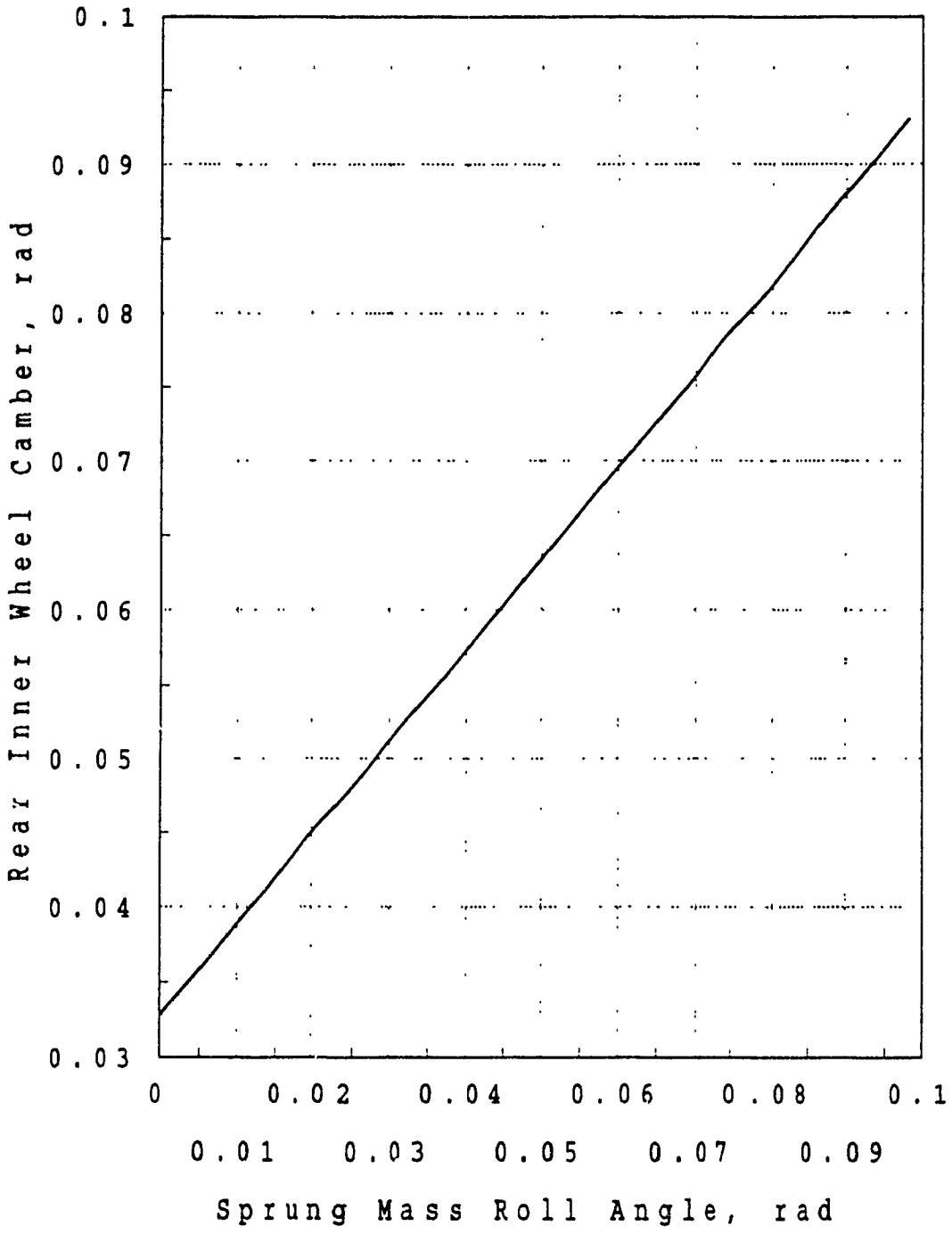

Fig. 4.13 Sprung Mass Roll Angle vs. Rear Inner Camber

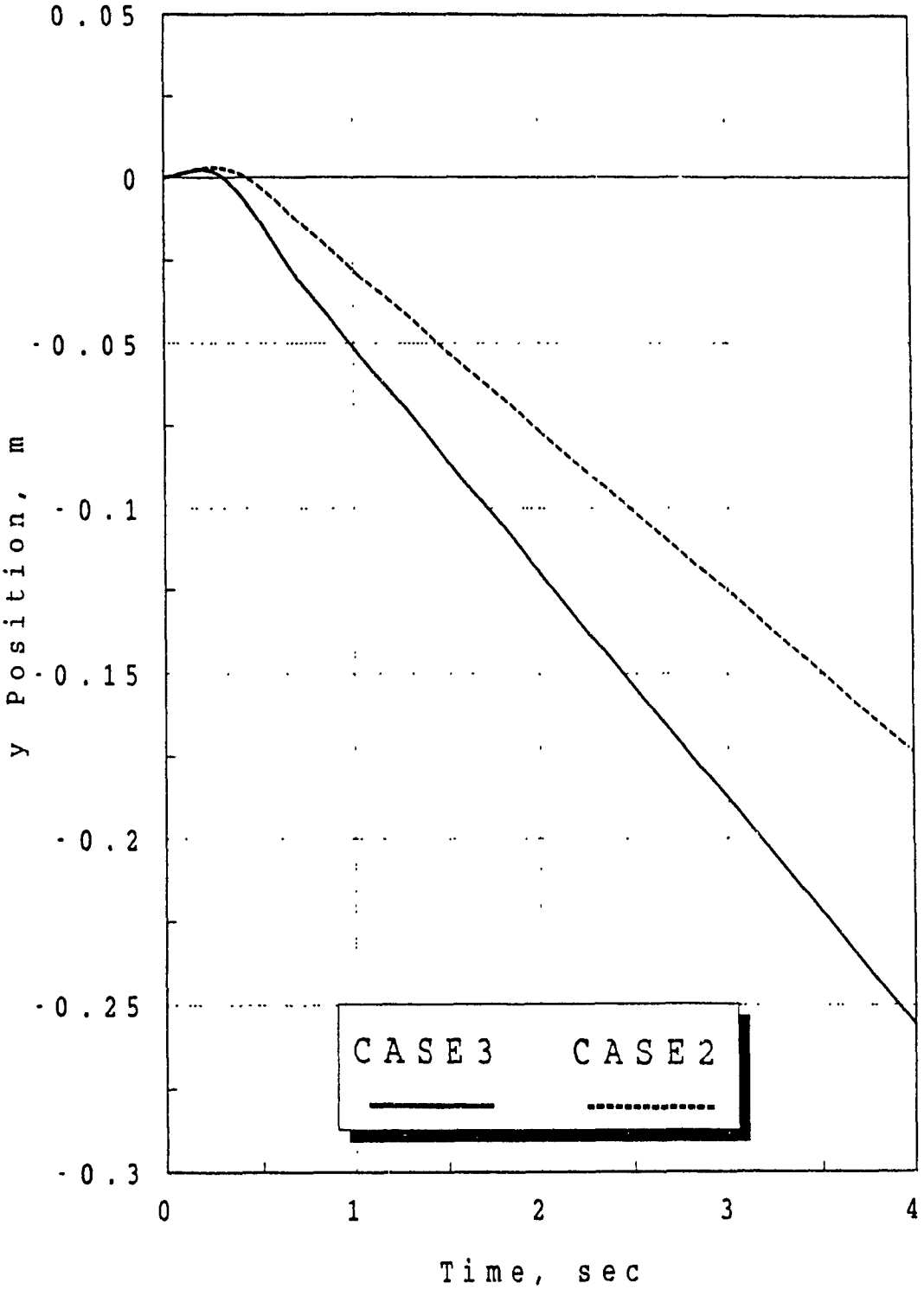

Fig. 4.14 CASE3 y Position vs. Time

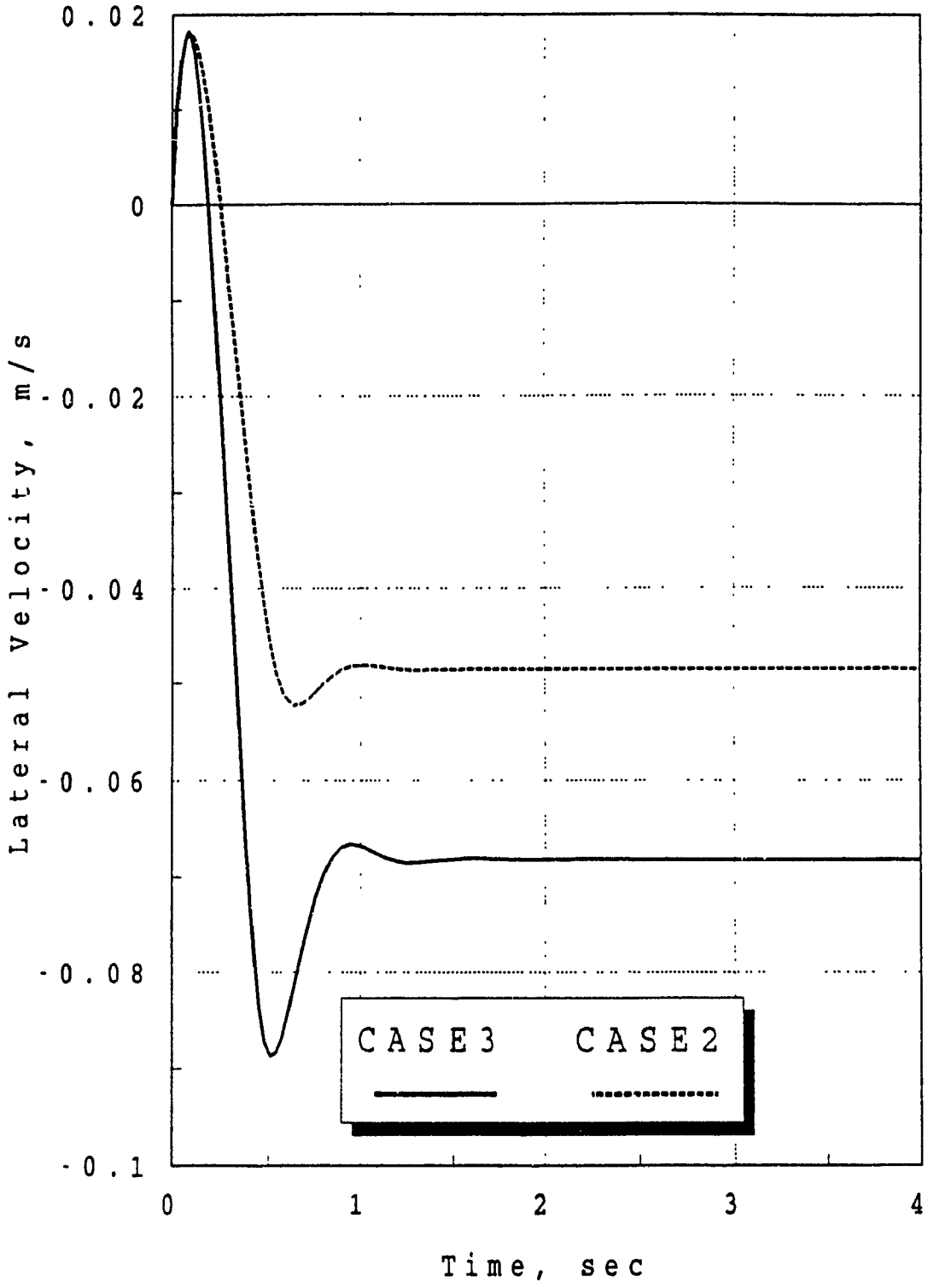

Fig. 4.15 CASE3 Lateral Velocity vs. Time

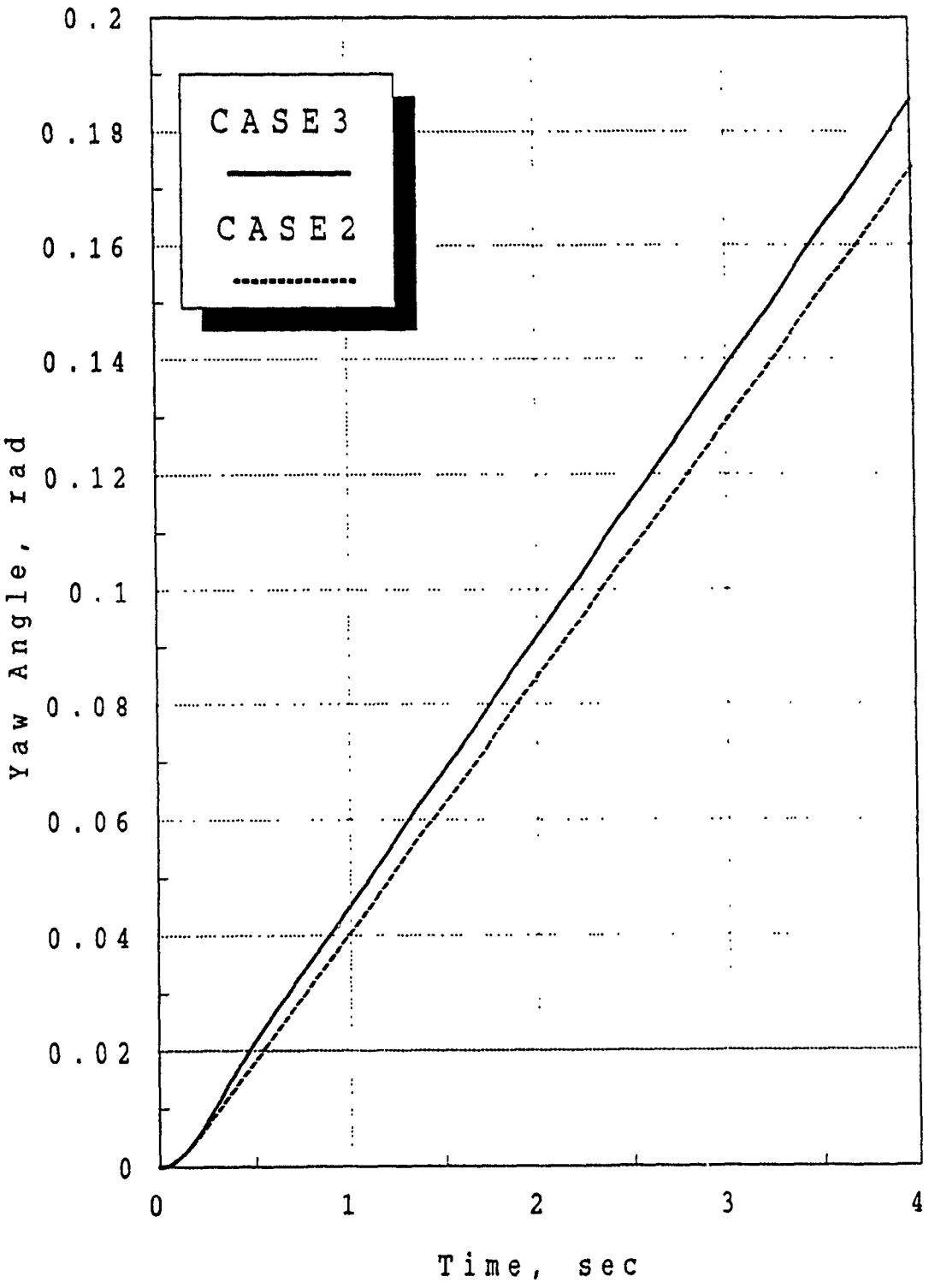

Fig. 4.16 CASE3 Yaw Angle vs. Time

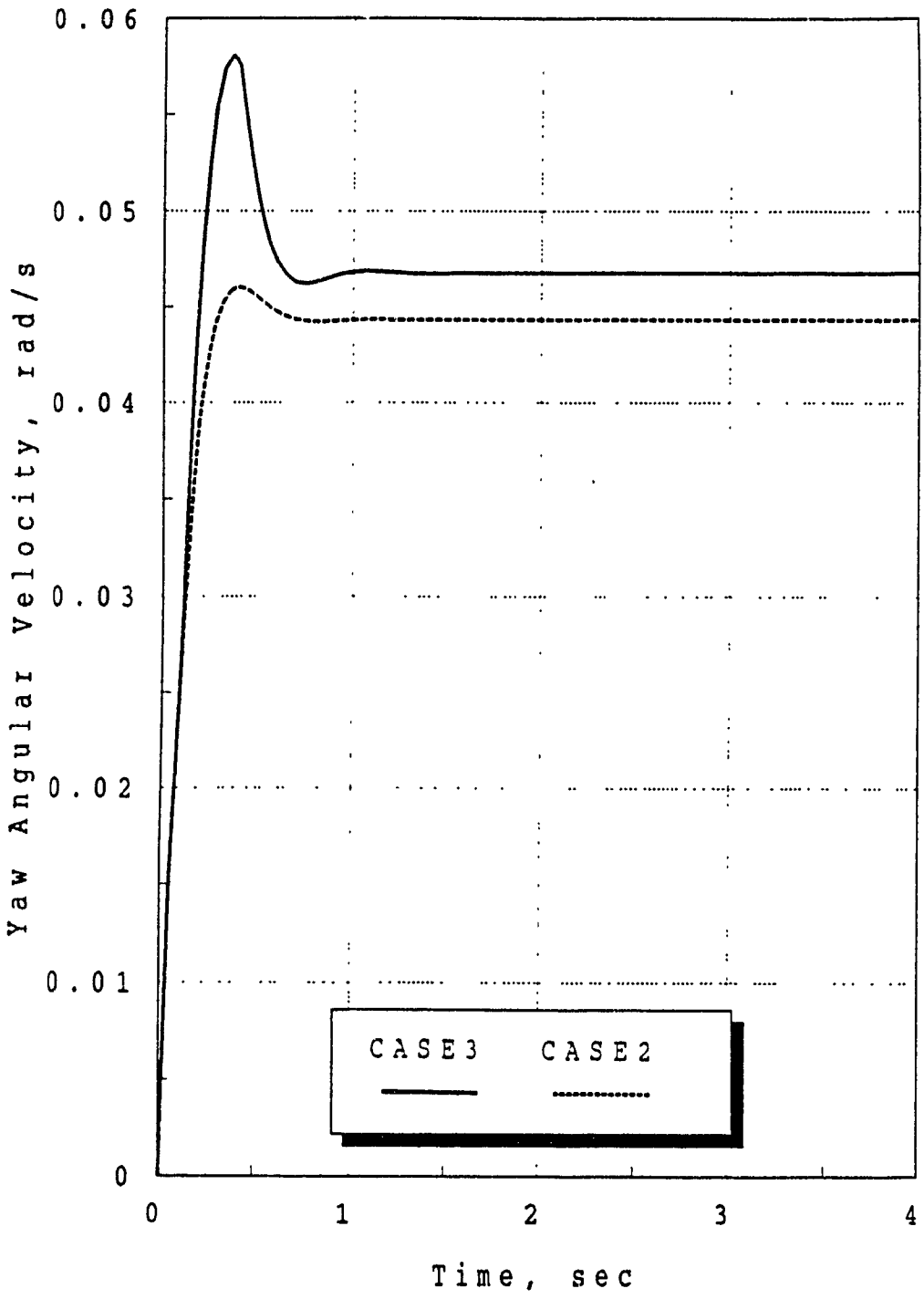

Fig. 4.17 CASE3 Yaw Angular Velocity vs. Time

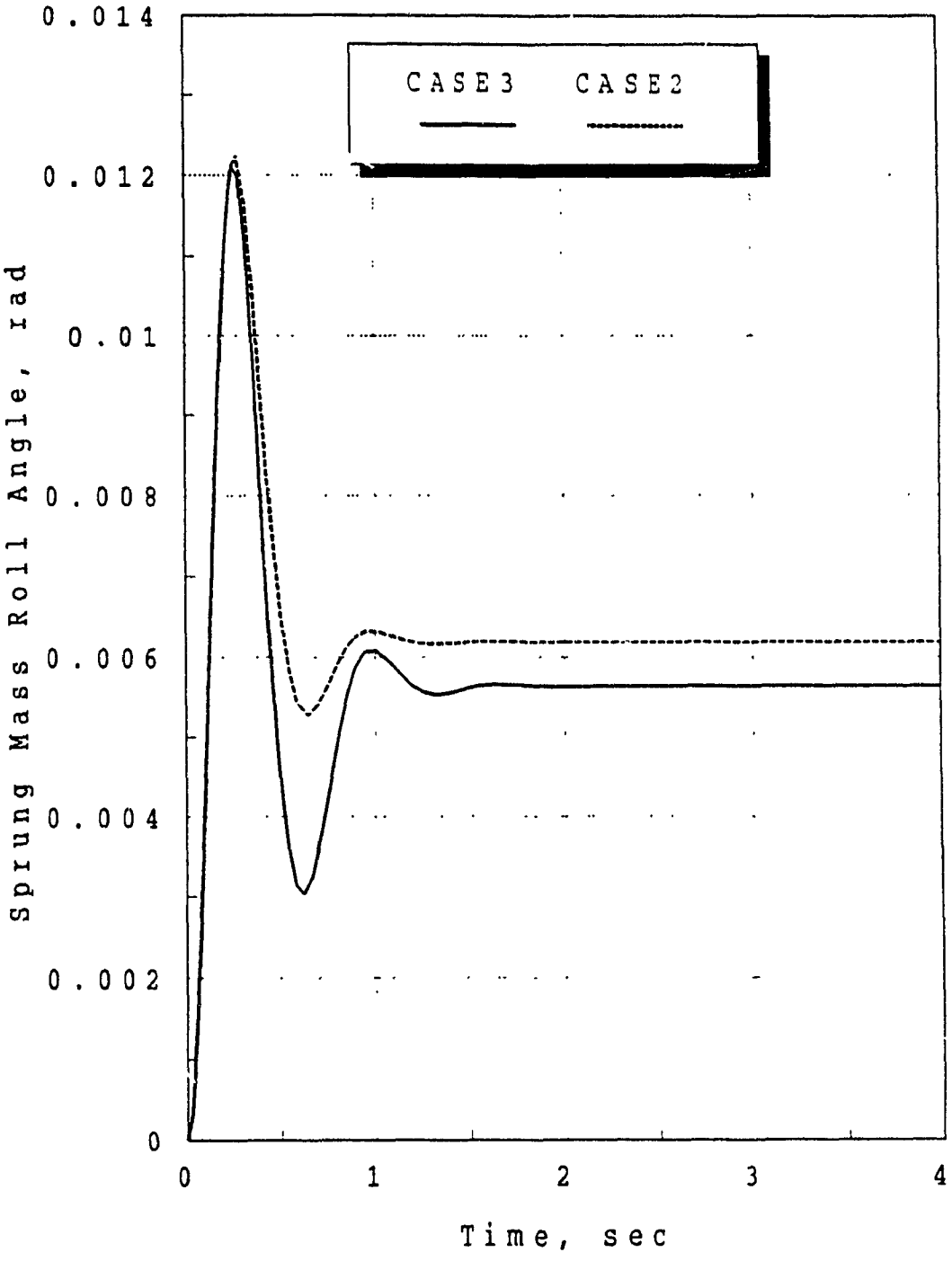

Fig. 4.18 CASE3 Sprung Mass Roll Angle vs. Time

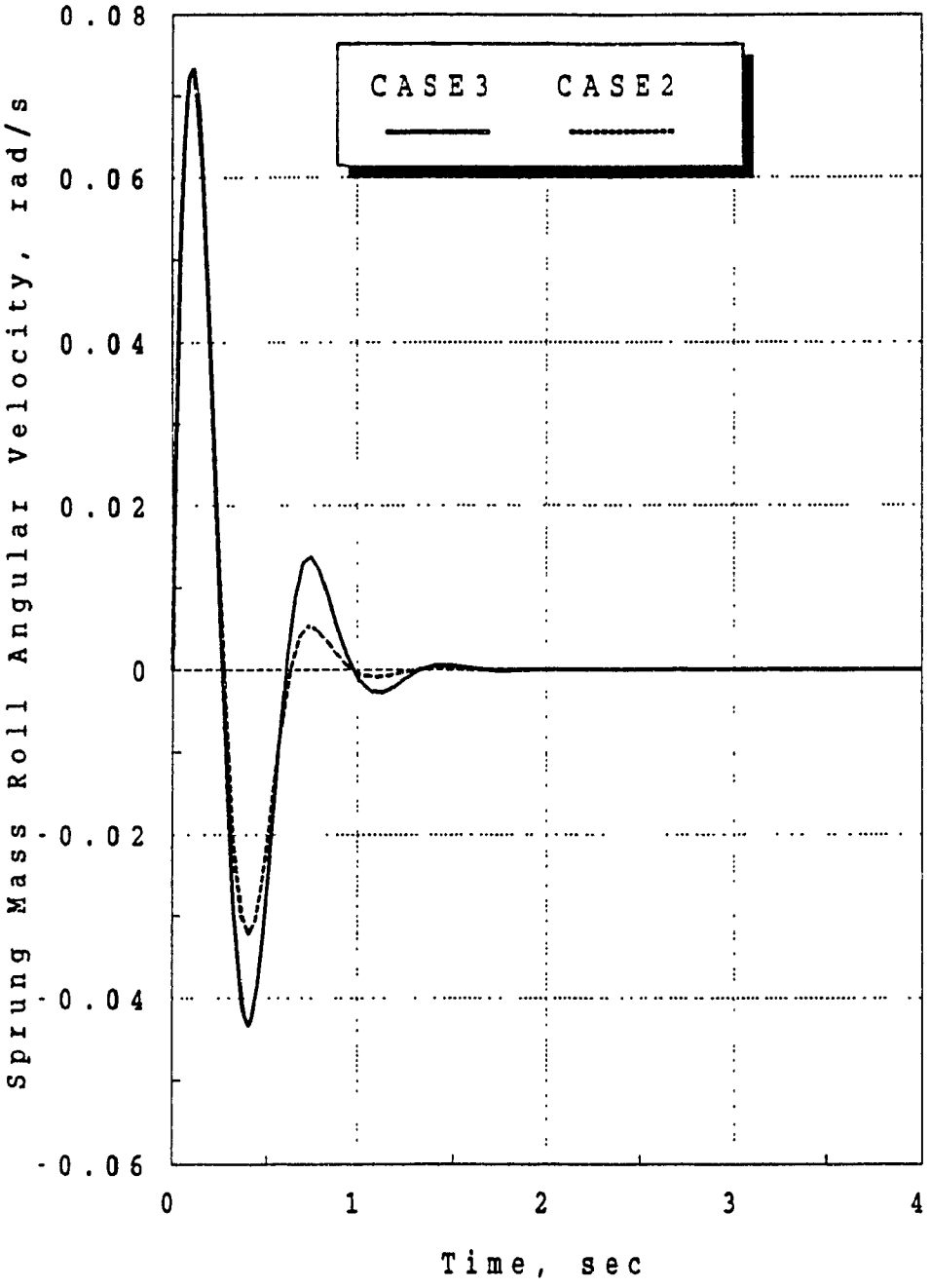

Fig. 4.19 CASE3 Sprung Mass Roll Angular Velocity vs. Time

4.5 Comparison of Linkage Analysis with GENKAD [44]

To gain confidence in the kinematic and kineto-static analyses and software for the suspension linkage by the velocity coefficients method described in the thesis, a comparison was made with GENKAD. A selected configuration of the linkage described in Section 3.3 was modelled and analysed with KINSTAT as well as with GENKAD. A comprehensive comparison of the numerical results was made. Detailed outputs of the linkage angles, dimensions across springs, velocity coefficients, and absolute sensitivities of velocity coefficients to input variables were collected and compared. The comparison was very thorough, being carried out over the full range of the linkage movement, and the agreement of the results was excellent. With very rare exceptions, all numerical results for each iteration agreed within at least four decimal places. This comparison provided very good confidence in the kinematic and kineto-static analyses for their implementation in the vehicle dynamic analysis.

4.6 3DOF Nonlinear Model With Suspension Linkage Analysis (CASE6)

In this section, the instantaneous location of roll centers and roll stiffness from the kinematic and kineto-static analyses are added to the vehicle handling and stability model with non-linear tire characteristics.

The sprung mass properties used in CASE6 are common to the previous cases. In addition, complete front and rear planar A-arm suspensions have been designed and analysed using the software. The 3DOF vehicle handling model has been modified to incorporate the non-linear suspension parameters.

Maximum non-linearities generally occur in the upper regions of the vehicle's performance envelope. To simulate vehicle behavior in the upper performance envelope, a step steer input of sufficient magnitude is applied. The peak vehicle lateral acceleration is estimated by examining the Pacejka tire side force curves. It is observed that the side force coefficient (FY/FZ) at the peak slip angle range (10-13 degrees) is approximately 0.9g, depending on the normal load FZ. Taking into account the fact that the lateral load transfer decreases the absolute capabilites of the tires, a peak lateral acceleration below 0.9g is expected.

By trial and error, it was found that a step steer input of 1.25 degrees resulted in a steady-state lateral accleration of approximately 0.8g. The magnitude of step steer angle is chosen so that the sprung mass roll angle will not be exceed

5 degrees ; this is to avoid excessive tire camber.

Three simulations are carried out. The first simulation uses constant roll centers and roll stiffnesses corresponding to zero roll angle. The second simulation uses constant roll centers and roll stiffnesses corresponding to the sprung mass roll angle at 0.8g lateral acceleration. The third simulation uses the instantaneous roll center locations and roll stiffnesses from linkage analysis. The vehicle handling model reads lookup tables from the kinematic and kineto-static analysis for the instantaneous roll center locations and roll stiffnesses.

The vehicle handling model parameters are the same as CASE3 except as specified in Tables 4.3 and 4.4:

TABLE 4.3: CASE6: ZERO ROLL ANGLE CASE

```
    hf = -0.094   m
    hr = -0.0343  m
    kf = 22370 Nm/rad
    kr = 16269 Nm/rad
    Lp = -1961 Nm/rad/s
tfinal = 2 sec
 delta = 0.0218 rads
```

TABLE 4.4: CASE6: ROLL ANGLE FOR 0.8g LATERAL ACCELERATION

```
    hf = -0.0849 m
    hr = 0.00056 m
    kf = 22200   Nm/rad
    kr = 12300   Nm/rad
tfinal = 2 sec
 delta = 0.0218  rads
```

The graphical results of the kineto-static analysis for front and rear linkages are seen in Fig. 4.20. A sweep of kinetic equilibrium positions with their corresponding roll centers is shown. The non-linear roll centers and roll stiffnesses are plotted in Figs. 4.21 to 4.24. The results of the handling analysis are seen in Figs. 4.25 to 4.31. The results from the full non-linear analysis are in all cases bracketed by the results from the "zero g" and "0.8 g" approximations. The steady-state lateral acceleration as well reaches a value which is between the two approximations. Thus the vehicle design synthesis is sensitive to suspension linkage non-linearities.

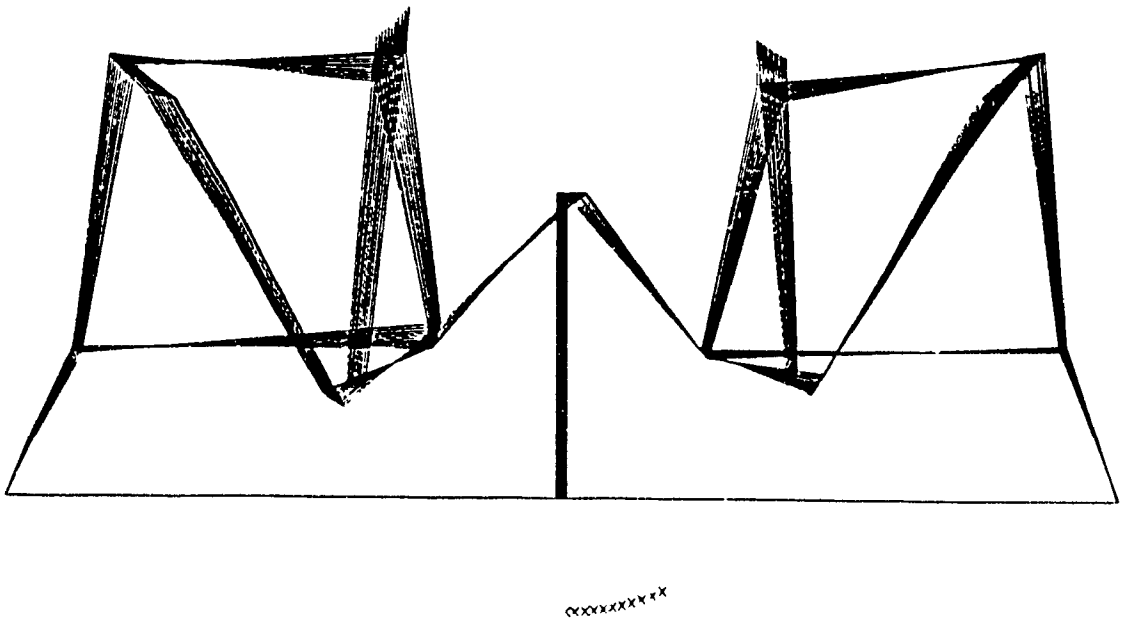

Fig. 4.20a CASE6: Kineto-Static Analysis of Front Suspension

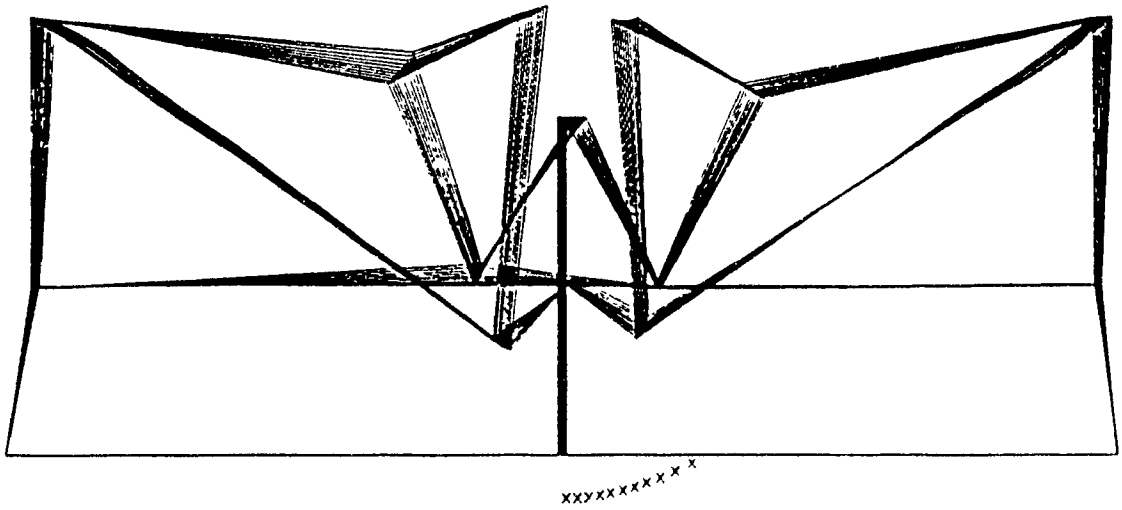

Fig. 4.20b CASE6: Kineto-Static Analysis of Rear Suspension

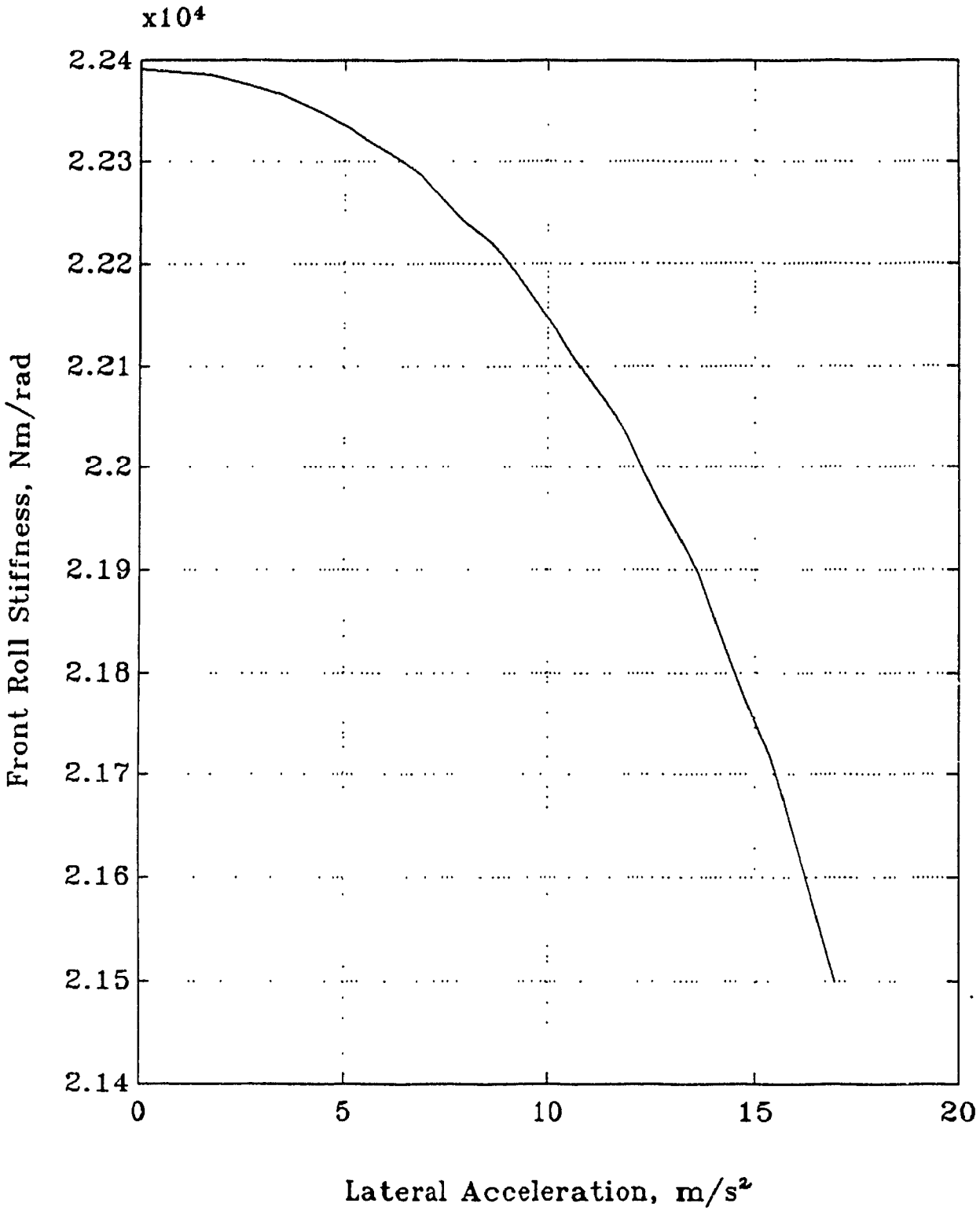

Fig. 4.21 CASE6: Front Roll Stiffness vs. Lateral Accleration

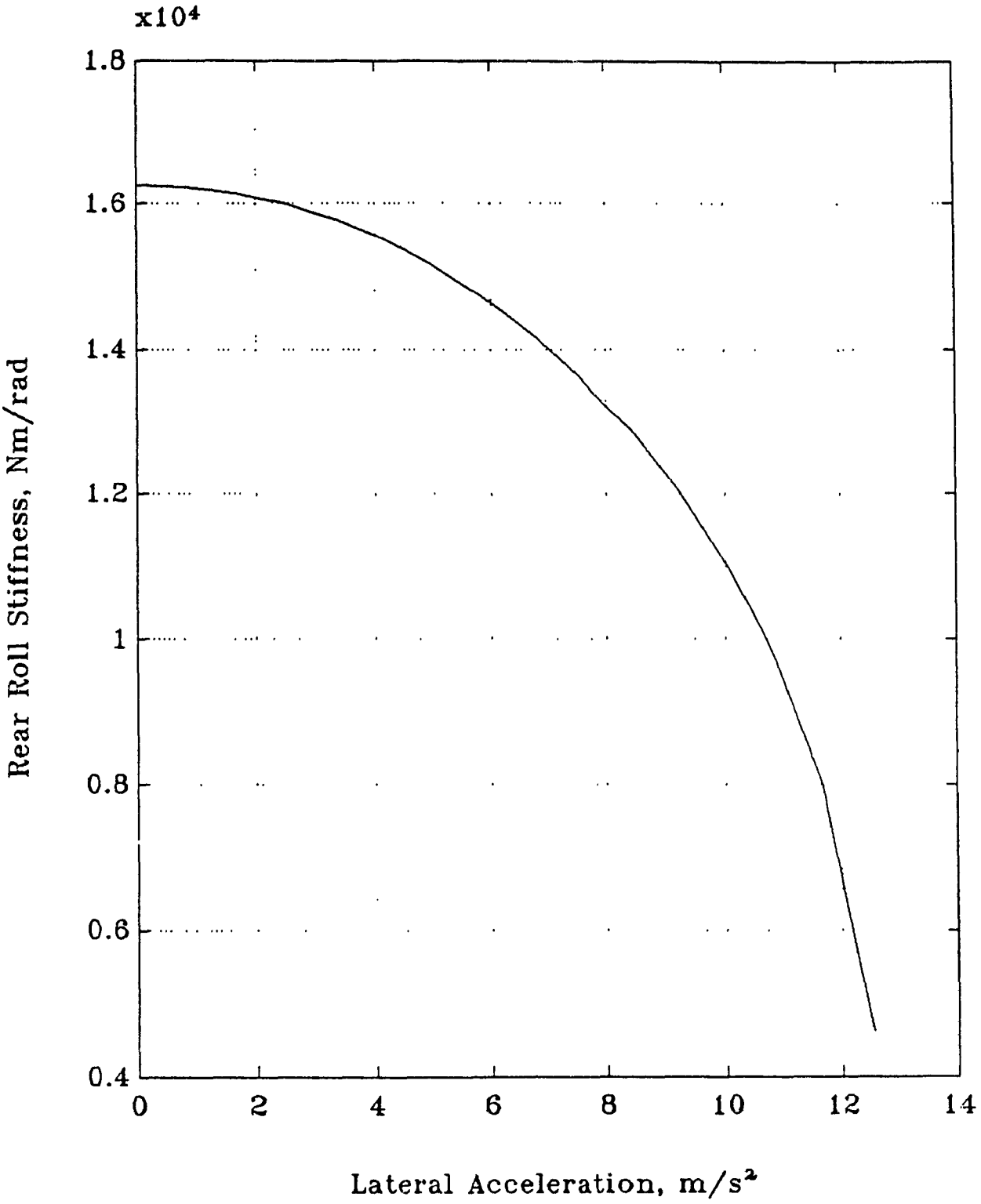

Fig. 4.22 CASE6: Rear Roll Stiffness vs. Lateral Acceleration

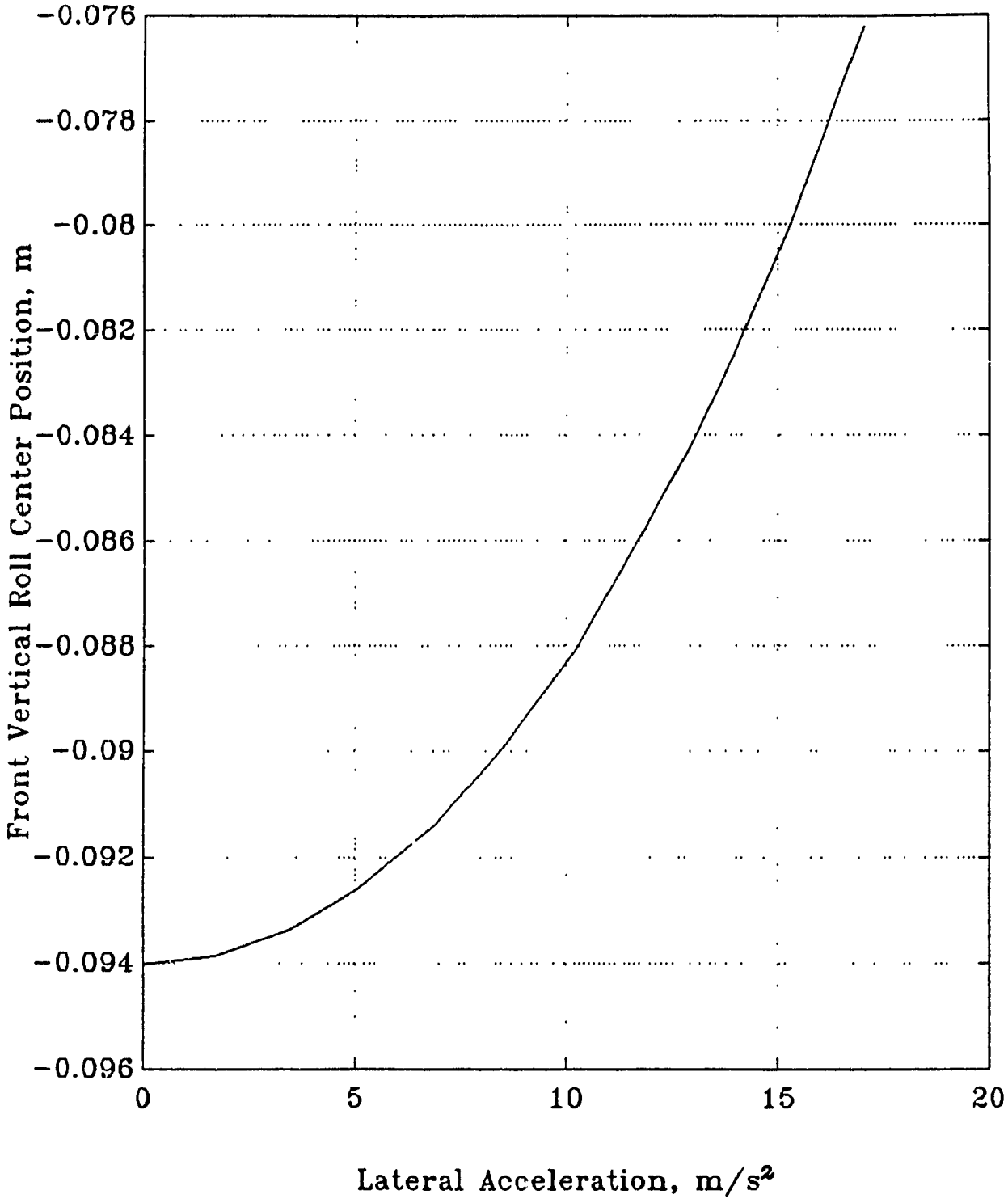

Fig. 4.23 CASE6: Front Roll Center vs. Lateral Acceleration

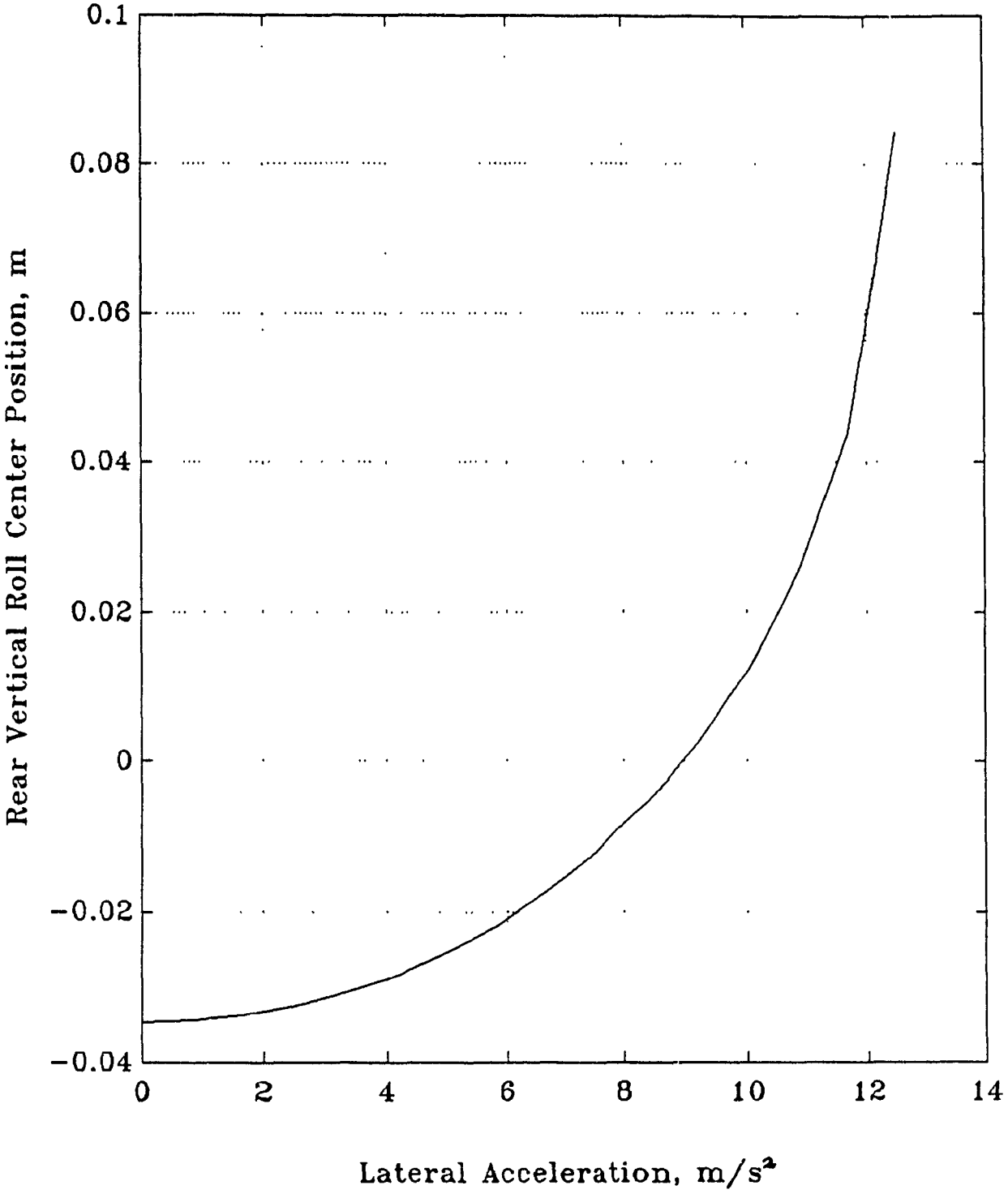

Fig. 4.24 CASE6: Rear Roll Center vs. Lateral Acceleration

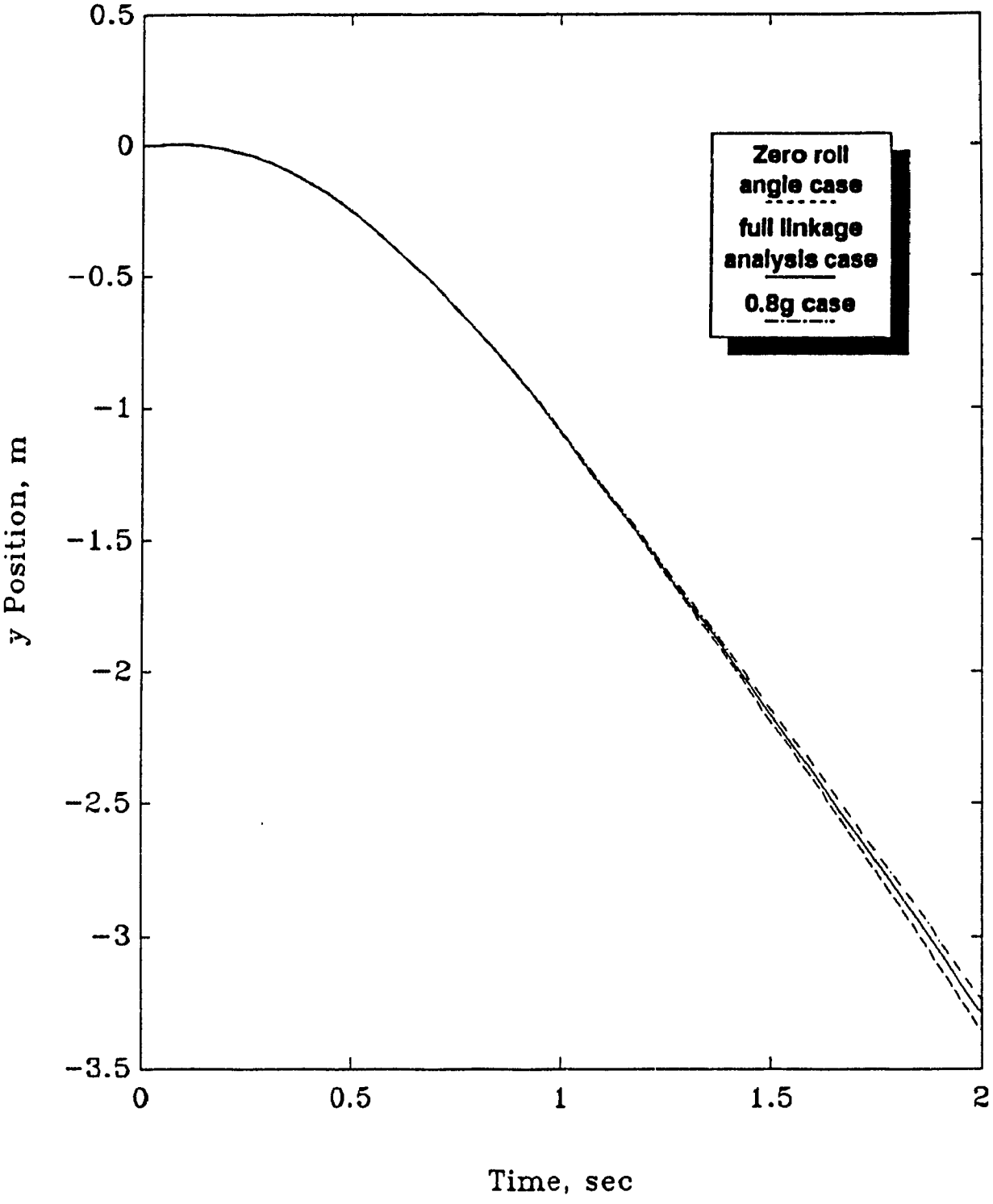

Fig. 4.25 CASE6: y Position vs. Time

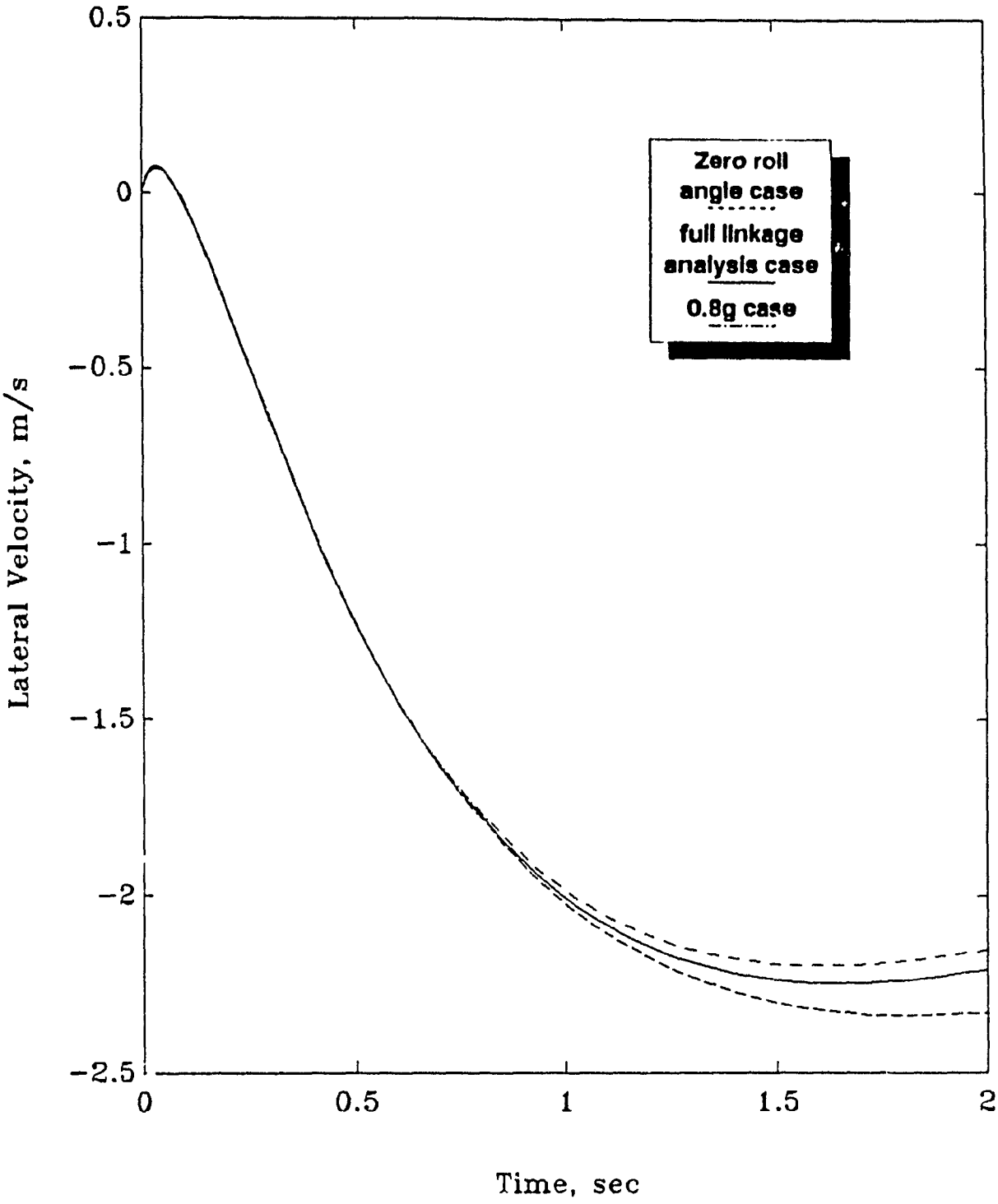

Fig. 4.26 CASE6: Lateral Velocity vs. Time

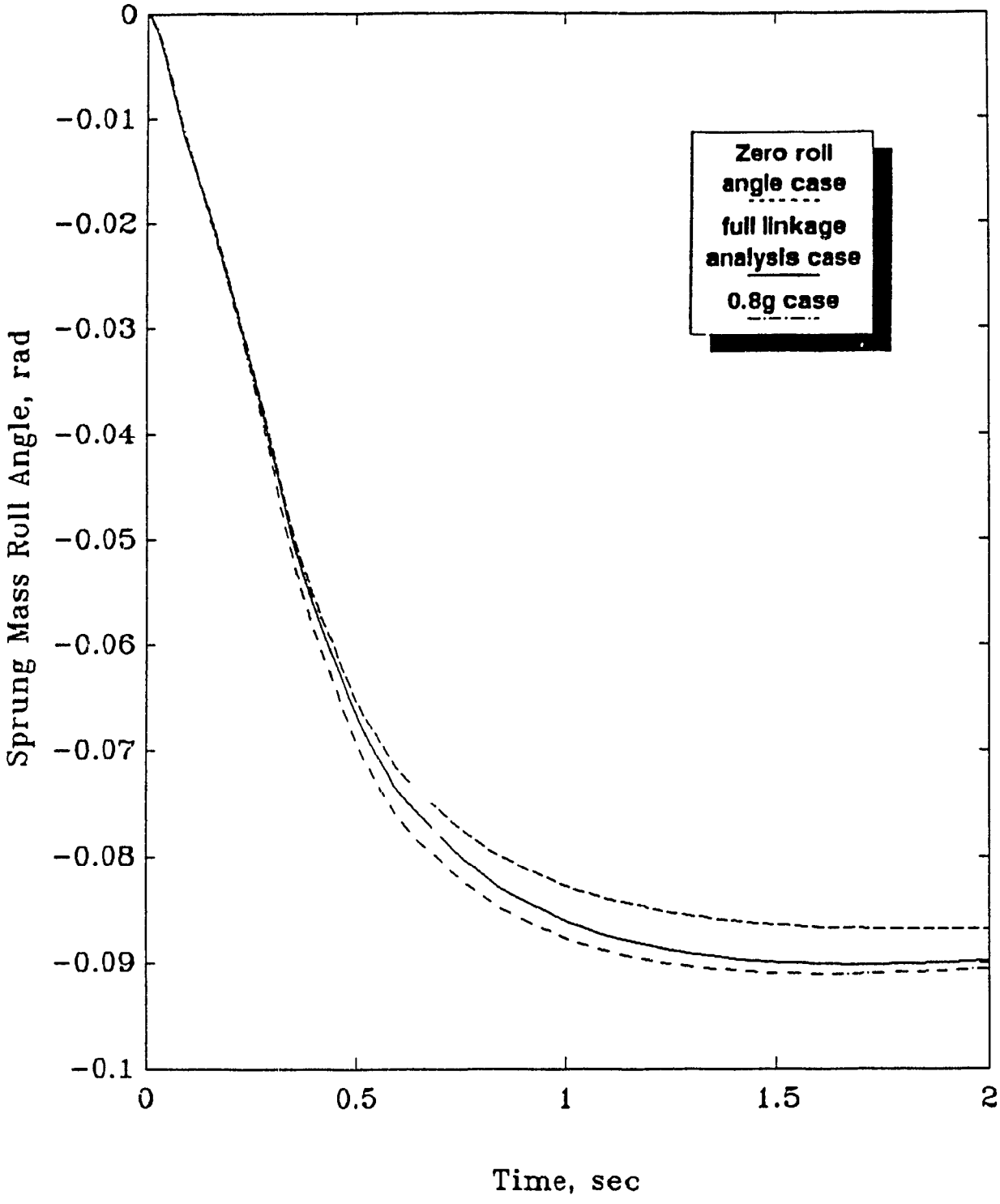

Fig. 4.27 CASE6: Roll Angle vs. Time

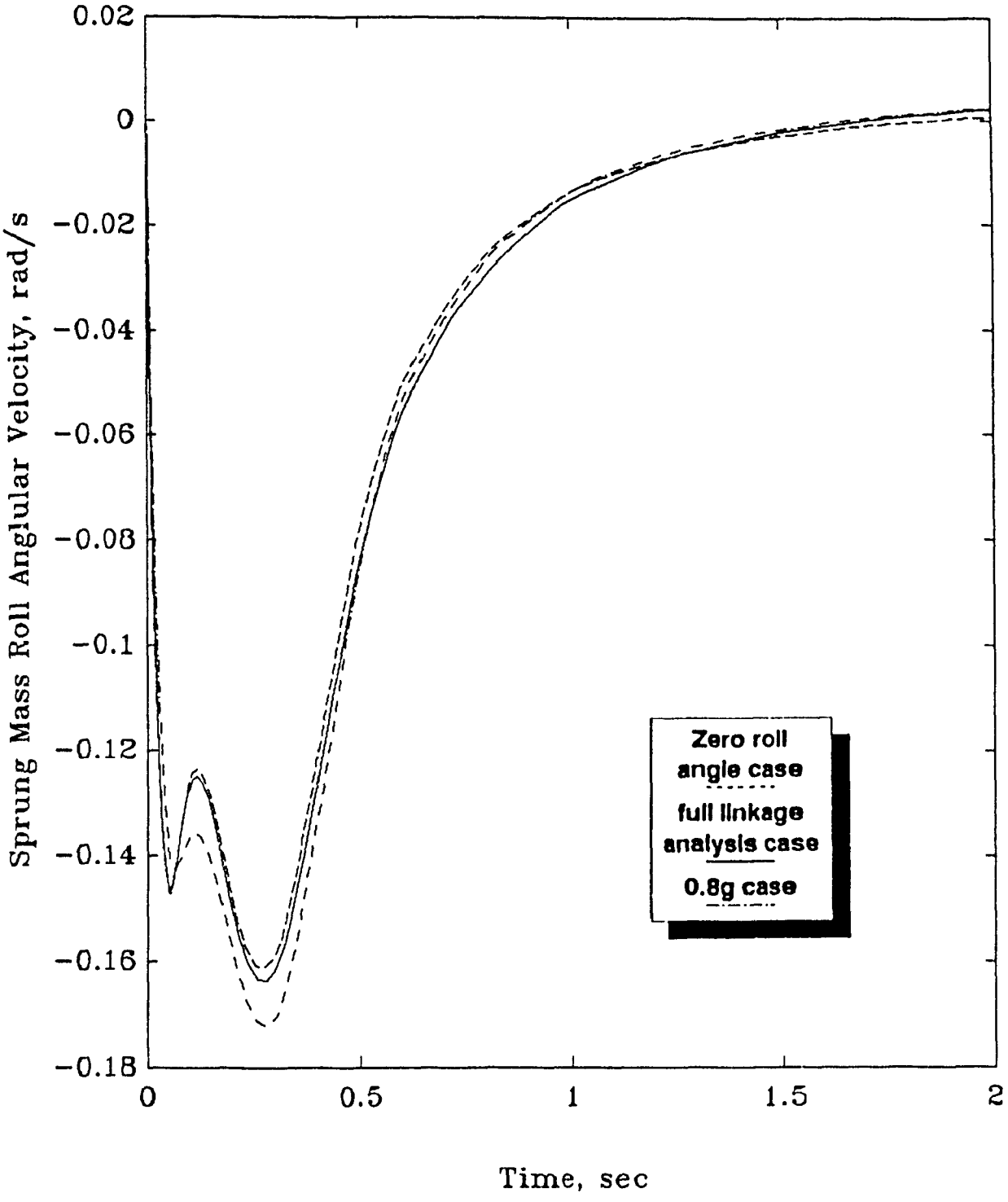

Fig. 4.28 CASE6: Roll Angular Velocity vs. Time

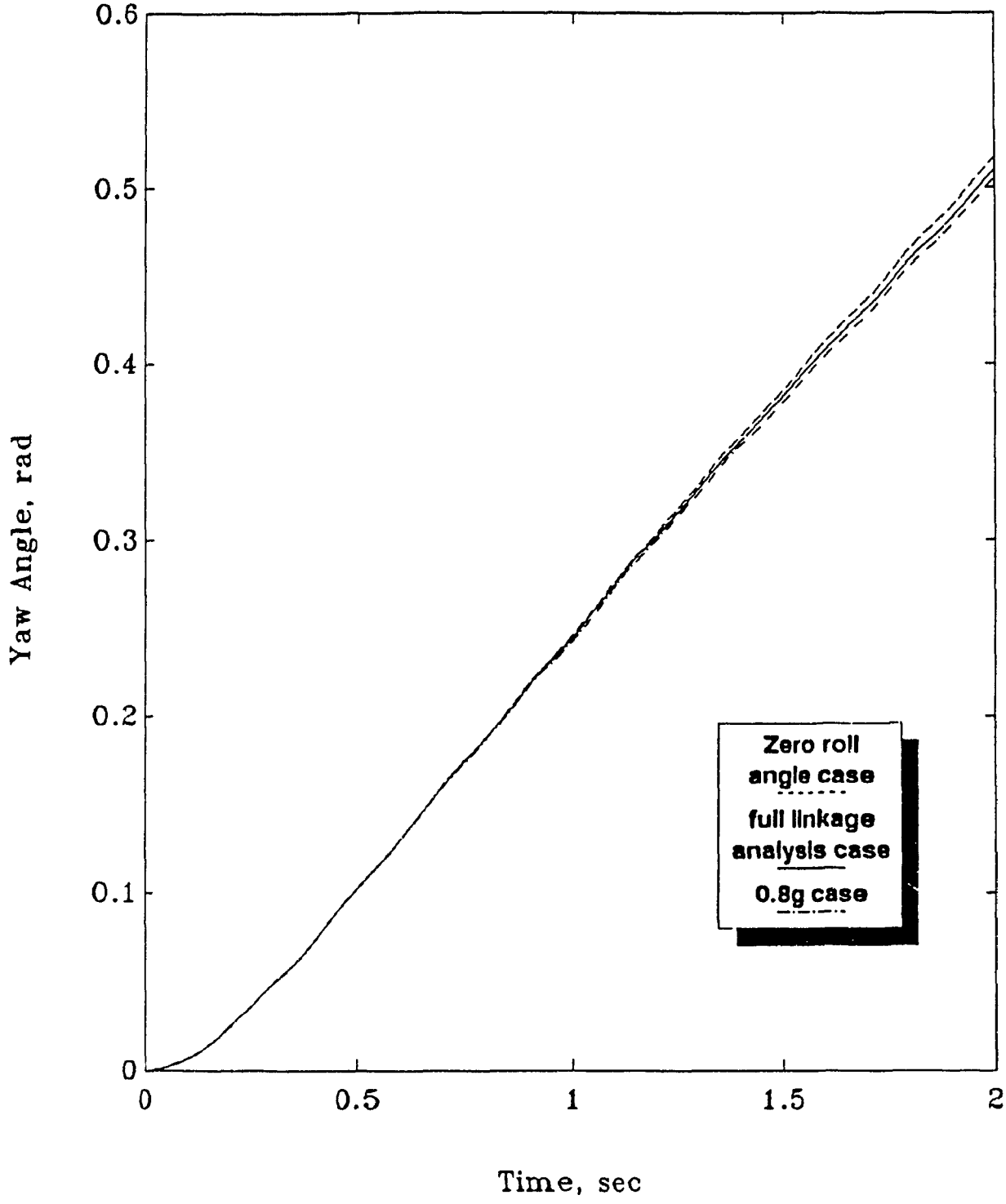

Fig. 4.29 CASE6: Yaw Angle vs. Time

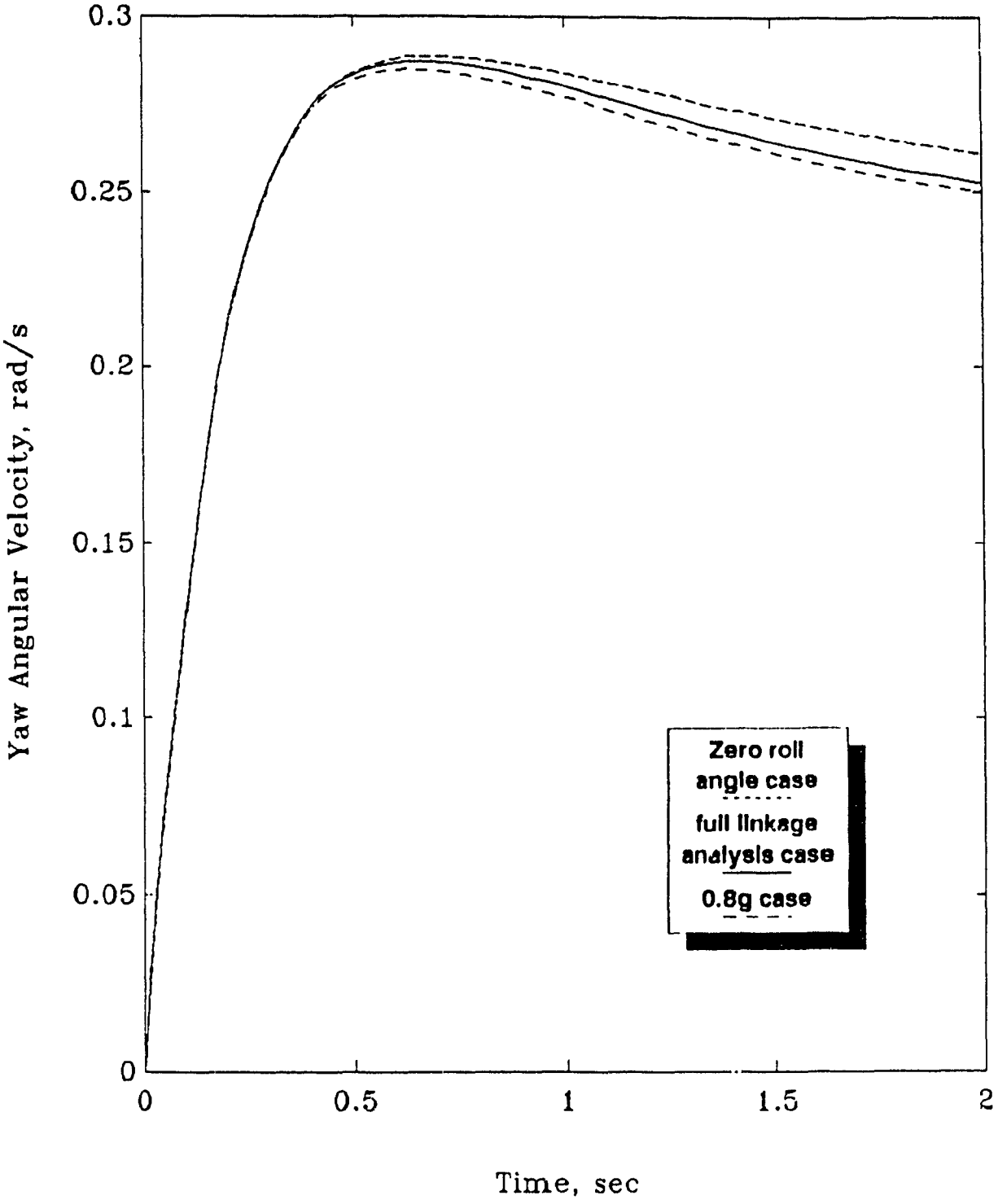

Fig. 4.30 CASE6: Yaw Angular Velocity vs. Time

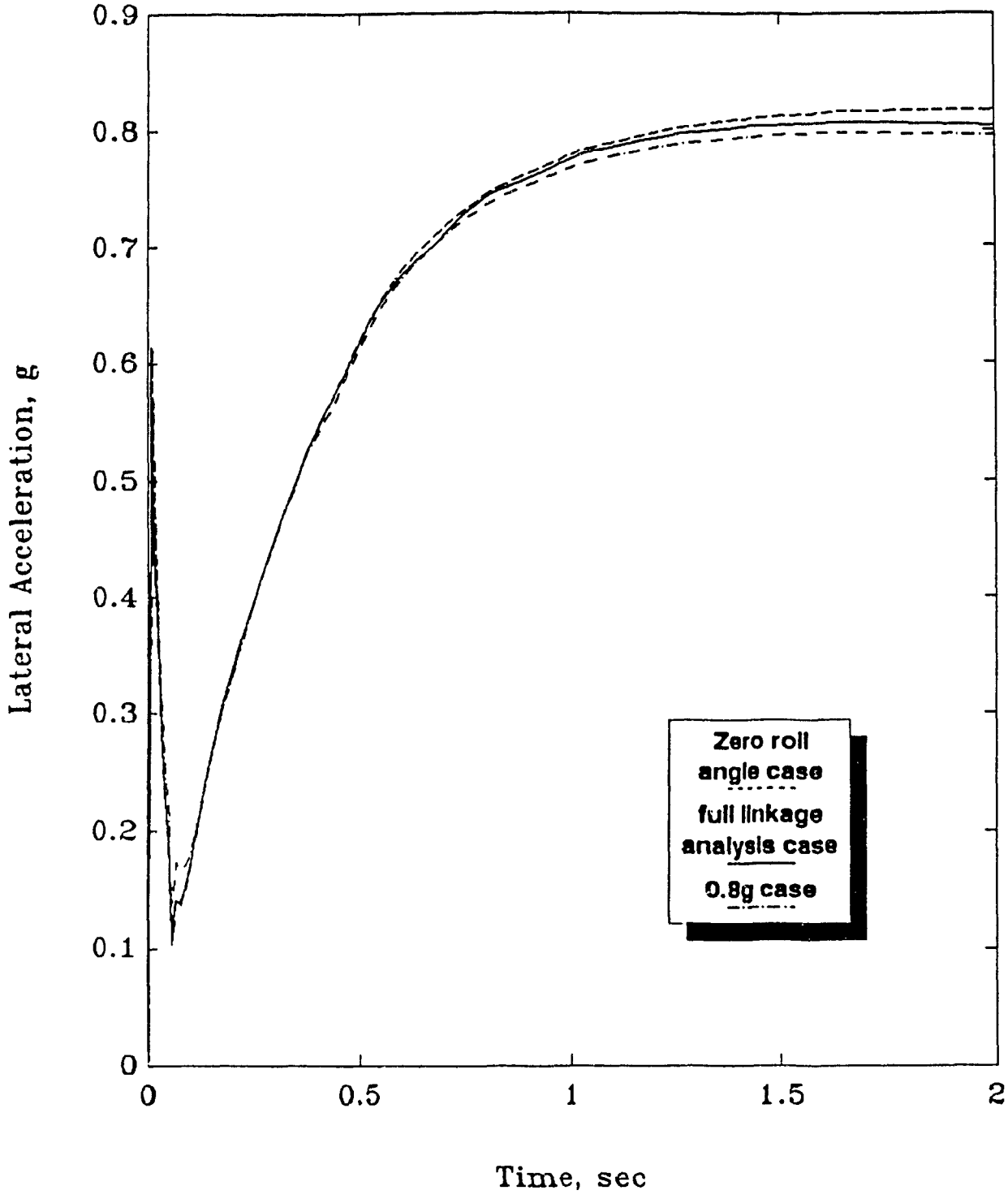

Fig. 4.31 CASE6: Lateral Acceleration vs. Time

4.7 Parametric Study

4.7.1 Parametric Study of Total Roll Stiffness

In the previous section (Section 4.6) it is demonstrated that kinematic suspension nonlinearities do have an effect on vehicle handling response at high lateral accelerations. It is also noted that a limiting factor is excessive roll angle causing the tires to operate at high camber angles. In this section, the total roll stiffness will be varied and the effects on the sprung mass roll angle and the vehicle handling will be observed.

Total roll stiffness is changed by adding auxiliary roll stiffnesses to the front and rear axles while maintaining the baseline roll-stiffness distribution. With reference to Tables 4.5 and 4.6, the total roll stiffness k_{tot} is varied relative to the baseline configuration (100%). Each of the other columns is designated by the total roll stiffness percentage relative to that of the baseline. The total roll stiffness k_{tot} is defined as follows:

$$k_{tot} = k_{f_{CASE6}} + k_{faux} + k_{r_{CASE6}} + k_{raux}$$

The baseline configuration is that of CASE6. The roll damping ratio in each case is maintained at 0.3. Adding roll stiffness is a physically realizable task; it is accomplished by the use of anti-roll bars. A reduction in roll stiffness at an axle would require a decrease in spring rate at that axle.

TABLE 4.5: CASE7 Roll Stiffness and Roll Damping

Step Steer 1.25 deg., tfinal=2 sec.

	95%	97.5%	100%	125%	150%	175%
kf	21293	21853	22391	28017	33620	39224
kr	15419	15825	16253	20288	24346	28403
ktot	36712	37678	38644	48305	57966	67627
|Lp|	1912	1937	1961.5	2193	2402	2595
kfaux	-1098	-537.8	0	5626	11229	16833
kraux	-834	-428.3	0	4035	8093	12150
ltype	----	-.-.	solid	....	++++	****

TABLE 4.6: CASE7 Roll Stiffness and Roll Damping

Step Steer=2 deg., tfinal=2 sec.

	112.5%	125%	137.5%	150%	175%
kf	25215	28017	30819	33620	39224
kr	18259	20288	22317	24346	28403
ktot	43475	48305	53136	57966	67627
|Lp|	2080	2193	2300	2402	2595
kfaux	2824	5625	8428	11229	16833
kraux	2006	4035	6064	8093	12150
ltype	----	-.-.	....	++++	****

The lower limit of the roll stiffness is set by the maximum allowable sprung mass roll angle; the upper limit is set by the assumption that an anti-roll bar that is too stiff will limit wheel independence. Two sets of trials are carried out for step steer inputs of 1.25 and 2 degrees.

It should be noted that the roll stiffness values k_f and k_r are for the zero roll angle. Since the front and rear suspension linkages exhibit a change in roll stiffness as the sprung mass rolls, it is likely that the handling of the vehicle will change. This is demonstrated in Figs. 4.34 and 4.35, which show that the understeer numbers change as the total roll stiffness changes.

Figs. 4.32 and 4.33 show that lateral acceleration increases with total roll stiffness.

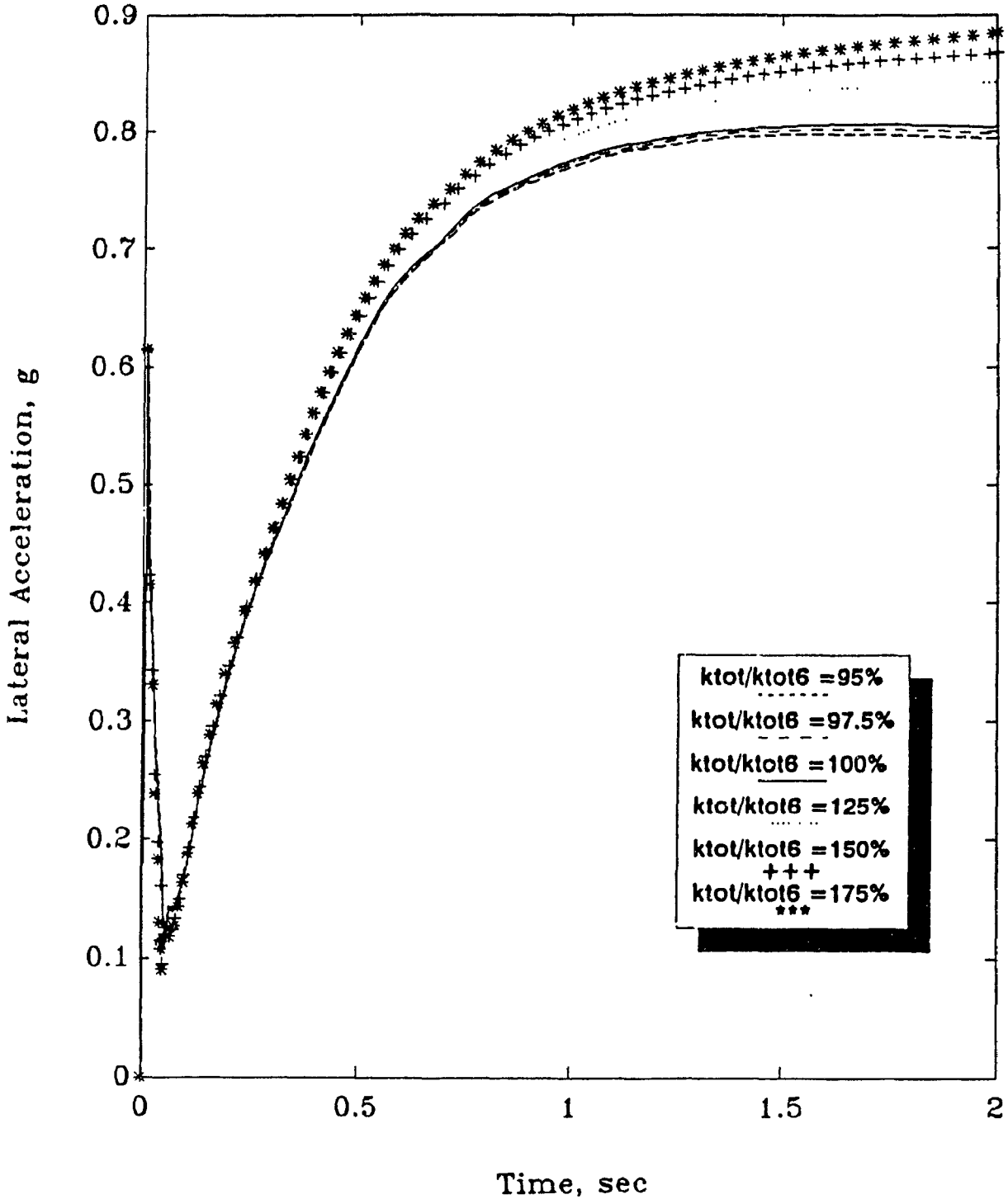

Fig. 4.32 CASE7: 1.25 deg. Step Steer, Lateral Acc. vs. Time

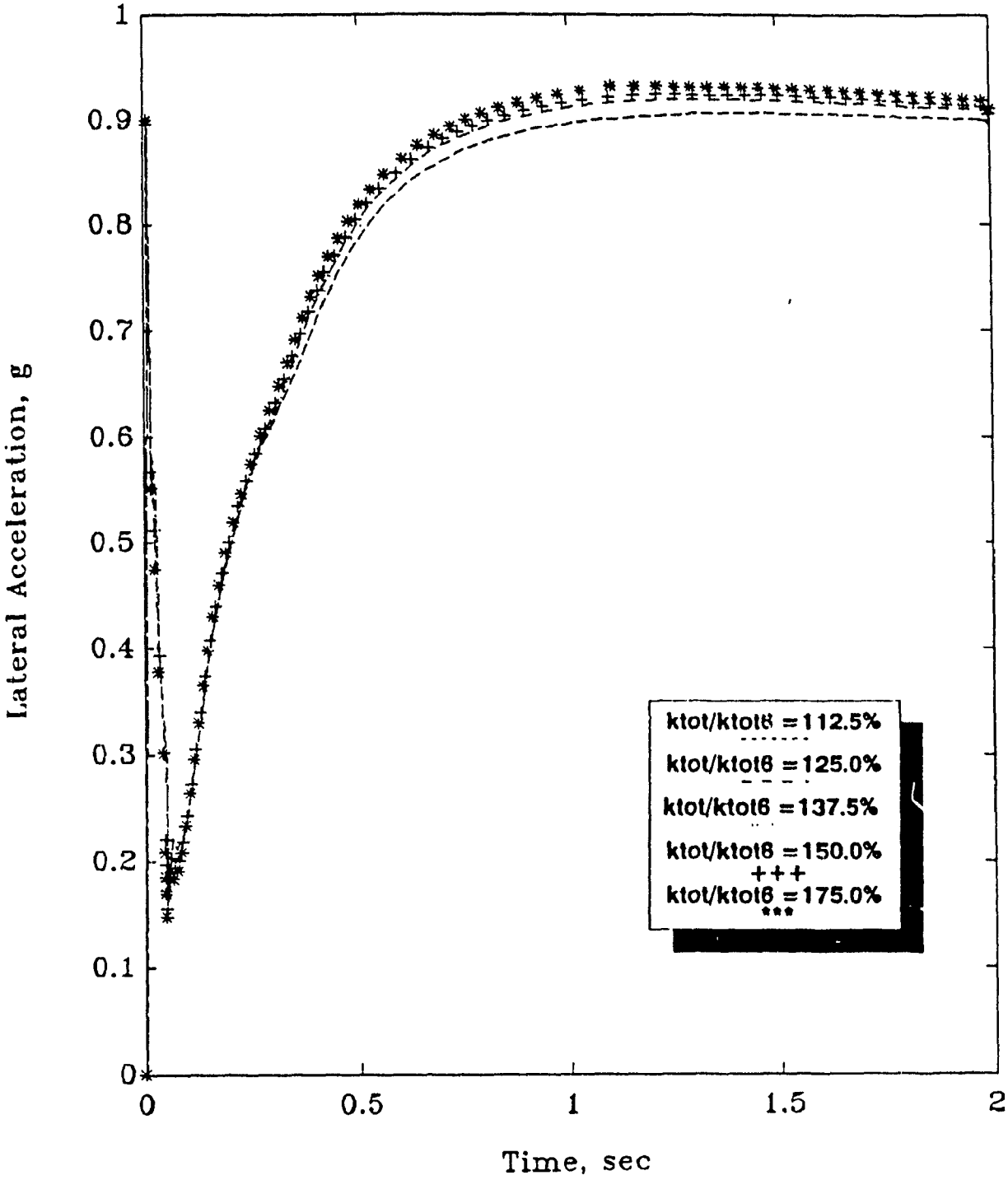

Fig. 4.33 CASE7: 2.0 deg. Step Steer, Lateral Acc. vs. Time

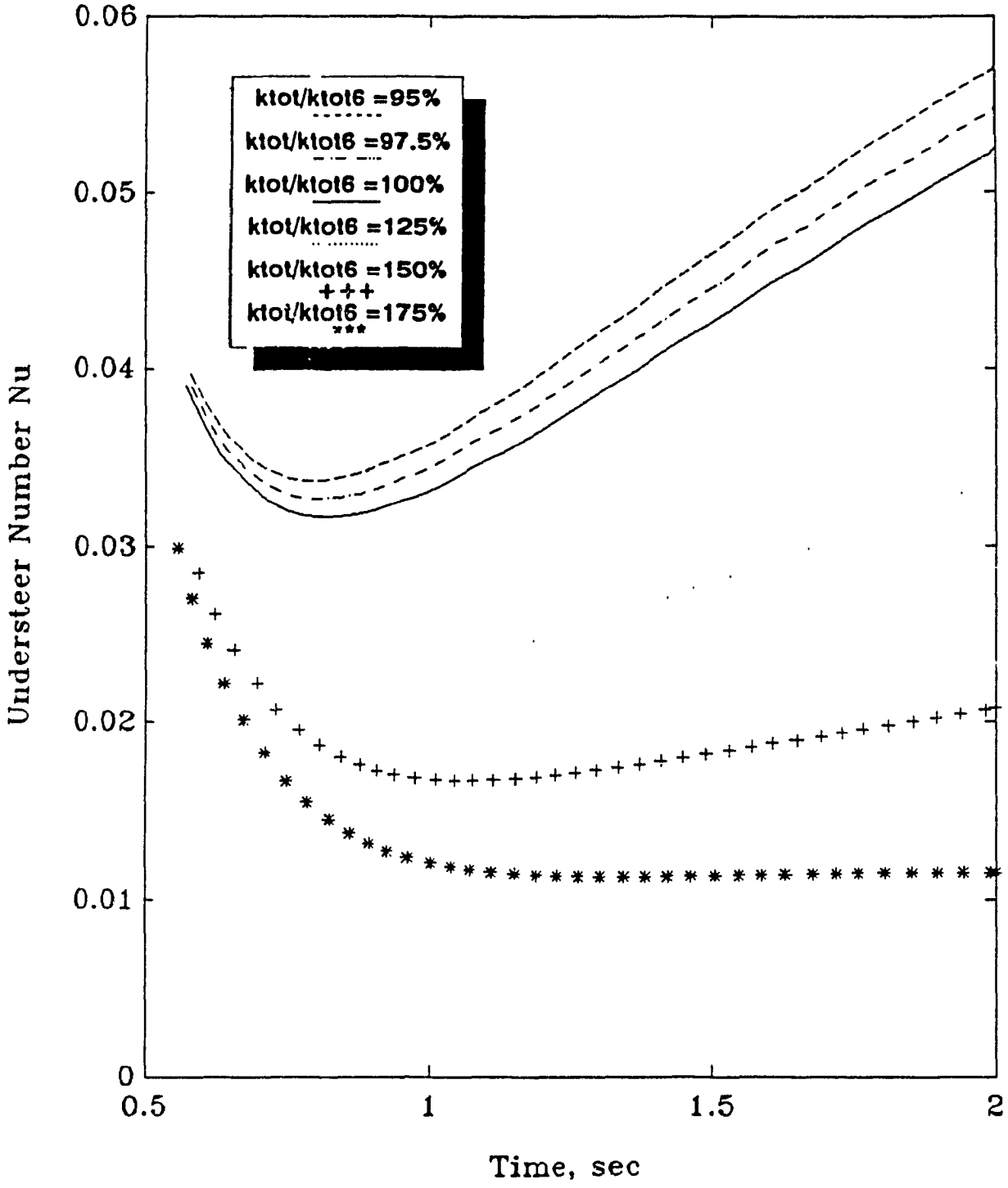

Fig. 4.34 CASE7: 1.25 deg. Step Steer, Understeer vs. Time

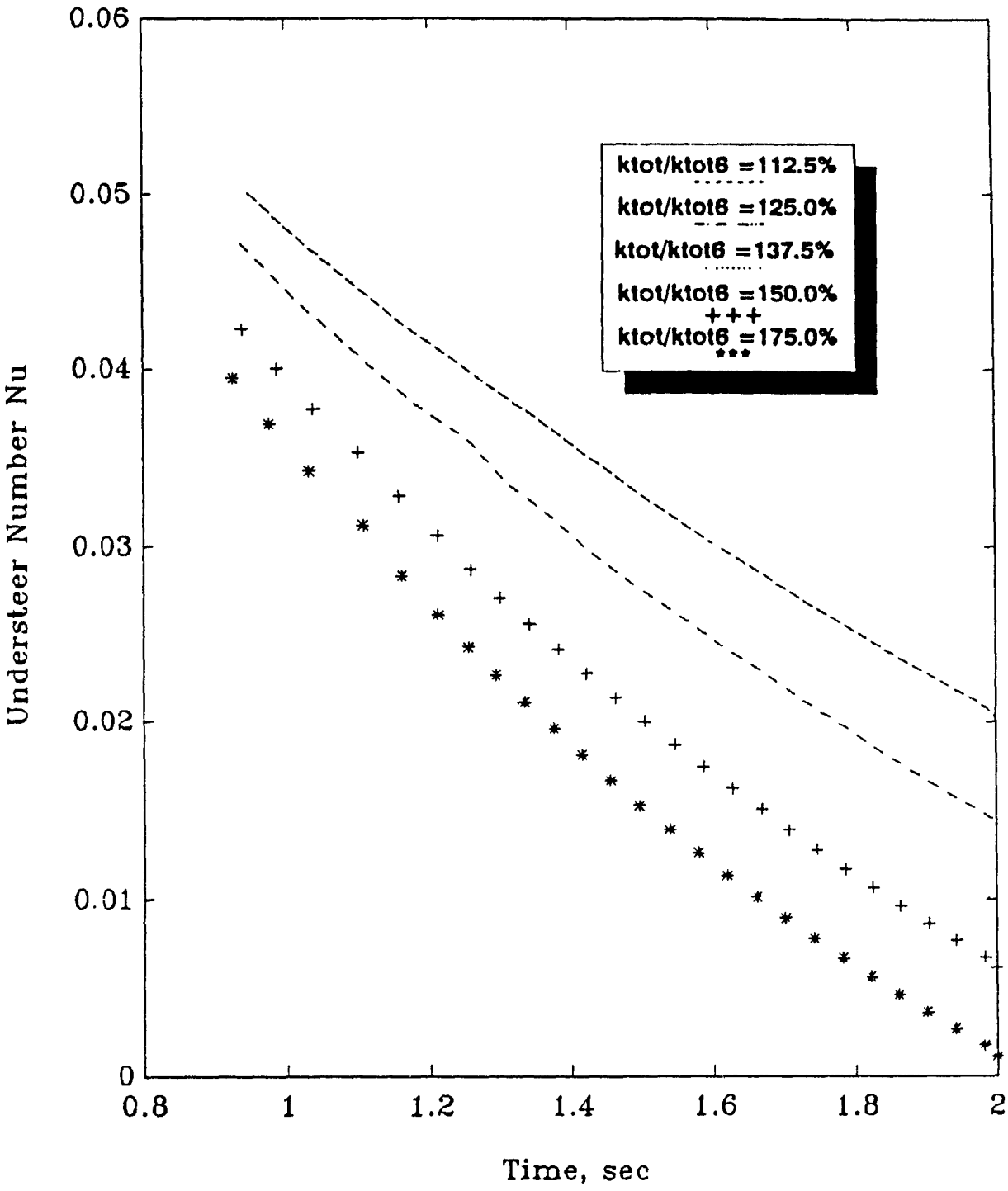

Fig. 4.35 CASE7: 2.0 deg. Step Steer, Understeer vs. Time

4.7.2 Parametric Study of CG Position

The center of gravity position a/L is varied and the effects on the vehicle handling response are observed. The wheelbase L is kept a constant. The range of test values is seen in Table 4.7.

TABLE 4.7: CASE8: CG Position Variation

Step Steer = 1.25 deg., tfinal = 2 sec, kaux = 0

a/L	0.45	0.50	0.55	0.61	0.65
a(m)	0.944	1.0485	1.153	1.28	1.363
b(m)	1.153	1.0485	0.944	0.817	0.734
ltype	----	-.-.	....	solid(baseline)	****

The results of the study are shown in Figs. 4.36 to 4.43. The test case with the most rearward CG position produced the highest lateral acceleration and the least understeer. This is to be expected, in light of the substantially forward-biased roll stiffness distribution for the baseline vehicle parameters (a/L=0.61). Moving the CG forward from the baseline (understeering) case resulted in increased understeer and diminished lateral acceleration. Thus the already overloaded front tires were having increasingly detrimental lateral weight transfer conditions imposed on them. Moving the CG position back from the baseline resulted in improved handling and stability, because tire loading conditions became more equalized.

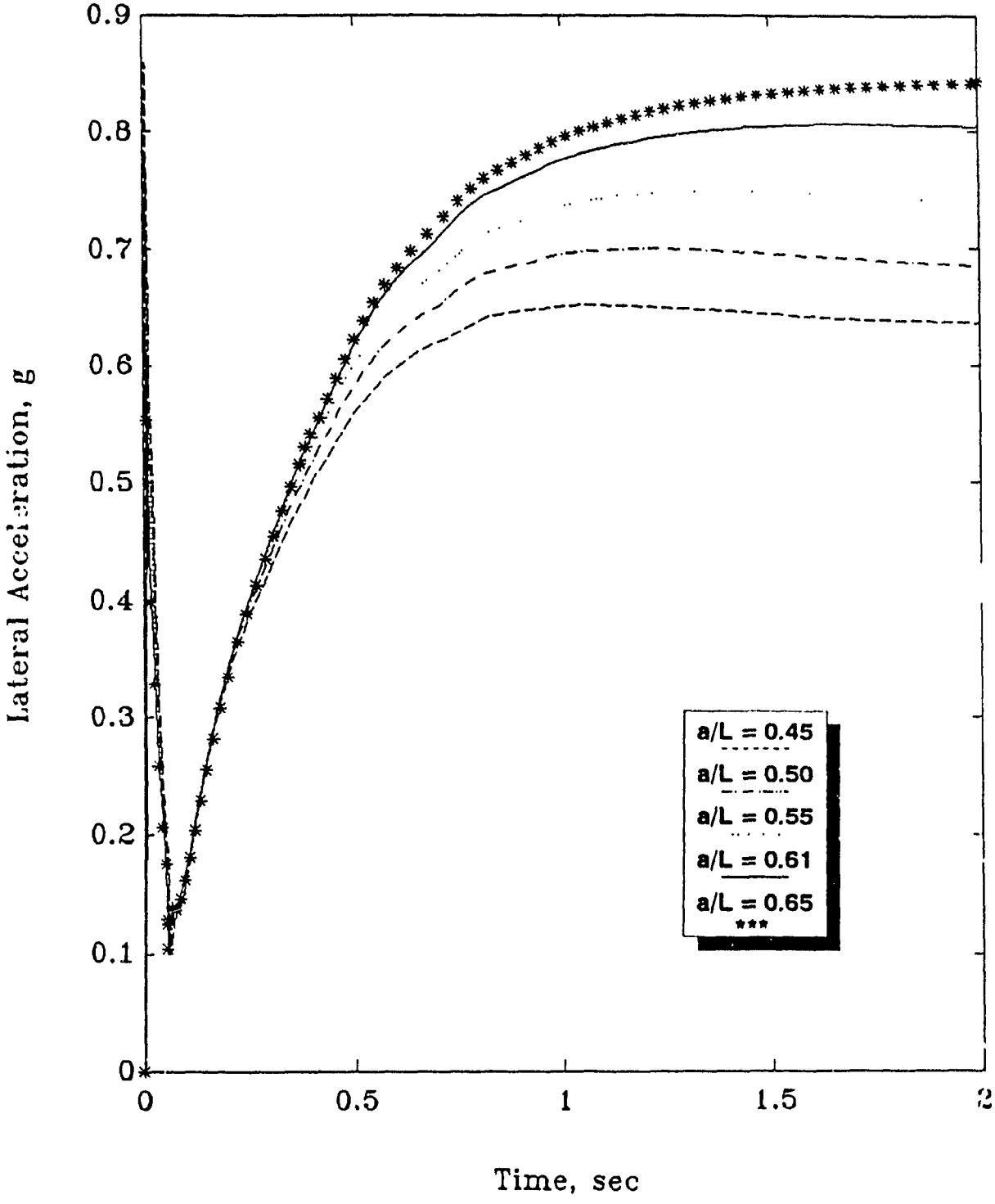

Fig. 4.36 CASE8: 1.25 deg. Step Steer, Lateral Acc. vs. Time

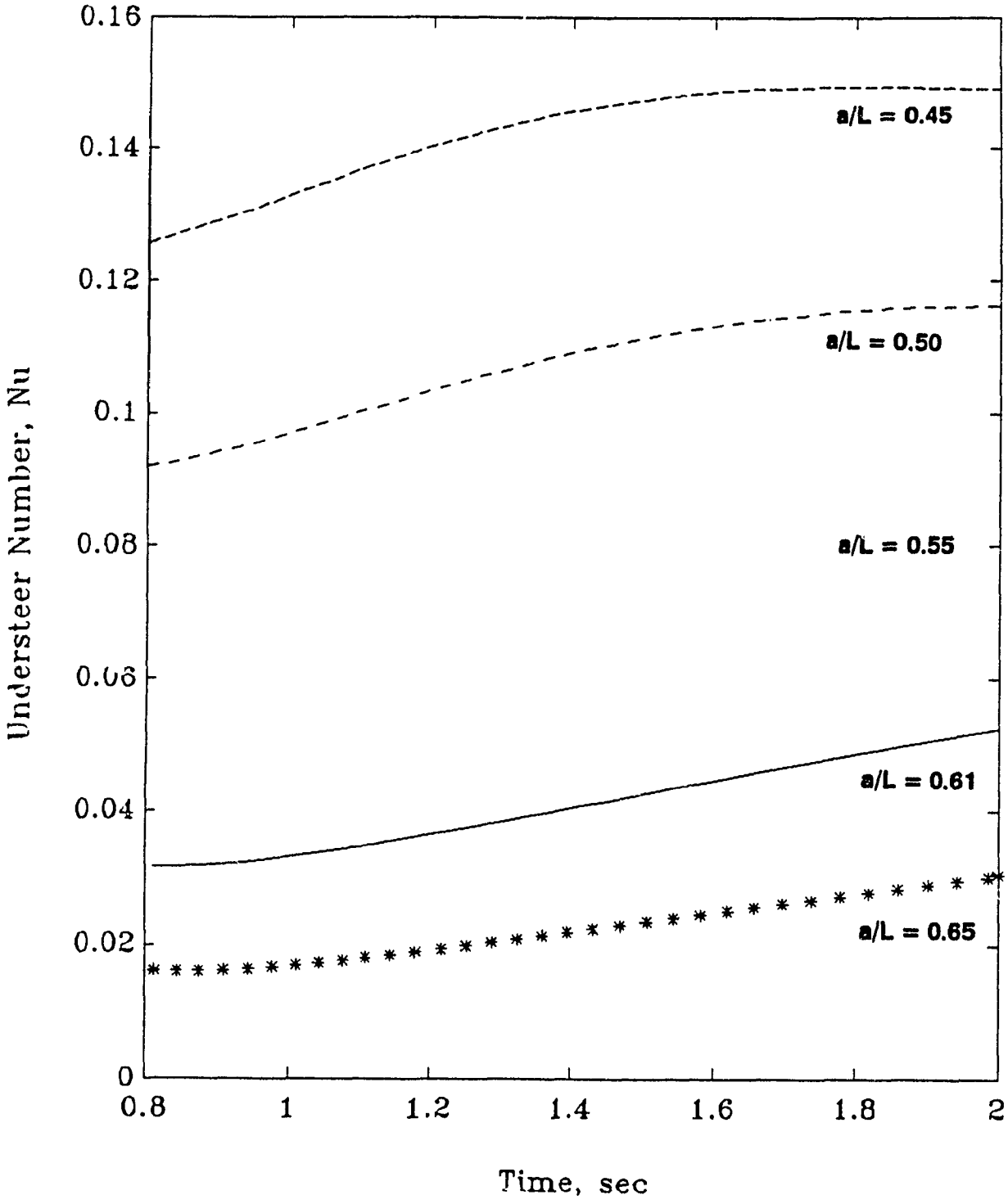

Fig. 4.37 CASE8: 1.25 deg. Step Steer, Understeer vs. Time

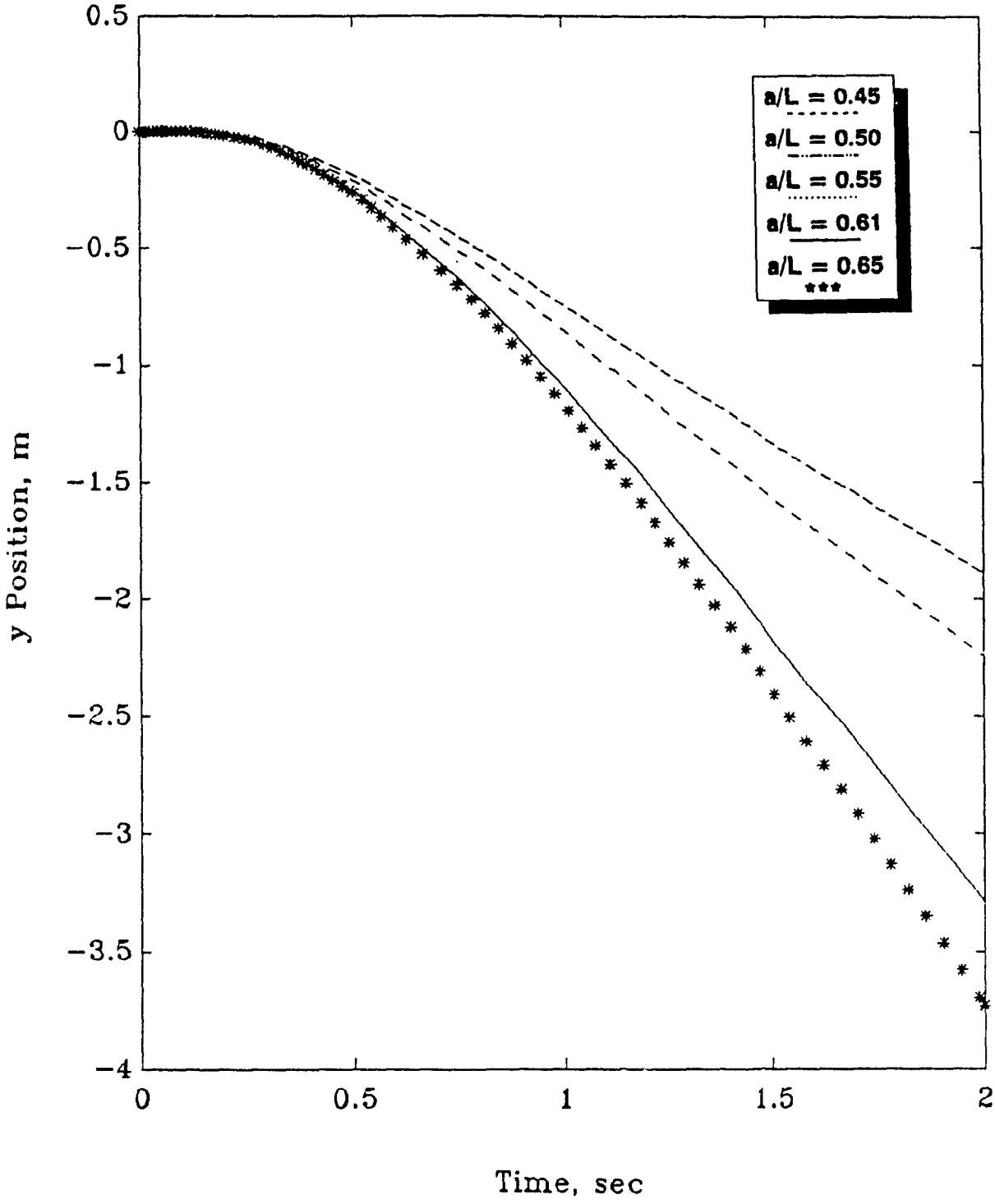

Fig. 4.38 CASE8: y Position vs. Time

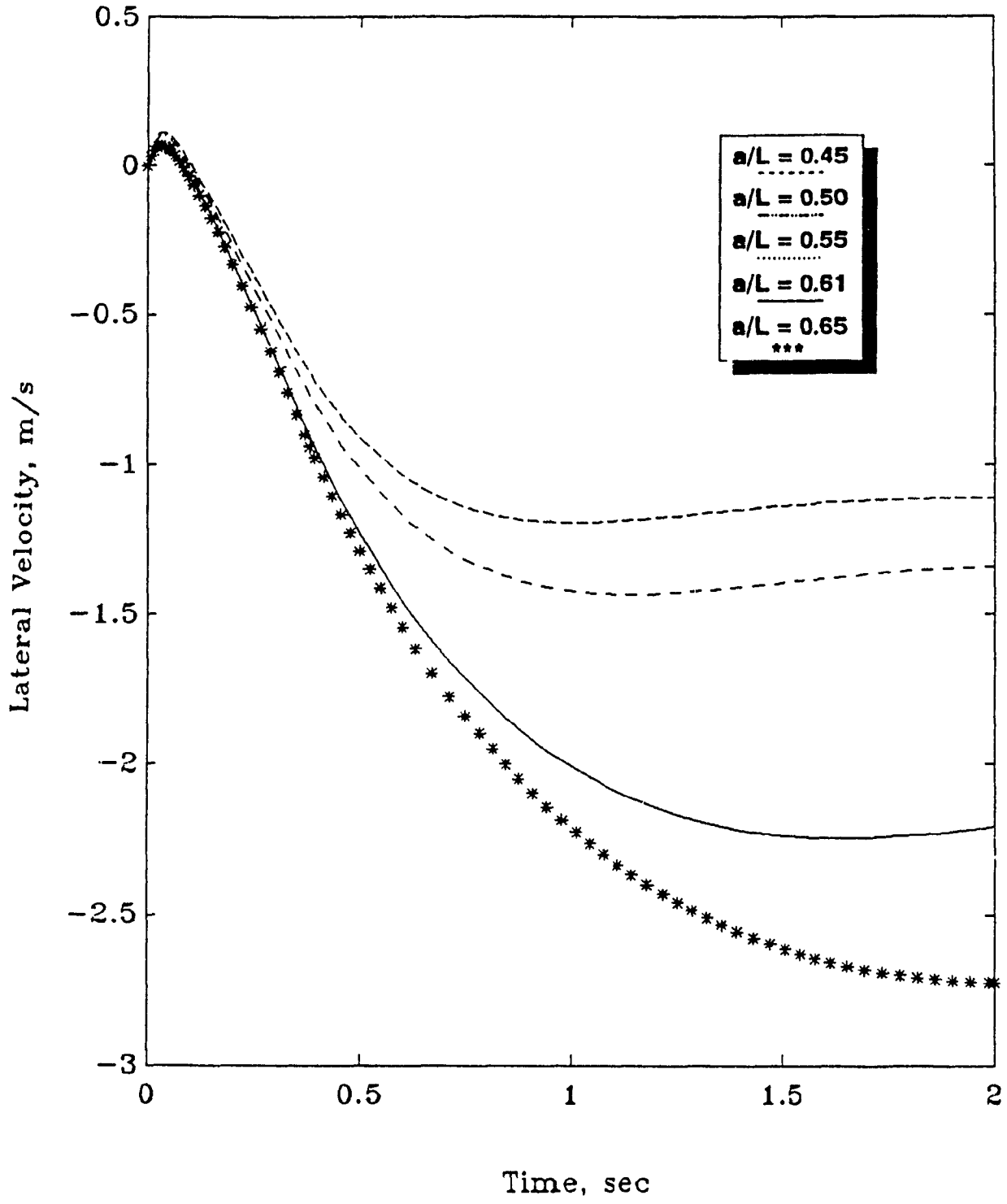

Fig. 4.39 CASE8: Lateral Velocity vs. Time

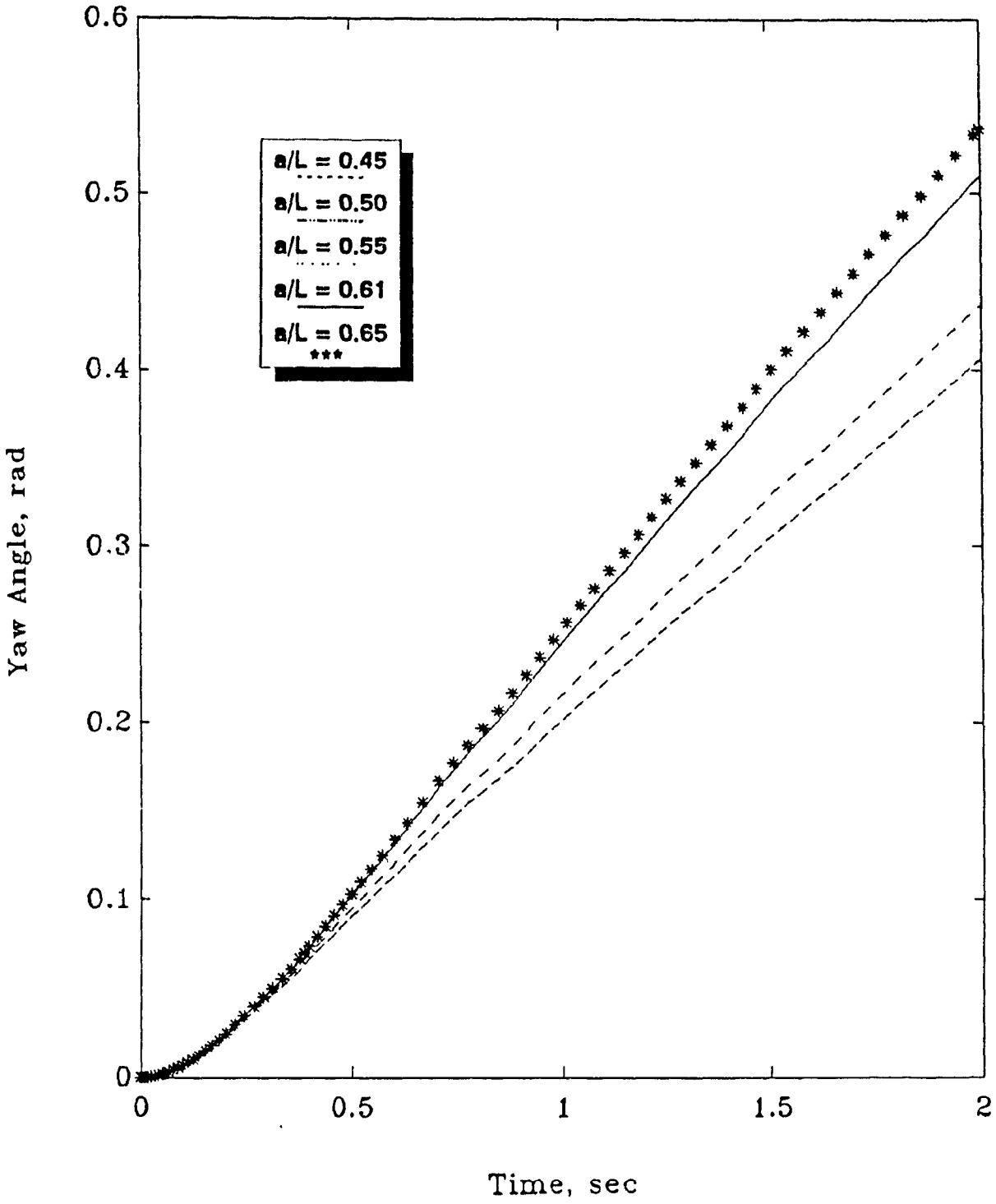

Fig. 4.40 CASE8: Yaw Angle vs. Time

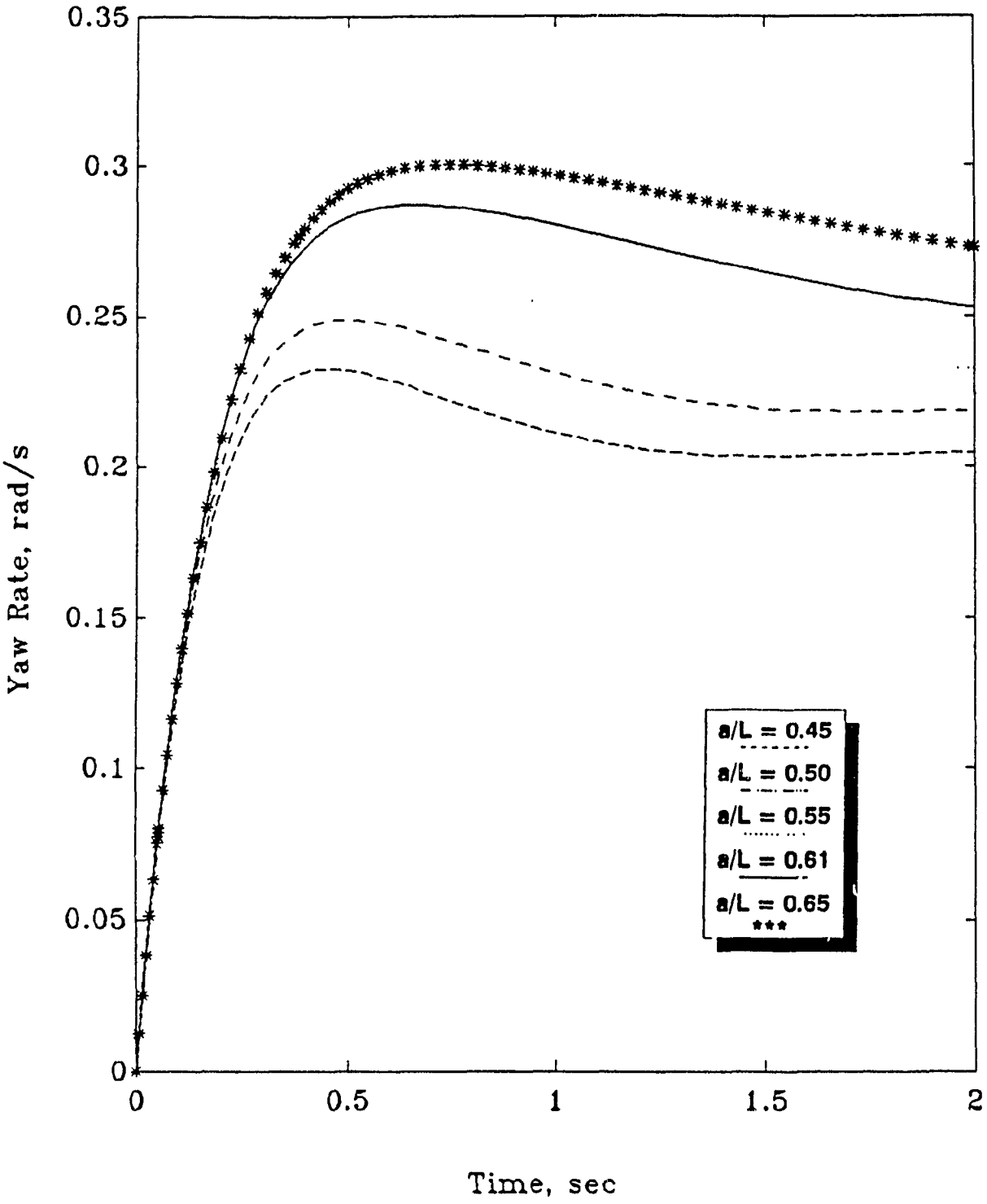

Fig. 4.41 CASE8: Yaw Angular Velocity vs. Time

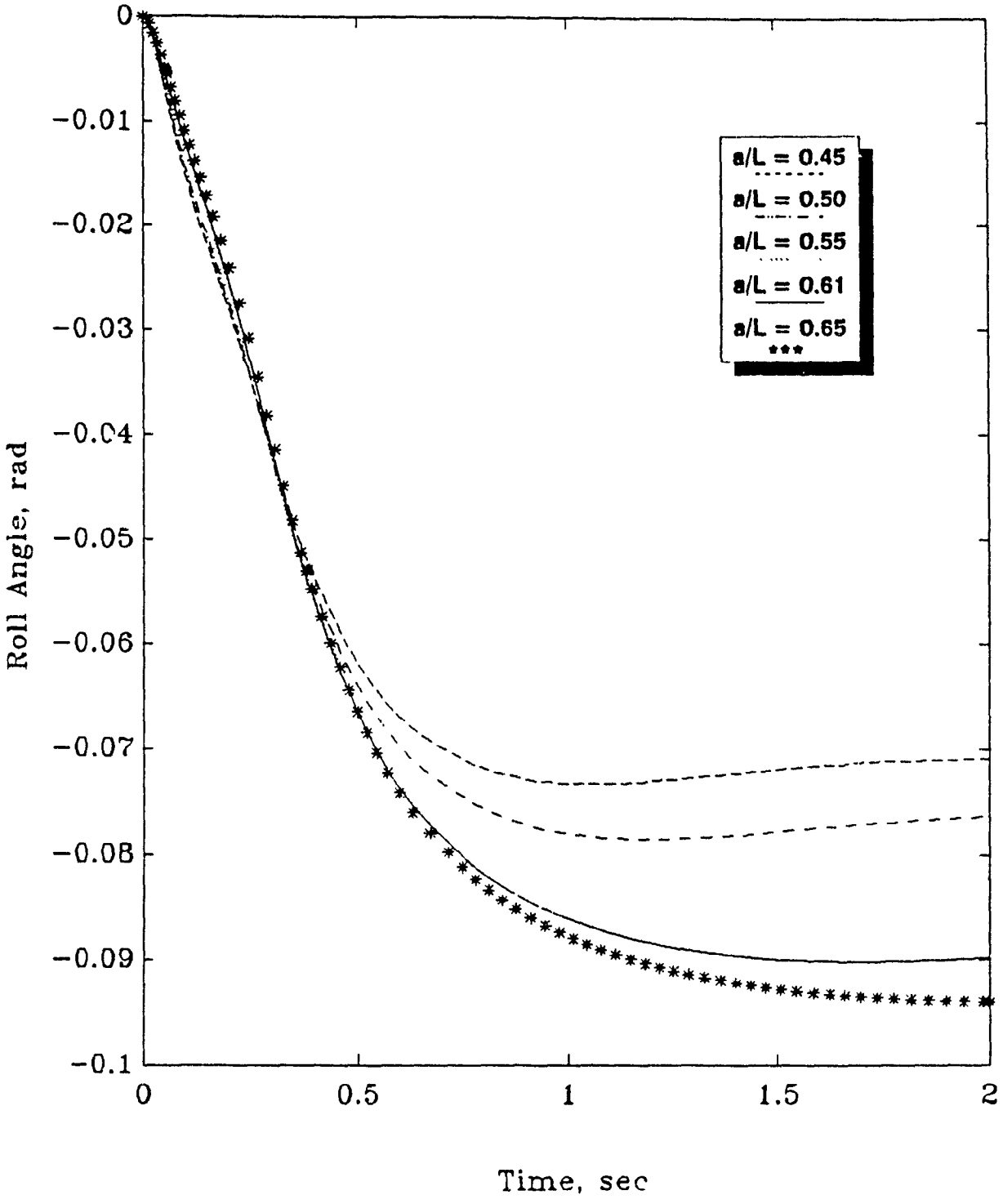

Fig. 4.42 CASE8: Roll Angle vs. Time

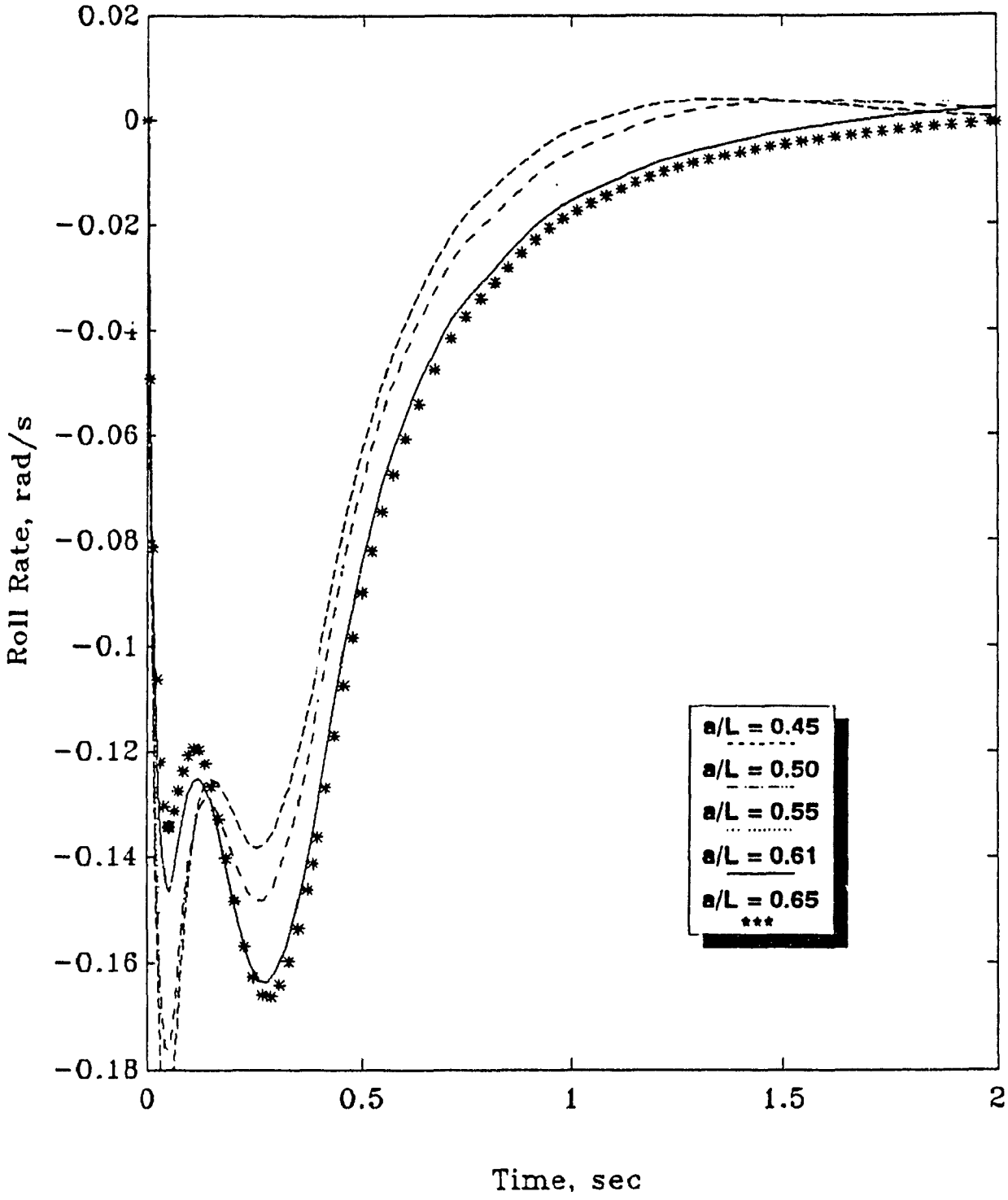

Fig. 4.43 CASE8: Roll Angular Velocity vs. Time

4.7.3 Parametric Study of CG Height

The center of gravity height h is varied and the effects on the vehicle handling response are observed. The simulation failed at first when the CG position is raised, due to excessive roll angle. This was overcome by increasing the total roll stiffness by 50 percent, in the form of constant auxiliary roll stiffness. The baseline 58/42 front/rear roll stiffness distribution is maintained and the roll damping ratio is 0.3. The range of test values is seen in Table 4.8:

TABLE 4.8: CASE9: CG Height Variation

h/h6	79%	90%	100%	105%	110%
h (m)	0.381	0.4318	0.4813	0.5054	0.5286
ltype	----	-.-.	solid	....	++++

The results of this study are seen in Figs. 4.44 and 4.45. It is clear that lowering the CG height will increase the maximum lateral acceleration capability. Lowering the CG height also decreased understeer slightly. This could be explained by the fact that the front/rear roll stiffness distribution would be changed due to a slightly different sprung mass roll angle. More precisely, as the sprung mass rolls, the linkage non-linearities effect a change in the roll stiffness distribution. This shows how sensitive the vehicle design synthesis is to suspension non-linearities.

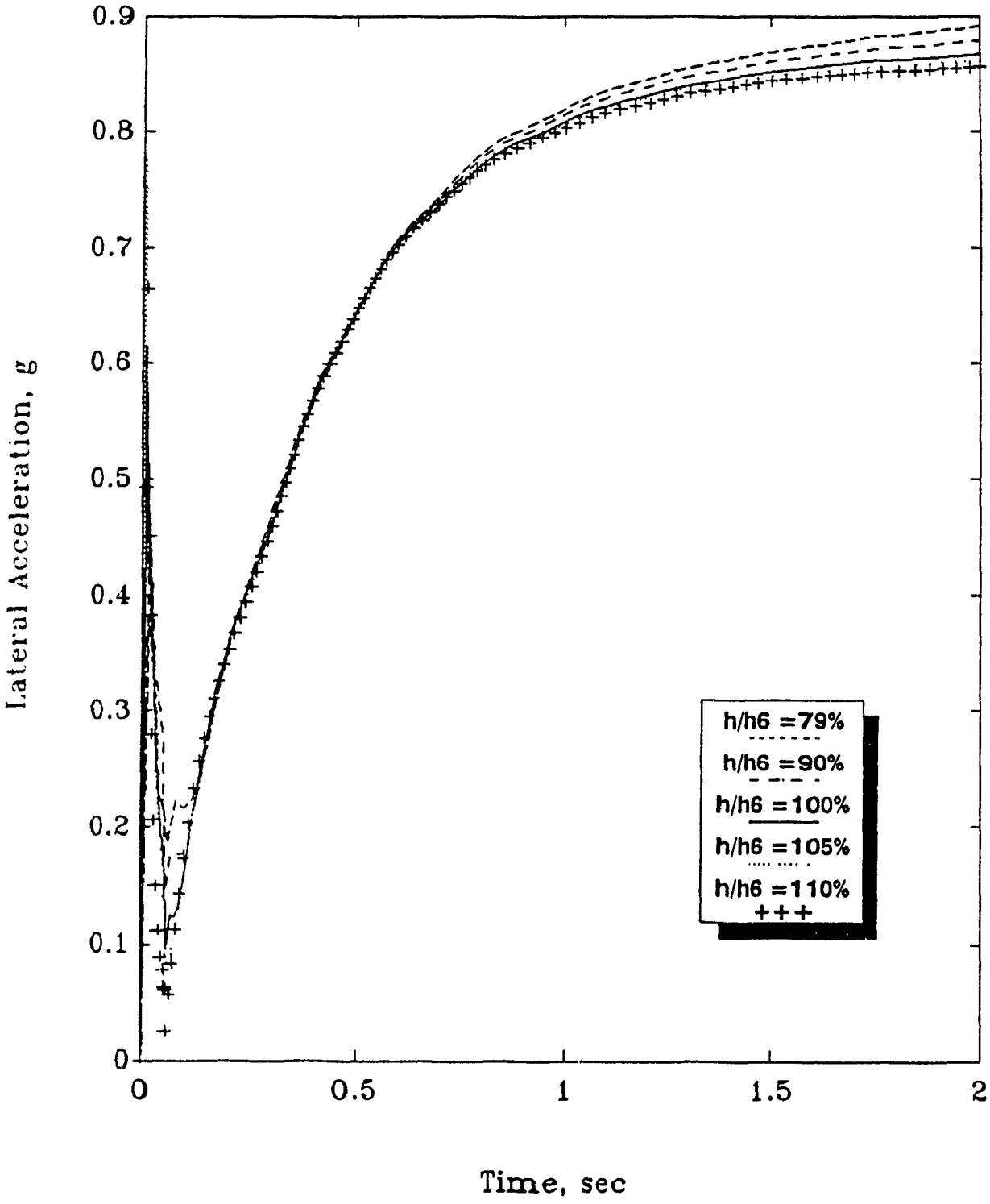

Fig. 4.44 CASE9: 1.25 Step Steer, Lateral Acc. vs. Time

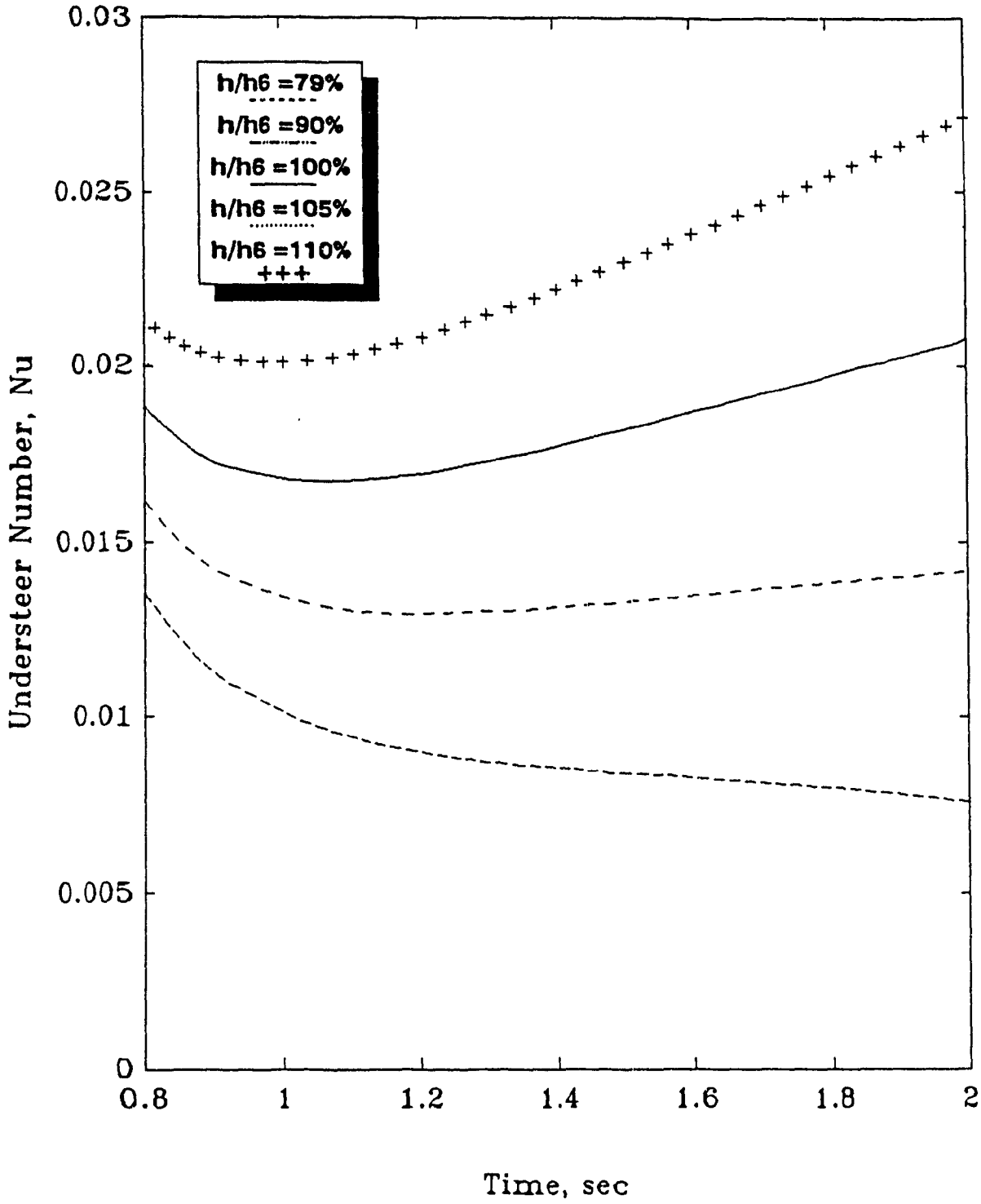

Fig. 4.45 CASE9: 1.25 Step Steer, Understeer vs. Time

4.7.4 Parametric Study of Wheelbase

The wheelbase L is varied and the effects on the vehicle handling response are observed. The baseline vehicle parameters with instantaneous roll center locations and roll stiffnesses are used. No auxiliary roll stiffness is used. The wheelbase variation is seen in Table 4.9.

TABLE 4.9: CASE10: Wheelbase Variation

Step Steer = 1.25 deg., tfinal = 2 sec.

L/L6	86%	90%	100%	109%	120%
L (m)	1.796	1.934	2.097	2.285	2.514
tf/L	0.7	0.65	0.6	0.55	0.50
a (m)	1.096	1.180	1.28	1.395	1.534
b (m)	0.7	0.754	0.817	0.890	0.980
ltype	———	-.-.	solid	....	++++

The results are seen in Figs. 4.46 to 4.53. It can be seen that the vehicle with the shortest wheelbase experienced the most yaw, lateral acceleration and understeer. It should be noted that the mass distribution and moments of inertia were not varied. For a large variation of wheelbase from the baseline configuration, it would be impossible to maintain the same moments of inertia.

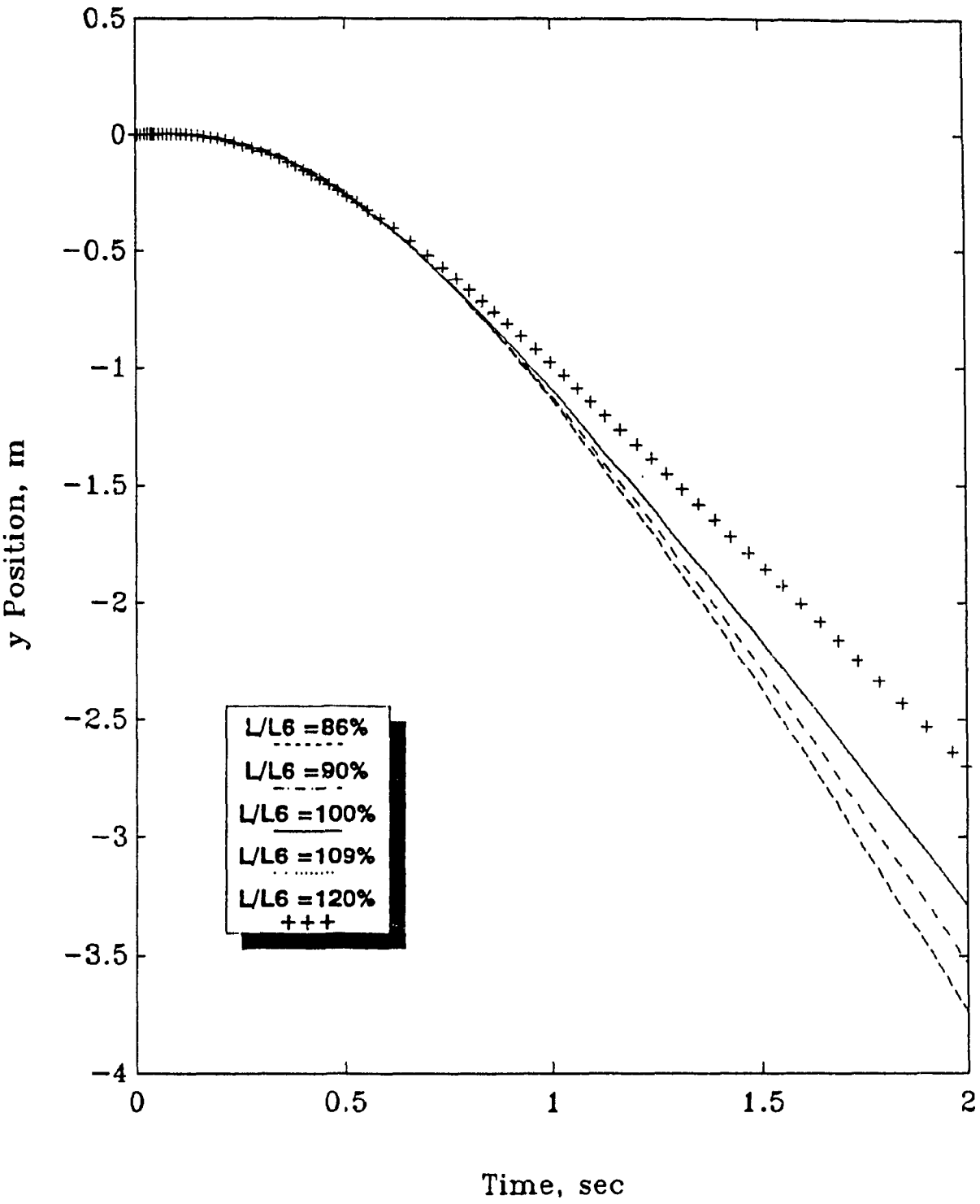

Fig. 4.46 CASE10: y Position vs. Time

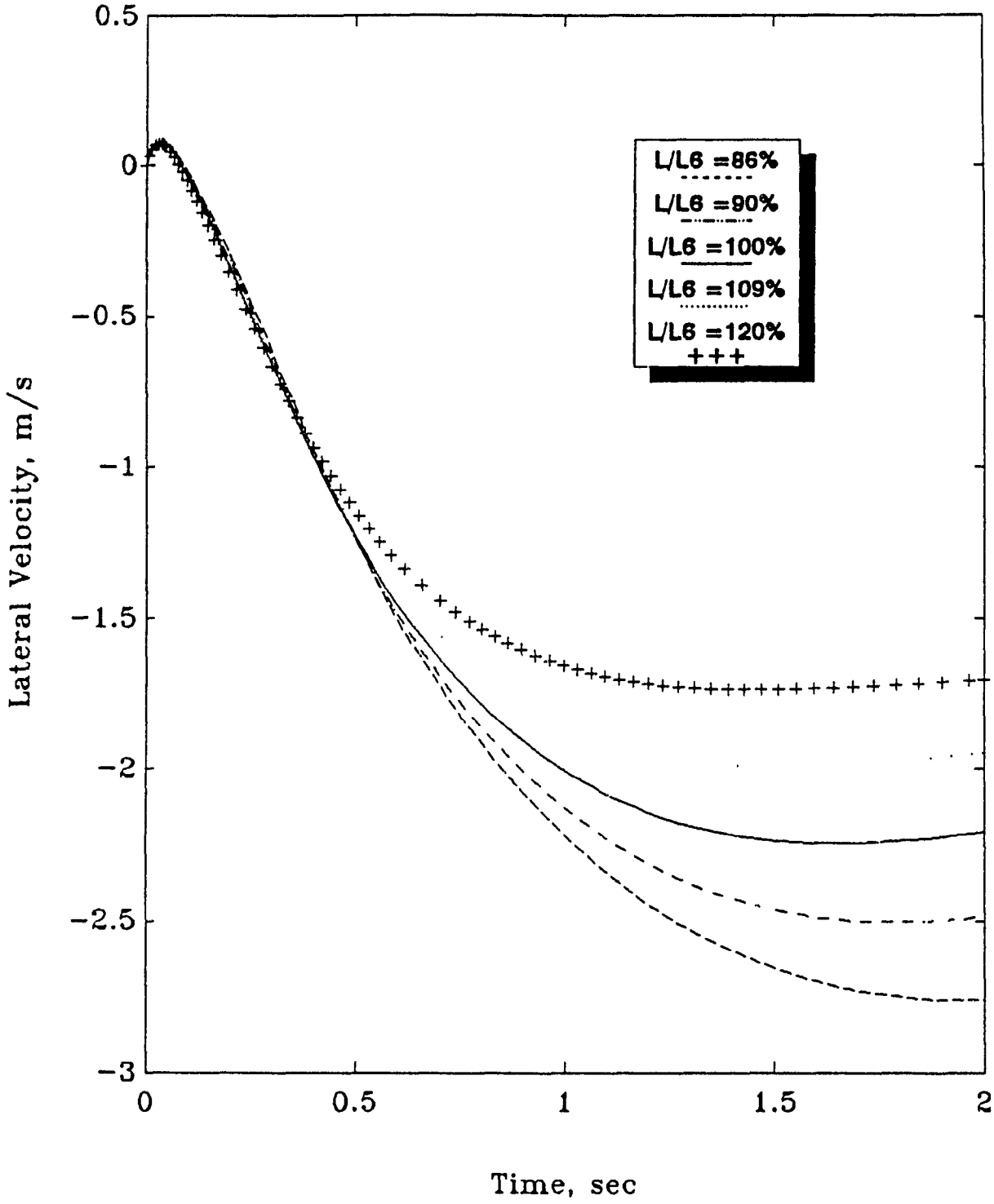

Fig. 4.47 CASE10: Lateral Velocity vs. Time

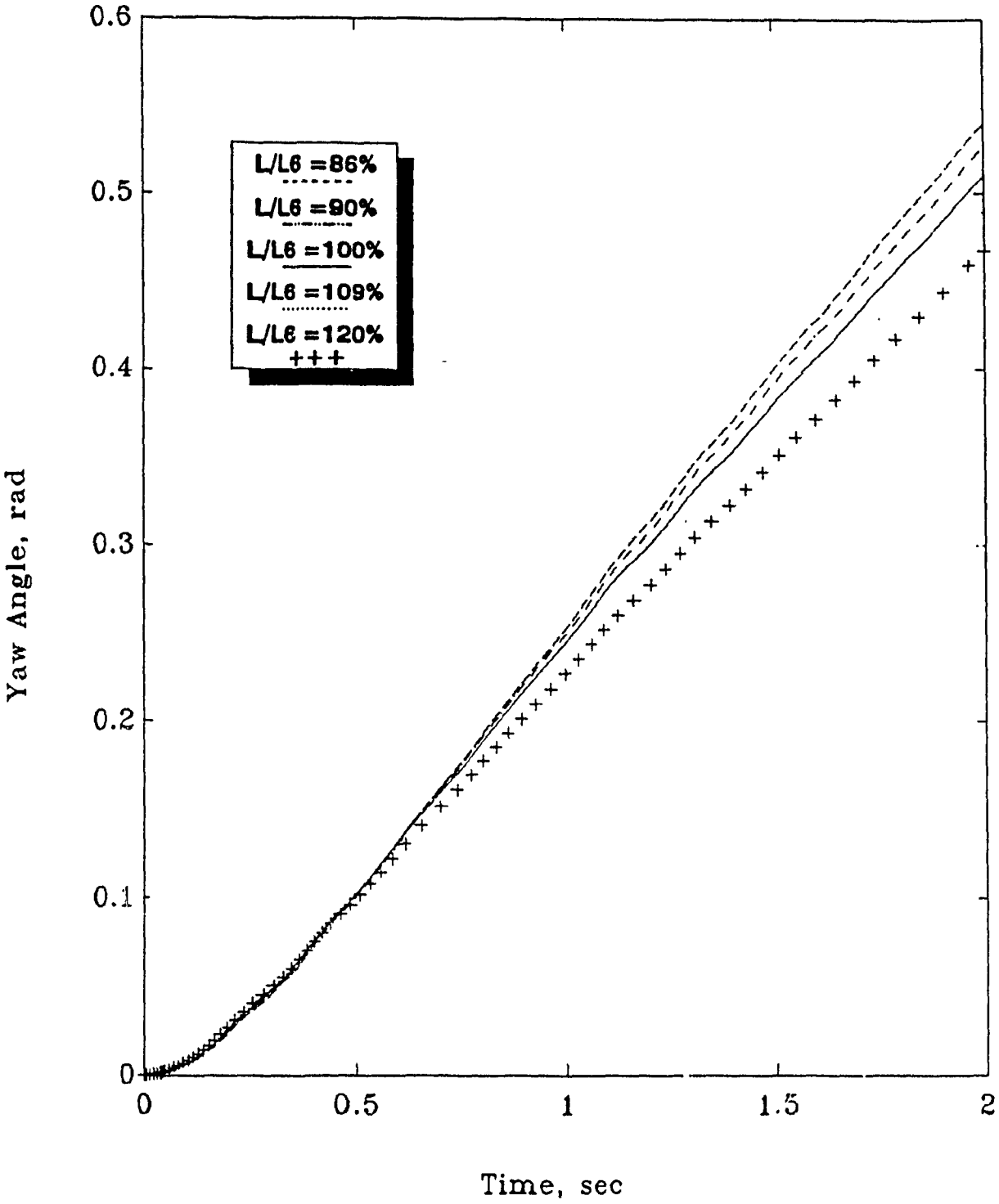

Fig. 4.48 CASE10: Yaw Angle vs. Time

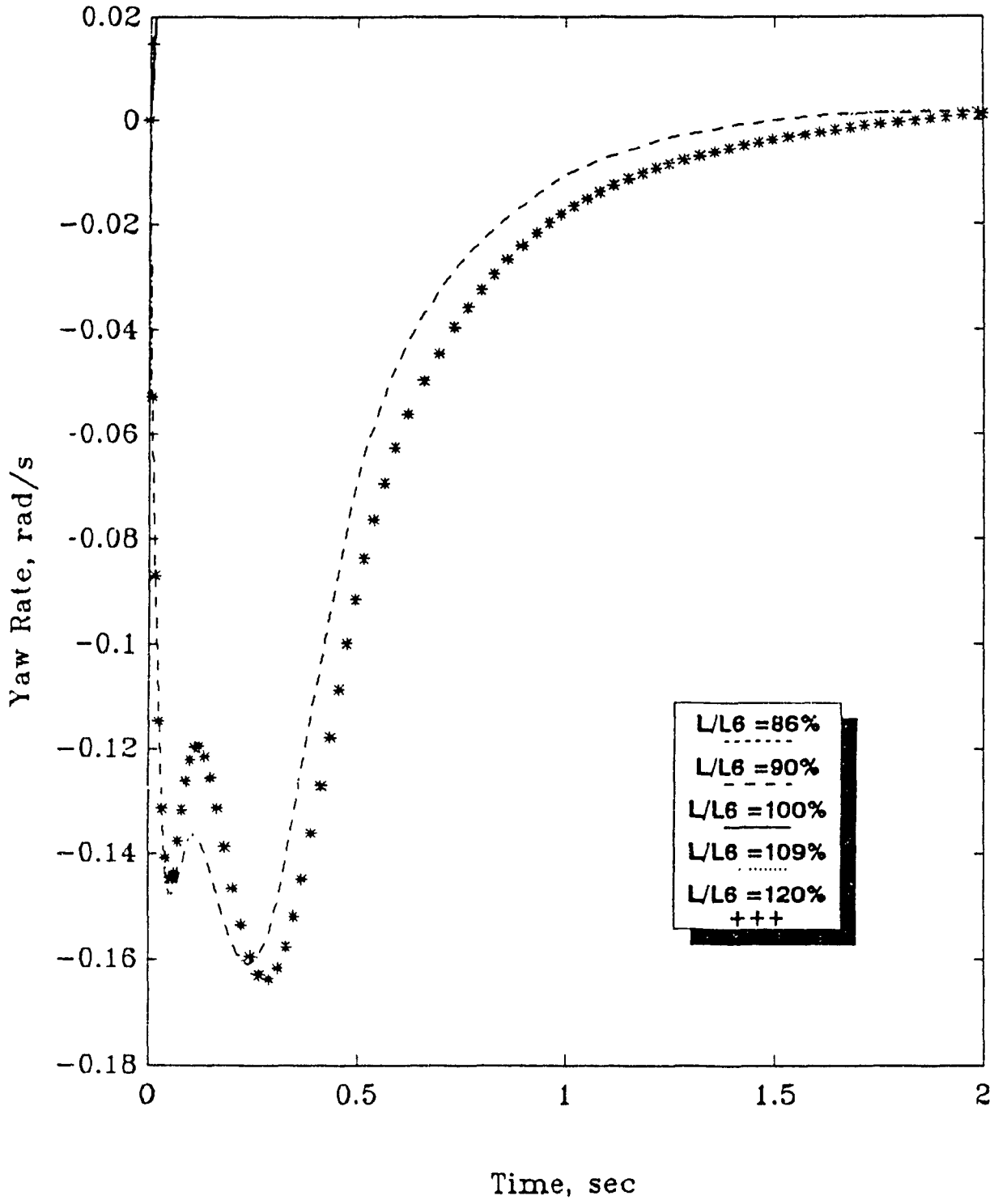

Fig. 4.49 CASE10: Yaw Angular Velocity vs. Time

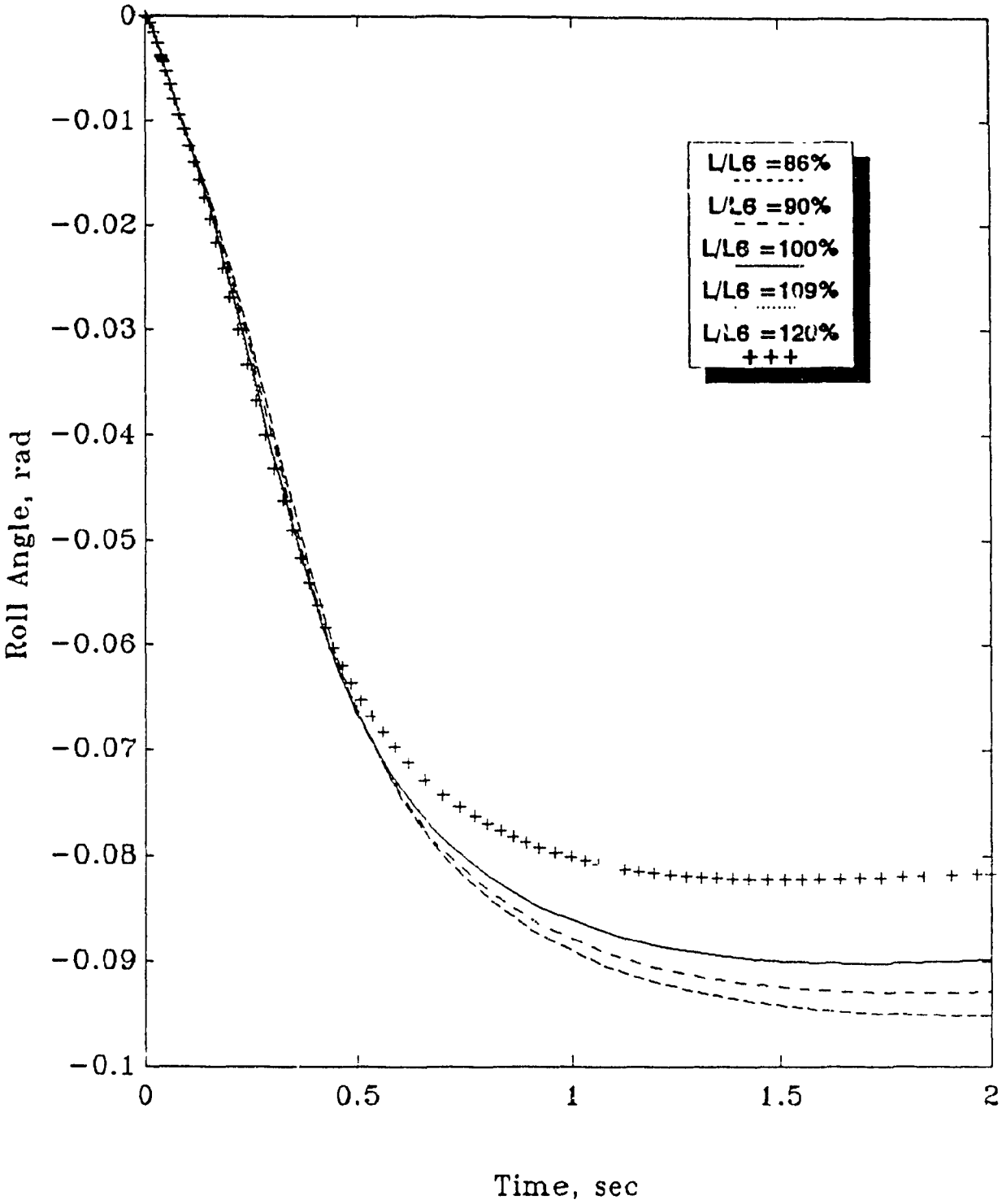

Fig. 4.50 CASE10: Roll Angle vs. Time

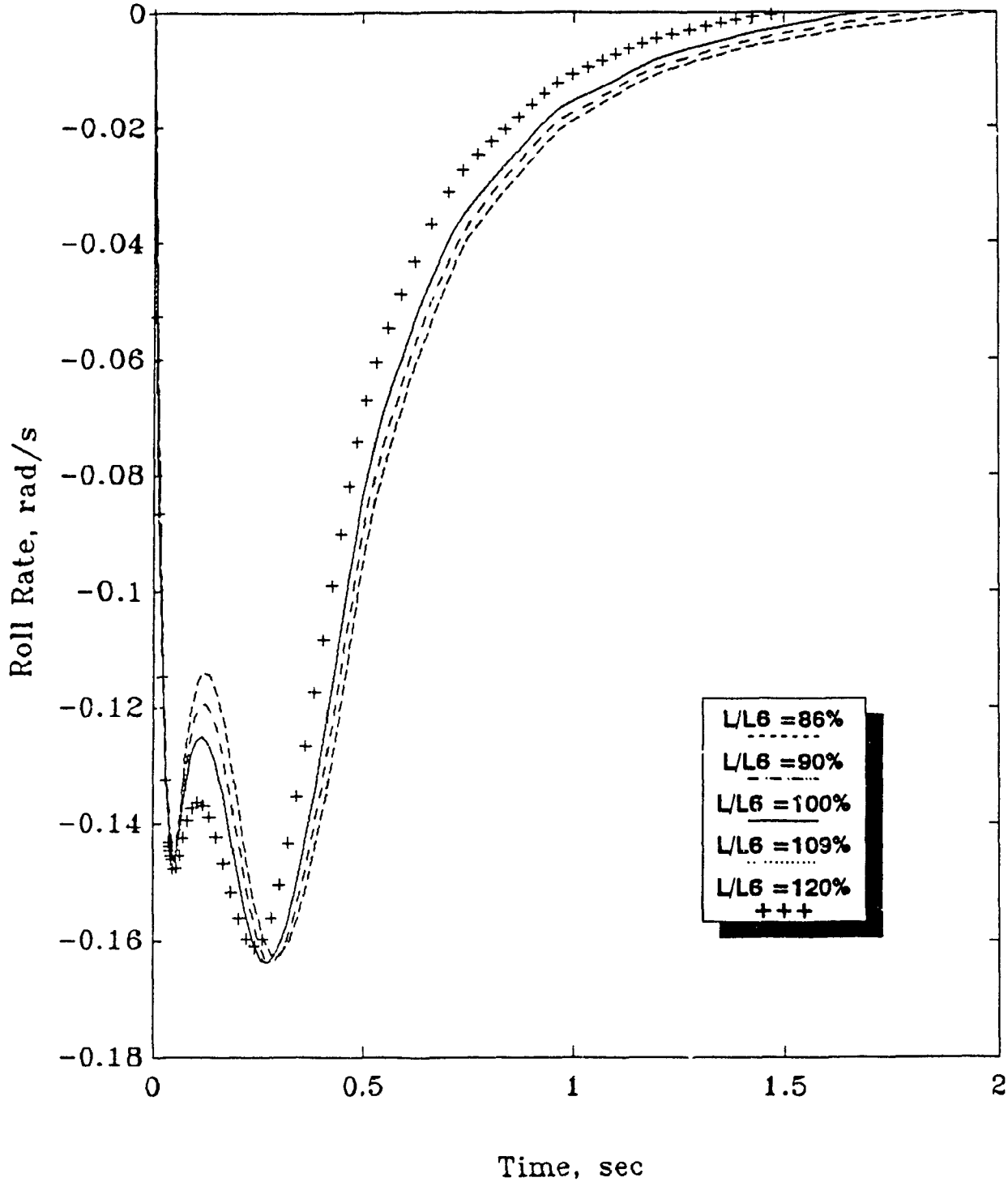

Fig. 4.51 CASE10: Roll Angular Velocity vs. Time

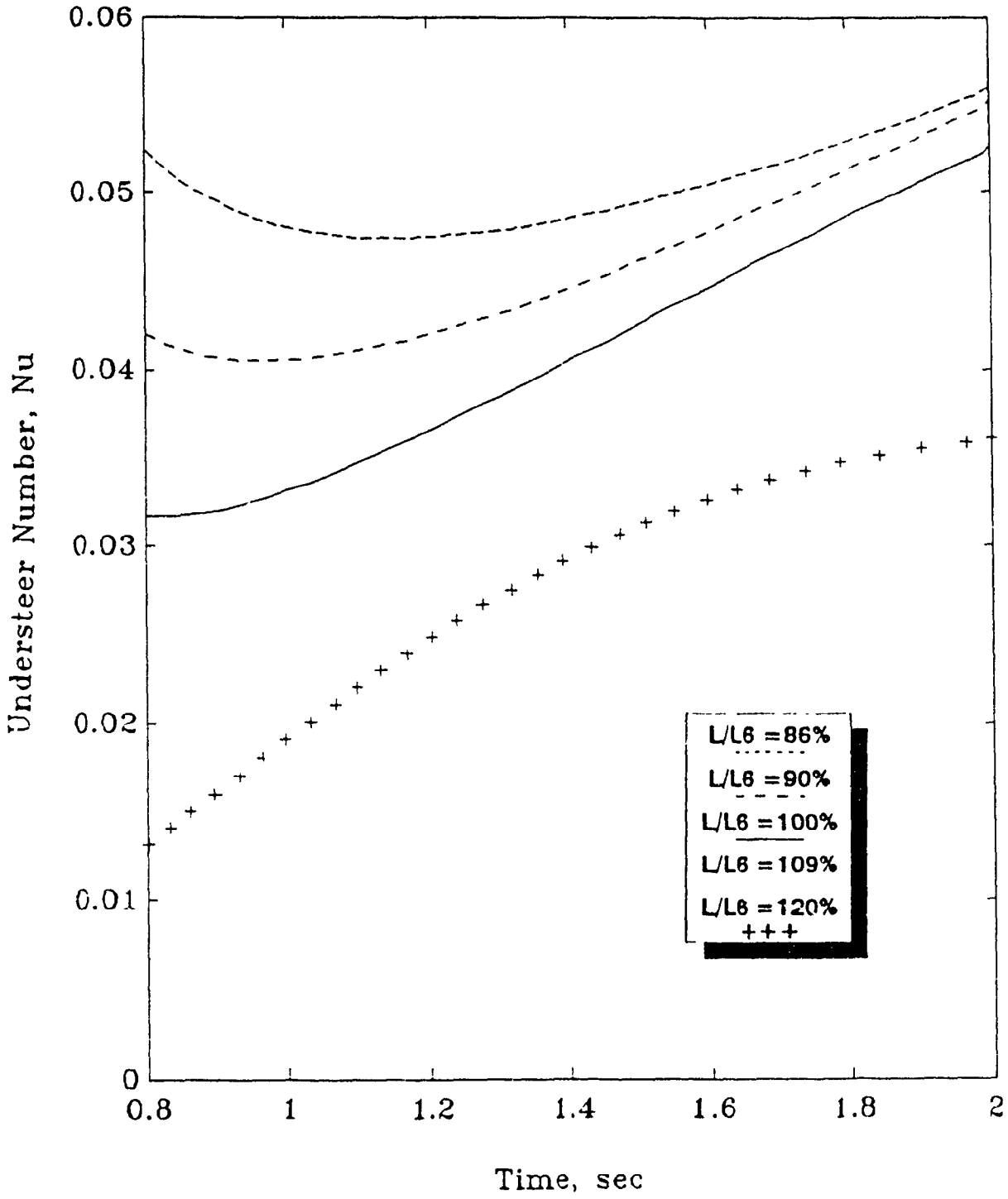

Fig. 4.52 CASE10: 1.25 deg. Step Steer, Understeer vs. Time

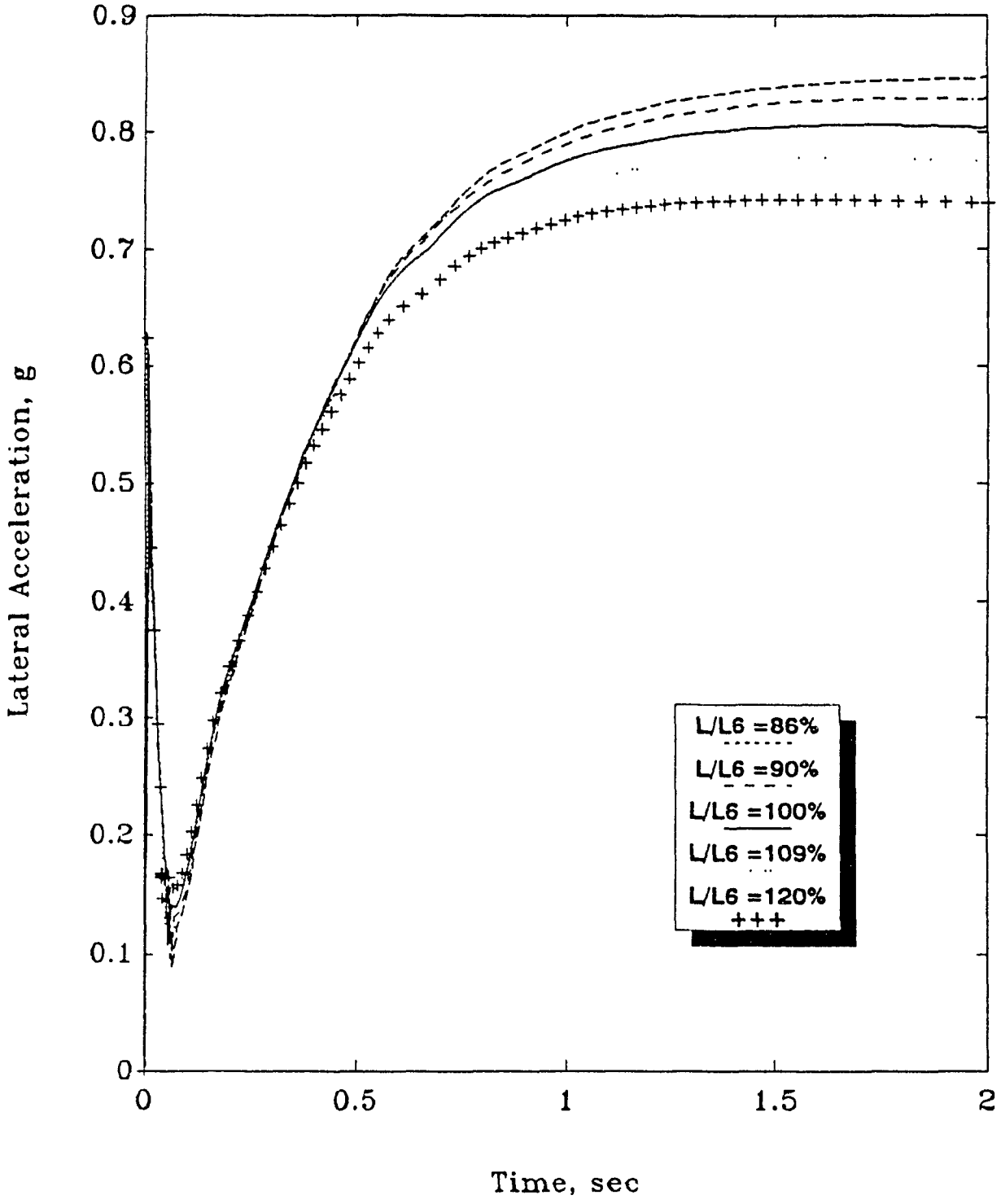

Fig. 4.53 CASE10: 1.25 deg. Step Steer, Lateral Acc. vs. Time

4.7.5 Parametric Study of Roll Stiffness Distribution

The roll stiffness distribution kf/ktot is varied and the effects on the vehicle handling response are observed. Changing the roll stiffness distribution is analogous to altering the anti-roll bar size or spring stiffness at one axle of a vehicle. The roll stiffness proportions are shown in Table 4.10.

TABLE 4.10: CASE11: Roll Stiffness Distribution

Step Steer = 1.25 deg., tr1nal = 2 sec.

kf/ktot	0.40	0.50	0.58	0.70	0.80
kf0	22391	22391	22391	22391	22391
kr0	16253	16253	16253	16253	16253
ktot	55978	44782	38644	54177	81265
kfaux	0	0	0	15533	42621
kraux	17333	6138	0	0	0
|Lp|	2361	2112	1961	2322	2844
ltype	----	-.-.-	solid	....	++++

* where ktot = kf0 + kr0 + kfaux + kraux

Results are shown in Figs. 4.54 and 4.55. Shifting the roll stiffness distribution towards the front axle improved the lateral acceleration and decreased understeer. These trends can be explained by the fact that the vehicle model has

a rearward weight bias. By increasing the proportion of front roll stiffness, lateral weight transfer at the front axle is increased, resulting in a more neutral-handling vehicle. The vehicle handling model with suspension analysis is able to illustrate this.

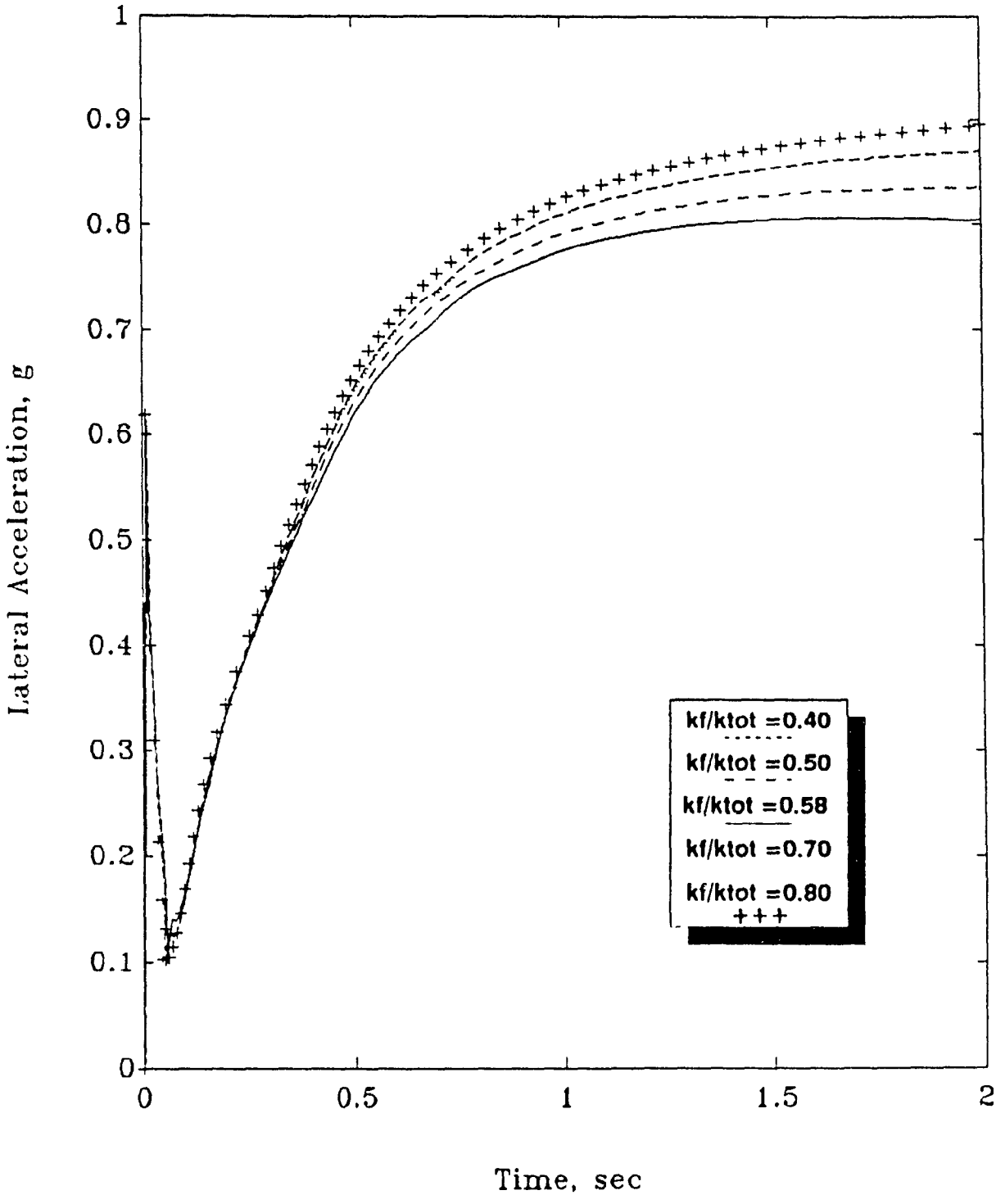

Fig. 4.54 CASE11: 1.25 deg. Step Steer, Lateral Acc. vs. Time

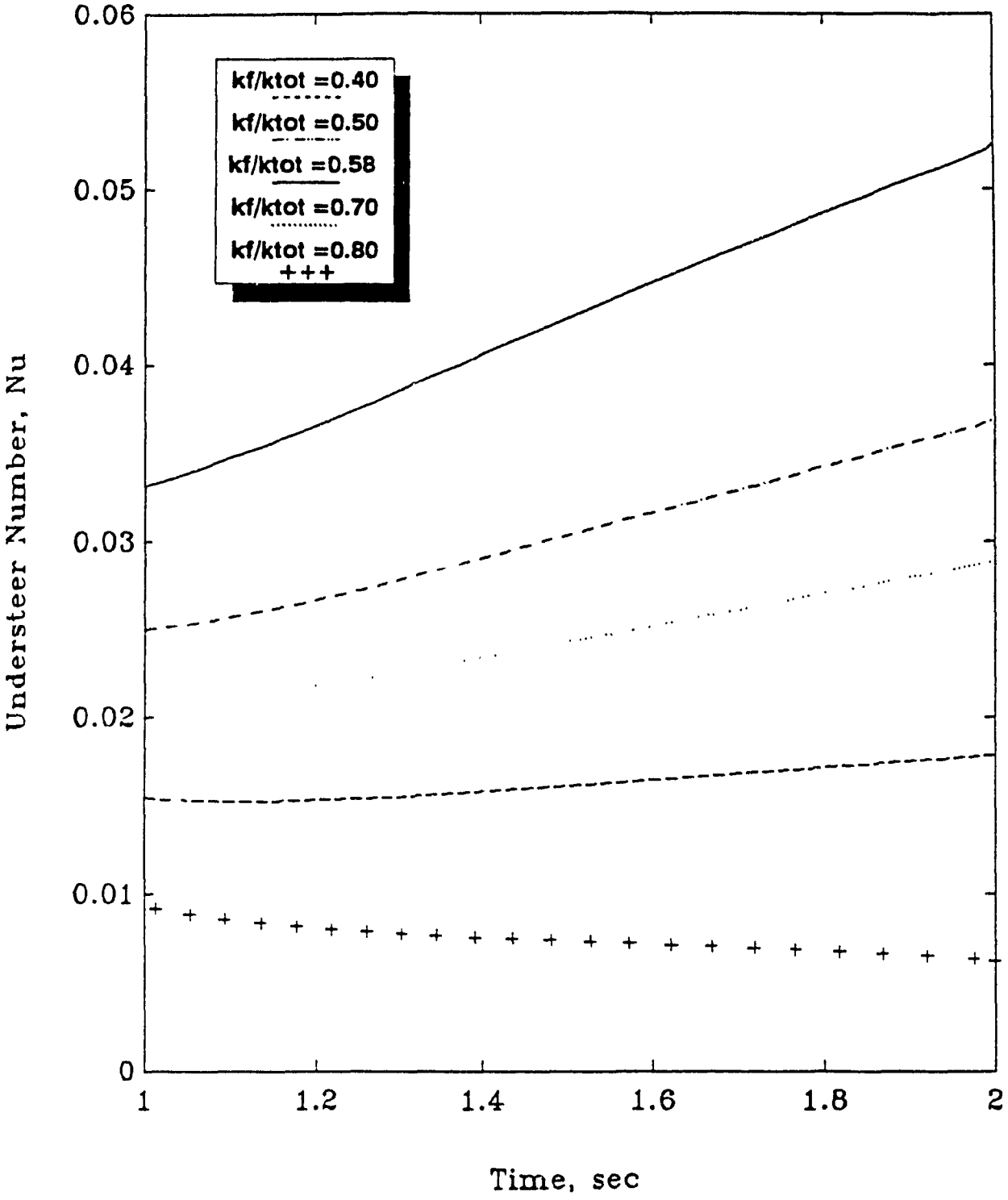

Fig. 4.55 CASE11: 1.25 deg. Step Steer, Understeer vs. Time

4.8 Summary

In this chapter, the mathematical modeling, analysis, and design synthesis for vehicle handling and stability, as developed in Chapter 3, has been demonstrated. Confidence has been gained in the solution of the vehicle handling model. The suspension analysis by the method of velocity coefficients has been used to include the instantaneous roll center locations and roll stiffnesses in the vehicle handling model. The parametric study using the vehicle handling model with non-linearities produced good handling and stability trends.

In conclusion, it is possible to include the influence of roll center movement and roll stiffness variation in a vehicle handling analysis and synthesis procedure. The method of velocity coefficients is used to obtain the instantaneous roll center location and roll stiffness. The advantage of the velocity coefficients method is that the kinematics analysis can be performed separately, and then included in the vehicle handling and stability analysis. In this way, the problem is conveniently broken down into small, manageable parts.

CHAPTER 5

Conclusions and Recommendations for Future Work

5.1 Conclusions

A computer-aided vehicle design synthesis procedure for handling and stability is developed. The vehicle suspension system components for handling and stability are described. The qualitative effect of each component on vehicle handling has been discussed. Selection methods based on analytical techniques presented in the literature are presented for the tires, springs and dampers.

The various stages of a design synthesis for the handling of a vehicle with pullrod A-arm suspension linkages are described in detail. The mathematical modeling, analysis, and design synthesis for vehicle handling and stability is developed. The suspension analysis by the method of velocity coefficients has been used to include instantaneous location of roll centers and roll stiffnesses in the vehicle handling model. The design synthesis procedure is implemented as a MATLAB-based software. The software consists of four modules called CGFIND, SPRING, KINSTAT, and DYNAMIC. CGFIND computes the best center of gravity location. SPRING computes the chassis spring rates. KINSTAT computes the non-linear roll centers and roll stiffnesses. DYNAMIC computes the transient and steady-state handling response for the vehicle, taking into account the selected tire and chassis non-linearities.

Case studies on a typical vehicle have been presented to gain confidence in the design synthesis procedure. The parametric study using the vehicle handling model with non-linearities produced good handling and stability trends.

In conclusion, it is possible to include the influence of instantaneous location of roll centers and roll stiffnesses in a vehicle handling analysis and synthesis procedure. The advantage of the procedure adopted in the thesis is that the kinematics analysis can be performed separately, and then included in the vehicle handling and stability analysis. In this way, the problem is broken down into small, manageable parts. The highlights of the thesis include:

- Discussion of selection methods for tires, springs, and dampers.
- A 3DOF mathematical modelling of a fixed control vehicle travelling on a smooth, level road, that includes the calculation of lateral weight transfer and a nonlinear tire model which provides tire lateral forces and self-aligning torques as a function of normal load, slip angle, and camber angle.
- Mathematical modelling of the planar A-arm pullrod suspension linkage and a kinematic and kineto-static analysis of the suspension linkage using the Newton-Raphson technique and velocity coefficients to fully describe its equilibrium force characteristics.

- Development of a procedure to find the best location of a vehicle's center of gravity based on two steady-state performance indices: understeer number N_u=0 and maximum lateral acceleration.
- Transient vehicle dynamic response evaluation in state-space form, using the fourth-order Runge-Kutta method in the MATLAB package.
- Case study on vehicle design synthesis.
- Parametric studies on the total roll stiffness, CG position a/L, CG height, wheelbase, and roll stiffness distribution.

5.2 Recommendations for Future Work

This thesis has provided a foundation for the development of a truly comprehensive vehicle design synthesis software. The range of possible modifications and improvements is probably limitless. However, some scope-limiting restrictions can be removed, and some further additions of a fundamental nature can provide a well-structured approach to the improvement of the synthesis procedure. These selected and influential changes are now noted.

-Modification of the mathematical model to include combined braking and cornering, or acceleration and cornering.
-Inclusion of aerodynamic loading.
-Inclusion of roll damping using the method of velocity coefficients and the nonlinear damper characteristics
-Anti-roll bar non-linearities
-Path follower model
-Additional degrees of freedom in mathematical model

At every stage of the analytical development, field testing, wherever possible, shall be carried out.

REFERENCES

1. Bernard, J.E., Segel, L., and Wild, R.E. "Tire Shear Force Generation During Combined Steering and Braking Maneuvers," SAE Transaction Paper No. 770852, 1978, pp. 2953-2969.

2. Pacejka, H.B. "Study of the Lateral Behaviour of an Automobile Moving Upon a Flat, Level Road and of An Analog Method of Solving the Problem," Cornell Aeronautical Laboratory Report No. YC-857-F-23, December 1957.

3. Radt, H.S., Jr., and Milliken, W.F. "Motions of Skidding Automobiles," SAE Preprint No. 205A (presented at SAE Summer Meeting, Chicago, Ill.), June 1960.

4. Ellis, J.R. "The Dynamics of Vehicles During Braking and Cornering," Institution of Mechanical Engineers, June 1963.

5. Deininger, W. "Einfluss der Auftreibskraft auf die Fahrstabilitaet von Kraftfahrzeugen," Automobiltechnische Zeitschrift, Vol. 67, No. 7, July 1965.

6. Krempl, G. "Untersuchungen an Kraftfahrzeugreifen," Automobiltechnische Zeitschrift, Vol. 69, No. 1, January 1967 and Vol. 69, No. 8, August 1967.

7. Holmes, K.E. and Stone, R.D. "Tire Forces as Functions of Cornering and Braking Slip on Wet Road Surfaces," Road Research Laboratory Report LR 254, 1969.

8. Dugoff, H., Fancher, P., and Segel, L. "An Analysis of Tire Traction Properties and Their Influence on Vehicle Dynamic Performance," 1970 International Automobile Safety Conference Compendium, Society of Automotive Engineers, New York.

9. Okada, T. et al. "Evaluation of Vehicle Handling and Stability by Computer Simulation at the First Stage of Vehicle Planning," SAE Transaction Paper No. 730525, 1973, pp. 1685-1707.

10. McHenry, R.R. and Deleys, N.J. "Vehicle Dynamics in Single Vehicle Accidents-Validation and Extensions of a Computer Simulation," Cornell Aeronautical Laboratory Report No. VJ-2251-V-3, December 1968.

11. Dugoff, H., Fancher, P.S., and Segel, L. "Tire performance characteristics affecting vehicle response to steering and braking control inputs," Final Report, Contract CST-460, Office of Vehicle Systems Research, US National Bureau of Standards, August, 1969.

12. Brewer, H.K. and Rice, R.S. "Tires-Stability and Control," SAE Technical Paper No. 830561, 1983, pp. 2.646-2.669.

13. Bakker, E., Nyborg, L., and Pacejka, H.B. "Tire Modelling for Use in Vehicle Dynamic Studies," SAE Technical Paper No. 870421, 1987, pp. 1-15.

14. Maalej, A.Y., Guenther, D.A., and Ellis, J.R. "Experimental Development of Tyre Force and Moment Models," International Journal of Vehicle Design, Vol. 10, No. 1, 1989, pp. 34-50.

15. Nalecz, A.G. "Investigation into the Effects of Suspension Design on Stability of Light Vehicles," SAE Technical Paper No. 870497, 1987, pp. 2.512-2.545.

16. Tapia, G.A. "Extended Tire Testing," Calspan Corporation, Contract No. DTNH22-81-C-07100, Final Report, 1983.

17. Segel, L. "Research in the Fundamentals of Automobile Control and Stability," SAE Transactions Vol. 65, 1957, pp. 527-540.

18. Broulhiet, G. "Suspension of Automobile Steering Mechanism: Shimmy and Tramp," Societe des Ingenieurs Civils de France, Bulletin 78, 1925.

19. Lind-Walker, G.E. "Directional Stability, Study of Factors Involved in Private Car Design," Automobile Engineer, Vol. 40, August-November 1950.

20. Scybor-Rylski, A.J. Road Vehicle Aerodynamics, 2nd. ed., Pentech Press, London, 1984.

21. Dominy, J.A. and Dominy, R.G. "Aerodynamic influences on the performance of the Grand Prix racing car," Proceedings of the Institution of Mechanical Engineers, Vol. 198D, No. 7, 1984, pp. 87-93.

22. Belingardi, G., Garavelli, M., Masserano, A., and Piombo, B. "On the Influence of Suspension Mechanism on the Dynamic Behaviour of a F.1 Racing Car," Proceedings of the 7th World Congress on The Theory of Machines and Mechanisms, Vol. 1, Seville, September 1987, pp. 455-458.

23. Dixon, J.C. "The Equations of Lateral Motion of the Two Degree-of-Freedom Model of the Four-Wheeled Road Vehicle," SAE Technical Paper No. 901732, 1990, pp. 25-33.

24. **Racing by the Numbers**, pamphlet, Mitchell Software, Menlo Park, CA, 1990.

25. **TLS100 Suspension Design Software**, Documentation and Operating Instructions, BTS Software, Inc., 1990.

26. Schaeffer, G. "Programme Tour 3.6: A Simulation Program to Optimise Road Performances of Racing Cars," 2e Session Technique Mechanique et Structure, S.I.A. No. 89037, September 1989, pp. 142-146.

27. Maalej, A. "Application of Suspension Derivative Formulation to Ground Vehicle Modeling and Simulation," Ph.D. Thesis, Ohio State University, 1988.

28. Bloxham, J. "Portuguese GP," Autosport, Vol. 112, No. 13, pp. 30-41.

29. Smith, C. Engineer to Win, Motorbooks International, Inc., Osceola, WI, 1984.

30. Staniforth, A. Competition Car Suspension: Design-Construction-Tuning, Haynes Publishing Group, Yeovil, Somerset, 1988.

31. Ellis, J.R. Vehicle Dynamics, Business Books Limited, London, 1969.

32. Adler, U. (ed.) Bosch Automotive Handbook, 2nd ed., Robert Bosch Ltd., Stuttgart, 1986.

33. Miles, J., Sears, K., and Booen, J. "High Performance Suspension for Front Wheel Drive," Automotive Technology International 1991, 1991, pp. 33-38.

34. **Vehicle Dynamics Terminology**, SAE Publication J1121, SAE Recommended Practice, 1988 SAE Handbook, Society of Automotive Engineers, 1988, pp. 17.16-17.20.

35. **Vehicle Dynamics Terminology**, SAE Publication J760e, SAE Recommended Practice, 1988 SAE Handbook, Society of Automotive Engineers, 1988, pp. 34.209-34.218.

36. Thompson, A.G. "Suspension Design for Optimum Road-Holding," SAE Technical Paper No. 830663, 1983, pp. 2.1135-2.1150.

37. **Owner's Manual, Fox Factory Shox**, Fox Factory, Inc. Campbell, CA, 1988.

38. Sugizaki, M. "Design features and driving comfort of motorcycles," Int. J. of Vehicle Design, Special Issue on Vehicle Safety, 1986, pp. 157-177.

39. Scott, D. "Global Viewpoints: Self-stabilizing suspension," Automotive Engineering, Vol. 94, No. 11, 1986, pp. 74-77.

40. Puhn, F. How to Make Your Car Handle, HPBooks, Inc., Tucson, Arizona, 1981.

41. **PRO-MATLAB User's Guide**, The MathWorks, Inc., Sherborn, MA, 1986.

42. Van Valkenburgh, P. Race Car Engineering and Mechanics, Dodd, Mead and Co., New York, 1976.

43. Nalecz, A.G. and Bindemann, A.C. "Handling Properties of Four Wheel Steering Vehicles," SAE Transaction Paper No. 890080, 1989, pp. 63-82.

44. Alanoly, J. "Computerized Analysis and Design of Vehicle Multibody Systems," Ph.D. Thesis, Concordia University, 1989.

45. Paul, B. Kinematics and Dynamics of Planar Machinery, Prentice-Hall, Inc., Englewood Cliffs, NJ, 1979.

46. Dominy, J. "Frictional aspects of F.1 racing car performance," TRIBOLOGY international, June 1981, pp. 167-170.

47. Dixon, J.C. "Limit steady state vehicle handling," Proc. Instn. Mech. Engrs., Vol. 201 No. D4, 1987, pp. 281-291.

48. Smith, C. Tune to Win, Aero Publishers, Inc., Fallbrook, CA, 1978.